
Electronic Thesis and Dissertation Repository

4-8-2015 12:00 AM

Helical Pile Installation Torque and Capacity Correlations

Jared Louis Harnish, *The University of Western Ontario*

Supervisor: Hesham El Naggar, *The University of Western Ontario*

A thesis submitted in partial fulfillment of the requirements for the Master of Engineering
Science degree in Civil and Environmental Engineering

© Jared Louis Harnish 2015

Follow this and additional works at: <https://ir.lib.uwo.ca/etd>



Part of the [Civil Engineering Commons](#), and the [Geotechnical Engineering Commons](#)

Recommended Citation

Harnish, Jared Louis, "Helical Pile Installation Torque and Capacity Correlations" (2015). *Electronic Thesis and Dissertation Repository*. 2855.

<https://ir.lib.uwo.ca/etd/2855>

This Dissertation/Thesis is brought to you for free and open access by Scholarship@Western. It has been accepted for inclusion in Electronic Thesis and Dissertation Repository by an authorized administrator of Scholarship@Western. For more information, please contact wlsadmin@uwo.ca.

HELICAL PILE INSTALLATION TORQUE AND CAPACITY CORRELATIONS

Monograph

by

Jared Harnish

Graduate Program in Geotechnical Engineering

A thesis submitted in partial fulfillment
of the requirements for the degree of
Masters of Science in Engineering

The School of Graduate and Postdoctoral Studies
The University of Western Ontario
London, Ontario, Canada

© Jared Harnish 2015

Abstract

Large diameter helical piles are being utilized increasingly to support large compressive and tensile loads. Both the magnitude of the required installation torque and the pile capacity can be directly attributed to the soil shearing resistance developed over the embedded area of the pile including the shaft and helical plates. Hence, the pile capacity can be correlated to the installation torque. Such correlations are widely used in the helical pile industry as a means for quality control/quality assurance. However, the reliability of capacity-torque correlations for predicting the behavior of large diameter helical piles is adversely affected by the inaccurate measurement of the installation torque employing hydraulic pressure torque indicators. In the current study, a torque pin was fabricated using a strain gauge methodology to facilitate accurate measurement of installation torque. A total of 17 piles, including seven fully instrumented, were installed while monitoring the installation torque continuously with depth using the fabricated device. The results of installation torque monitoring were demonstrated to be accurate and repeatable. In addition, six compressive and four tensile axial load tests were conducted on the test piles. The load test results were analyzed to determine the interpreted ultimate capacity of the test piles. The results demonstrate that the ultimate capacity of large diameter helical piles can be determined from the pile load tests data employing the interpreted failure criteria proposed by Elkasabgy and El Nagggar (2015) and Fuller & Hoy (1970). The measured installation torque and the corresponding ultimate capacity values were used to define the torque-to-capacity correlation based on embedded pile area, which is suitable for large diameter piles with single and double helices. Furthermore, the results from the seven test piles that were instrumented with strain gauges provided a description of the load transfer mechanism at various levels of axial loading. It was found that significant settlement may be required to mobilize the bearing resistance provided by the lead helix for both compressive and tensile loading conditions. Finally, the trailing helix provides significant capacity contribution under compression loading but little contribution under tensile loading.

Keywords

Helical pile, axial load test, installation torque, torque-to-capacity, ultimate failure load analysis, glacial till.

Acknowledgments

I would like to thank my supervisor Dr. M. H. El Naggar for his guidance and unwavering support as well as his inspiring outlook on the engineering profession. His promotion for freedom of thought and exploration is a treasure to the engineering community.

I would like to thank Tom Bradka, Ashref Alzawi, Ben Kasprick and the entire Helical Pier Systems team. Their financial and intellectual support during the research project was invaluable. Opportunities such as these may not be possible without such institutions as the Natural Sciences and Engineering Council of Canada (NSERC).

A special thanks goes to my colleagues Andrew MacDonald, and Jesus Gonzalez for their insightful discussions and sympathetic tirades.

Lastly, my academic achievements would not have been possible without my beloved wife Amy Harnish, whose love and encouragement made this endeavor possible.

Table of Contents

Abstract	ii
Acknowledgments.....	iii
Table of Contents	iv
List of Tables	viii
List of Figures	ix
List of Appendices	xiv
Chapter 1	1
1 Introduction	1
1.1 Research Objectives and Scope of Work.....	1
1.2 Thesis Organization	2
Chapter 2	4
2 Literature Review	4
2.1 Theoretical Axial Capacity	6
2.1.1 Compressive Individual Plate Bearing Method	7
2.1.2 Compressive Cylindrical Shear Method	10
2.1.3 Uplift Resistance.....	10
2.1.4 Shaft Adhesion.....	11
2.1.5 Uplift Capacity Factor N_{cu}	13
2.1.6 Geometric Considerations.....	14
2.2 Empirical Axial Capacity.....	18
2.3 Helical Pile Installation Torque	22
2.4 Static Pile Load Testing	24
2.5 Ultimate Capacity & Load Settlement Interpretation	24

2.6 Capacity to Torque Correlations	28
2.6.1 Hoyt and Clemence, 1989	29
2.6.2 Ghaly and Hanna, 1991	31
2.6.3 Zhang, 1999	35
2.6.4 Tappenden, 2007	35
2.6.5 Perko, 2009	37
Chapter 3	40
3 Site Investigation & Test Pile Configuration	40
3.1 Site Location	40
3.2 CPT Testing	41
3.2.1 CPT Results	41
3.2.2 Soil Properties	43
3.3 Test Pile Configurations & Instrumentation	51
3.3.1 Pile Configurations	51
3.3.2 Strain Gauge Installation	53
3.3.3 Installation Procedure & Layout	55
Chapter 4	56
4 Installation Torque	56
4.1 Measurement of installation parameters	56
4.1.1 Torque Pin	58
4.1.2 Hydraulic Pressure	60
4.1.3 Installation Rate	62
4.2 Torque Measurement Sensitivity	63
4.2.1 Effects of Crowd on Installation Torque Generation	63
4.2.2 Hydraulic Versus Mechanical Torque Measurements	67

4.2.3	Effects of Installation Rate on Torque	70
4.3	Installation Torque Results	70
4.4	Average and Final Installation Torque	75
4.5	Installation Torque Prediction.....	75
Chapter 5	81
5	Axial Pile Load Tests	81
5.1	Setup & Layout	81
5.2	Procedure	84
5.3	Pile Load Test Results	85
5.4	Interpreted Ultimate Capacity	85
5.5	Load Test Results.....	85
5.5.1	Compressive Load Tests	85
5.5.2	Uplift Load Tests	90
5.5.3	Comparison of interpreted failure load criteria.....	92
5.6	Capacity-Torque-Correlations	94
5.6.1	CTC factors	94
5.6.2	Capacity-Torque-Correlation Curve Fitting	95
5.6.3	Evaluation of Capacity to Torque Correlation Factors	95
5.6.4	Proposed Capacity to Torque Correlation Using Pile Embedded Area....	97
5.7	Load Transfer Results	98
5.7.1	Load Transfer Curves for Piles Under Compression Loading.....	99
5.7.2	Load Transfer Distribution for Piles Under Uplift Loading	104
5.7.3	Load Transfer Behavior	106
5.8	Accuracy of Capacity Prediction Approaches	107
5.8.1	Individual Plate Bearing Predictions	108

5.8.2	LCPC Method Predictions	109
5.8.3	Modified LCPC Predictions.....	110
5.8.4	Capacity to Torque Correlation Predictions	111
Chapter 6	114
6	Summary	114
6.1	Conclusions.....	114
6.2	Recommendations for Future Work.....	115
References	117
Appendices	121
Curriculum Vitae	123

List of Tables

Table 2-1: Bearing Capacity Factors, k_c (Canadian Geotechnical Society, 2006).....	20
Table 2-2: Friction Coefficient, α (Canadian Geotechnical Society, 2006).....	21
Table 3-1: Unit Weight Estimate based on SBT.....	44
Table 3-2: Peak shear strength (S_{up}) and remolded shear strength (S_{ur}) values averaged over 1 m intervals.....	50
Table 3-3: Pile Configuration and Testing Summary	53
Table 5-1: Ultimate capacity of tested piles	93
Table 5-2: Summary of correlation of torque to capacity factors	95
Table 5-3: Load Transfer Summary.....	107
Table 5-4: Predicted Capacity Summary	108

List of Figures

Figure 2-1: a) Individual Plate Bearing b) Cylindrical Shear (Perko, 2009)	7
Figure 2-2: Effective Shaft Adhesion a) Shallow Installation b) Transitional Installation c) Deep Installation (Narasimha Rao & Prasad, 1993)	13
Figure 2-3: Example Influence Cone (Perko, 2009)	17
Figure 2-4: Digger 1400 & Boom Truck	23
Figure 2-5: Typical Load Displacement Curves (Kulhawy, 2004)	25
Figure 2-6: Load Displacement Curve Regions (Kulhawy, 2004)	26
Figure 2-7: Histograms comparing the actual to calculated capacity ratios a) Cylindrical shear b) Individual plate bearing c) Torque-to-Capacity	31
Figure 2-8: Installation Torque Generation Model (Ghaly & Hanna, 1991)	33
Figure 2-9: Non-dimensional Torque Factor Formulation a) Theoretical formulation b) Experimental data fit (Ghaly & Hanna, 1991)	34
Figure 2-10: a): Axial measured pile capacity and required installation torque; b): Capacity to Torque Correlations based on shaft diameter (Tappenden, 2007)	36
Figure 2-11: Ratios of Predicted Ultimate Capacity, Q_t , to Measured Ultimate Capacity, Q_u , Using Torque Correlations Based on Diameter of Screw pile Shaft	37
Figure 2-12: Empirical Torque Correlation Line of Best Fit (Perko, 2009)	38
Figure 3-1: Test Site Location	41
Figure 3-2: CPT – Raw Data: a) Cone tip resistance (q_c); b) Sleeve friction (f_s); c) friction ratio; d) Pore pressure (u_2 & u_o)	43
Figure 3-3: a) Normalized tip resistance b) Normalized friction ratio	45

Figure 3-4: SBT chart	45
Figure 3-5: SBT; Soil type with for depth a) CPT #1;b) CPT #2; and c)C PT #3.....	46
Figure 3-6: Estimated OCR profiles	48
Figure 3-7: Undrained shear strength S_u estimated from: a) N_k ;b) OCR	49
Figure 3-8: Design Shear Strength Peak (S_{up}) and Remolded (S_{ur})	50
Figure 3-9: Test Pile Drawing.....	52
Figure 3-10: a) Double Helix Instrumented Pile with Installed Strain Gauges b) Double Helix Instrumented Pile Strain Gauges Coated in Protective Epoxy.....	54
Figure 3-11: Lamont Test Site Layout – Pile Locations & CPT Soundings	55
Figure 4-1: Boom Truck & Digger 1400	57
Figure 4-2: Torque Pin Calibration Table.....	59
Figure 4-3: Torque Sensors Calibration.....	59
Figure 4-4: Load Sensors Calibration	60
Figure 4-5: Hydraulic Pressure Transducer	61
Figure 4-6: Installation Rate Measurement.....	62
Figure 4-7: Install force profiles for 179 mm pile: a) C6S; b) T6S; c) C6D; and d) T6D	64
Figure 4-8: Install force profile for 219 mm pile a) C8S; b) T8S; c) C8D; and d)T8D	65
Figure 4-9: Install Force Profile for 273 mm pile a) C10S; and b) C10D	66
Figure 4-10: Crowd vs Torque Relationship	66
Figure 4-11: Hydraulic and mechanical torque: a) measured at low RPM for C10D; b) measured at high RPM for C6S; and c) measured at variable RPM for T8D	69

Figure 4-12: Torque Profile for Reaction Piles (RP1-8).....	71
Figure 4-13: Torque Profile for Test Piles; C6D, T6D, C6S, T6S	72
Figure 4-14: Torque Profiles for Test Piles; C8D, T8D, C8S, T8S.....	72
Figure 4-15: Torque Depth Profile Test Piles; C10S, C10D	73
Figure 4-16: Torque Depth Profile for Single Helix Piles.....	74
Figure 4-17: Torque Depth Profile for Double Helix Piles	74
Figure 4-18: Average and Final Installation Torque.....	75
Figure 4-19: 168.6 mm Diameter Pile with Single Helix Torque Prediction	78
Figure 4-20: 168.3 mm Diameter Pile with Double Helix Torque Prediction.....	78
Figure 4-21: 219 mm Diameter Pile with Single Helix Torque Prediction	79
Figure 4-22: 219 mm Diameter Pile with Double Helix Torque Prediction.....	79
Figure 4-23: 273 mm Diameter Pile with single Helix Torque Prediction.....	80
Figure 4-24: 273 mm Diameter Pile with Double helix Torque Prediction	80
Figure 5-1: Loading Setup a) Compression b) Tension.....	82
Figure 5-2: Reaction Setup a) Two Reaction Pile Setup b) Four Reaction Pile Setup	83
Figure 5-3: Data Acquisition System.....	84
Figure 5-4: Load Settlement Curve for Test Pile C6S.....	86
Figure 5-5: Load Settlement Curve for Test Pile C6D	87
Figure 5-6: Load Settlement Curve for Test Pile C8S.....	87
Figure 5-7: Load Settlement Curve for Test Pile C8D	88

Figure 5-8: Load Settlement Curve for Test Pile C10S	88
Figure 5-9: Load Settlement Curve for Test Pile C10D	89
Figure 5-10: Load Settlement Graph Test Pile T6S.....	90
Figure 5-11: Load Settlement Curve for Test Pile T6D	91
Figure 5-12: Load Settlement Curve for Test Pile T8S	91
Figure 5-13: Load Settlement Curve for Test Pile T8D	92
Figure 5-14: Comparison of Ultimate Failure Load from Different Criteria.....	93
Figure 5-15: Direct Torque –to –Capacity Correlation.....	96
Figure 5-16: Torque to Capacity vs Shaft Diameter	97
Figure 5-17: Torque to Capacity vs Embedded Area	98
Figure 5-18: Locations of strain guage stations	99
Figure 5-19: C6S Load Transfer Observations	101
Figure 5-20: C8S Load Transfer Observations	102
Figure 5-21: C8D Load Transfer Observations	102
Figure 5-22: C10S Load Transfer Observations	103
Figure 5-23: C10D Load Transfer Observations	103
Figure 5-24: T8S Load Transfer Observations	105
Figure 5-25: T8D Load Transfer Observations	105
Figure 5-26: Individual Plate Bearing Prediction Ratio Q_p/Q_u	109
Figure 5-27: LCPC Method Prediction Ratio Q_p/Q_u	110

Figure 5-28: Modified LCPC Method Prediction Ratio Q_p/Q_u	111
Figure 5-29: Torque-to-Capacity Prediction Ratio Q_p/Q_u	112
Figure 5-30: Comparison of Desk Design Prediction Ratio Q_p/Q_u	113

List of Appendices

Appendix A: Borehole Logs	121
---------------------------------	-----

Chapter 1

1 Introduction

Helical piles, also known as screw piles or screw anchors, were used historically for supporting small tensile forces. More recently, larger, higher capacity helical piles are used increasingly to support much larger compressive and tension loads. Their attractive features include a wide range of load carrying capacity, fast and low impact installation and ability to be loaded immediately after installations make them an appealing alternative to traditional deep foundation options such as driven piles, drilled shafts and micropiles.

As the capacity of the helical piles increases, the risk associated with their design solutions grows and so engineers must develop a better understanding of their performance and capacity evaluation. In situ verification of helical pile capacity is widely incorporated into the helical pile design methodology. Installation torque is often used as the quality assurance and quality control parameter governing as-built design specifications. In particular, the torque-to-capacity correlation, traditionally used for verification of pile capacity, which began as a mere ‘trade secret’, requires better understanding to be applied for the case of large diameter helical piles. Present literature reveals little research focused on the identification of the important factors that affect the generation of and/or error in measurement of installation torque.

1.1 Research Objectives and Scope of Work

Significant efforts have been dedicated over the years to empirically correlate the installation torque and the capacity of helical piles. However, a comprehensive relationship has not been attainable. There are a number of factors that affect installation torque such as pile configuration, soil conditions, and accuracy of torque measurements. Pile configurations such as pile shaft size and shape, number and diameter of helices, and pitch size are some parameters that affect installation torque. Soil conditions and groundwater levels also have considerable effects on pile installation and recorded torque values. In addition, installation procedures such as applying down-pressure (crowd) on the pile, use of pre-drilling process and speed of rotary head influence installation torque. Furthermore, the torque is determined through either measuring the differential hydraulic pressure using mechanical devices or by using an electronic load cell

attached to the pile head. The method employed may impact the torque measurements. The objective of this research is to investigate the significant parameters that affect the installation torque and understand if and where potential measurement errors may occur. Secondly, this research aims to investigate the relationship between installation torque and ultimate failure capacity of large diameter helical piles installed in glacial till.

Accurate measurement of torque effectively facilitates investigating the factors that affect the soil resistance to pile installation and hence the required installation torque. Consequently, suitable installation torque-to-capacity correlations can be developed and verified. A custom load pin was designed, fabricated and incorporated onto a helical pile drive head to accurately measure the installation torque. Seventeen piles were installed while continuously monitoring the installation torque with pile embedment depth. Axial pile load tests were subsequently conducted on ten helical piles, seven of which were instrumented with axial strain gauges. The installation torque, applied load, pile head displacement, and load transfer measurements along the piles were collected and analyzed in order to evaluate the required installation torque, and load transfer mechanisms for helical piles. The author was responsible for the installation of helical pile strain gauges, load testing, and test program design. Load cell construction was a joint effort including work by Terracene International while data acquisition was facilitated with the help of Dycor Technologies.

1.2 Thesis Organization

This thesis is organized into six chapters beginning with a brief introduction and literature review. The literature review presented in Chapter two focuses on the important aspects of helical pile design: axial capacity theory, installation torque measurement, ultimate capacity interpretation from load displacement, and torque-to-capacity correlations.

Chapter three provides a description of the test site, pile configurations and testing equipment. The soil investigation program and the resulting soil profile, and the representative soil parameters are presented. Furthermore, all details of the instrumentation employed to collect relevant information during the load tests are discussed.

Chapter four details the method of monitoring installation forces and presents the results from the 17 installed piles. All installation torque-depth profiles are investigated and compared to reveal the significant contributing factors, potential errors, and measurement sensitivities during installation. Furthermore, a basic model for predicting installation torque is presented.

The axial load testing program is described and the tests results are presented and discussed throughout Chapter five. The results are presented in terms of load-displacement curves as well as load transfer curves that were captured by the pile instrumentation. Additionally, the axial load tests results are combined with installation torque measurements to produce a set of capacity to torque correlations.

All significant findings and future research recommendation can be found in Chapter six.

Chapter 2

2 Literature Review

To effectively uncover the theoretical and practical issues affecting the accuracy of helical pile design, a literature review is provided on the main relevant topics: axial capacity theory, helical pile installation torque, load settlement and ultimate capacity interpretation, and the fundamental resulting Capacity to Torque Correlations (CTC). This review enables a better perspective for the scope of research continued herein.

Helical piles were first introduced as a deep foundation option in the early 1800's, (Perko, 2009) and the first available literature is credited to an Irish engineer, Alexander Mitchell, in 1848. Early uses for helical piles consisted of offshore anchorage in very soft marine soils most commonly required in the construction of lighthouse foundations. The early helical pile was similar to that of a screw made from cast or wrought iron. These large screw-like structures were then installed via manual torque provided by either several men or work horses. The application of early helical piles was limited by low-bearing and uplift capacities.

With the advent of powerful installation equipment and improved practical knowledge and engineering design, helical piles applications developed substantially. Their screw-like geometry gave promise for great uplift resistance in weak soils. Thus, by the mid-20th century, helical piles were utilized as anchorage for structures with appreciable uplift forces and most notably vital infrastructure experiencing overturning moments. The early development and refinement of helical pile design/fabrication focused on its uplift capacity. This emphasis formed much of the present knowledge base and standards of practice. Many engineers and construction industry professionals have recently promoted helical piles for their equally beneficial compressive resistance and minimal installation footprint. Helical piles have evolved into a niche of underpinning of failed or failing structures plagued by poor soil conditions. In these retrofitting applications, relatively small diameter and short piles are used. However, as the knowledge base and experiences of the industry continue to evolve, so do the helical piles applications. Presently, helical piles are utilized for a wide range of uplift, bearing, and/or lateral loading situations,

where they are employed to support structures ranging from bridges, short and tall buildings, machine foundations to pipeline supports.

The configuration of helical piles is designed to provide adequate loading capacity via a fast, reliable, and low disturbance installation method. A helical pile consists of one or more helical plate(s) welded to a central steel shaft. The design of a helical pile involves the choice of its shaft length and diameter as well as a specific arrangement of helices including their number, diameter, D , spacing to diameter ratio, S/D , and the embedment depth to diameter ratio (H/D) of the top helix. All these parameters can contribute considerably to the pile ultimate capacity. The design of helical piles also involves the selection of a reliable method and consideration of specified performance and loading criteria.

The central shaft shape is either hollow round pipe or solid square bar. The helical plates can range in diameter and pitch in order to provide a desired bearing force for the given soil embedment installation. The helix pitch and diameter are designed such that forward driving force (torque) is applied to the pile head during installation while minimizing the amount of potential soil disturbance.

Helical pile design has evolved from traditional foundation analysis such as Terzaghi's general bearing capacity formula (Terzaghi, 1943). Appropriate modifications were incorporated to account for the slender geometry of a pile foundation structure as well as the individual helical elements. These modifications have thus formulated two major methods for design and analysis: the individual plate bearing method and the cylindrical shear method. Each method has its analytical simplifications and approximations. Additionally, correction factors are proposed by many researchers to account for these simplifications. The application of either method and/or the associated corrections depends on both the assumed method of analysis as well as the intended use of the designed structure.

An alternative approach for the design and/or confirmation of capacity is also widely used by the helical pile industry professionals. The approach is empirical and relies on the CTC method. This approach continues to develop, incorporating different levels of sophistication providing theoretical basis and practical considerations. It is seen widely as a great advantage for helical piles in terms of providing on-site immediate confirmation of the pile capacity. It provides a

practical method of field testing the assumptions and simplifications made during the initial design process. Most often this confirmation is utilized as a indicator of design flaws, or in certain cases, indicating the potential for value engineering.

These approaches to helical pile design: individual plate bearing method; cylindrical shearing method; and confirmatory CTC method are explored in the following text.

2.1 Theoretical Axial Capacity

When determining the theoretical load bearing capacity of a helical pile within the bounds of traditional soil mechanics, there are two recognized methods: the individual plate bearing method and the cylindrical shear method. The suitability of either method is related to the size and spacing of helical bearing plates. If the helical plates are relatively far apart along the shaft of the pile, then the individual helical plates are considered to provide bearing capacity in isolation and their sum, in addition to the shaft resistance, provides the pile's total ultimate capacity. When the helical plates are relatively close, then it can be assumed that the helical plates will act as a group creating a cylindrical shearing surface of the soil between these plates. The pile capacity is then given by the sum of the shearing resistance along the upper shaft and the inter-helical soil cylinder and the bearing resistance along the bottom helix in compression, or the top helix in tension.

The distance between helical plates that creates either condition is not unequivocally established but depends upon the size, arrangement, and existing soil condition. There are several studies aimed at detailing the conditions required to assume either method; in practice, both methods are commonly used to evaluate the capacity, and the pile capacity is given by the lesser of the two values. The load carrying capacity achieved in both methods is realized through three primary load transfer mechanisms: skin friction occurring between soil and the pile shaft, bearing resistance via the surface area beneath the helical plates, and the soil-to-soil shearing surface located at the boundary of a mobilized cylindrical soil mass as demonstrated in Figure 2-1.

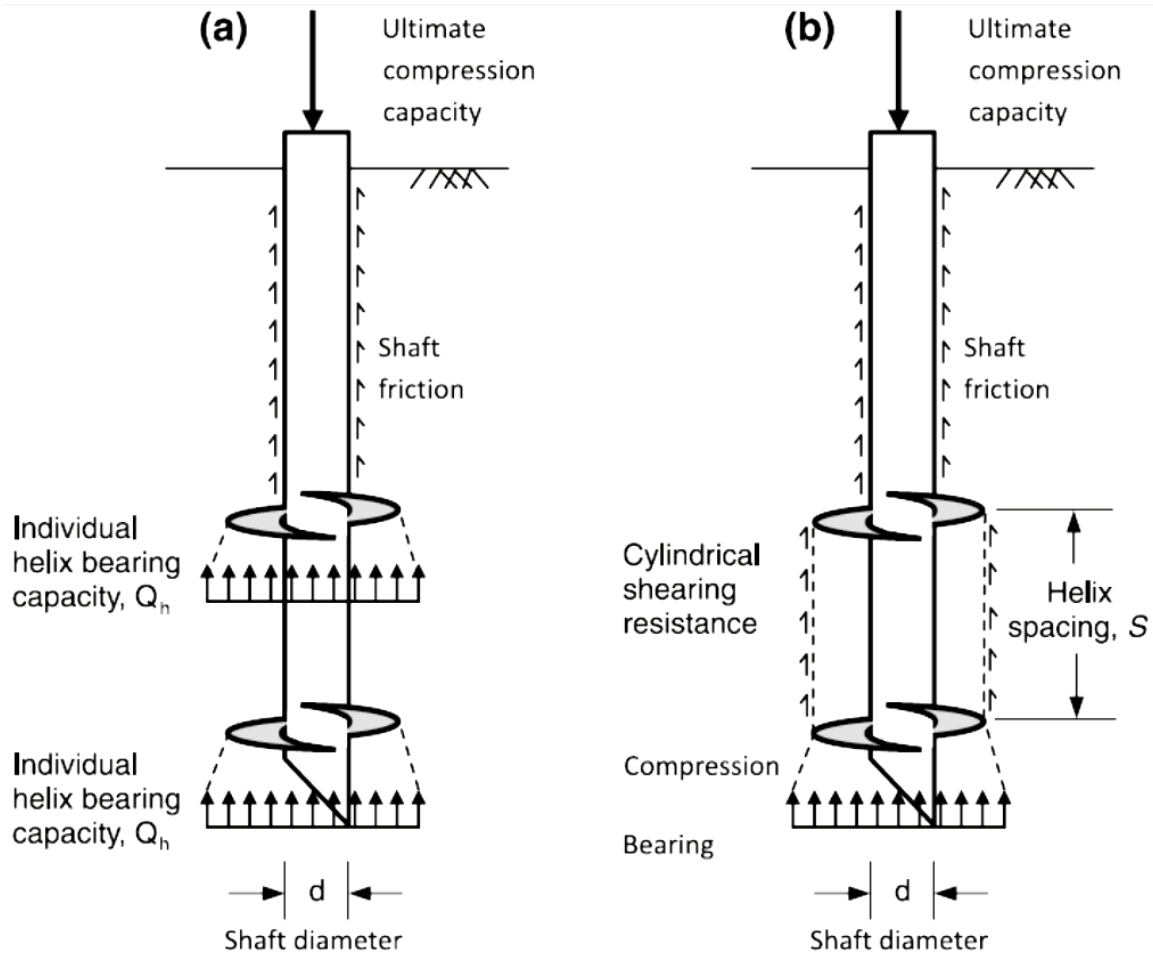


Figure 2-1: a) Individual Plate Bearing b) Cylindrical Shear (Perko, 2009)

2.1.1 Compressive Individual Plate Bearing Method

The individual plate bearing method of calculating compressive bearing capacity assumes that the pile configuration is such that each helical plate affixed to the pile shaft contributes individually to the bearing capacity of the system. The individual plate bearing capacity is calculated based upon a modification of Terzaghi's (1943) original shallow foundation bearing capacity equation, i.e. (Meyerhof, 1951):

$$q_{ult} = cN_cS_c d_c + q'N_qS_q d_q + 0.5\gamma BN_\gamma S_\gamma d_\gamma \quad (2-1)$$

Where c is soil cohesion, q' is the effective overburden pressure at bearing depth, γ is the soil unit weight, $B = D$ is the helix diameter, N_c , N_q , N_γ are bearing capacity factors dependent upon

the internal angle of friction, S_c , S_q , S_γ are shape factors dependent upon the geometry of the helical element, and d_c , d_q , d_γ are depth factors dependent upon the location of the helical element below grade. The bearing capacity factors proposed by Meyerhof are given by:

$$N_c = \frac{N_q - 1}{\tan \phi} \quad (2-1a)$$

$$N_q = e^{\pi \tan \phi} \tan^2 \left(45 + \frac{\phi}{2} \right) \quad (2-3b)$$

$$N_\gamma = (N_q - 1) \tan(1.4\phi) \quad (2-3c)$$

$$s_c = 1 + \left(\frac{N_q B}{N_c L} \right) \quad (2-3d)$$

$$s_q = 1 + \left(\frac{B}{L} \right) \tan \phi \quad (2-3e)$$

$$s_\gamma = 1 - 0.4 \left(\frac{B}{L} \right) \quad (2-3f)$$

$$d_c = 1 + 0.4(k) \quad (2-3g)$$

$$d_q = 1 + 2k \tan \phi (1 - \sin \phi)^2 \quad (2-3h)$$

$$d_\gamma = 1 \quad (2-3i)$$

$$k = \tan^{-1} \left(\frac{H}{B} \right) \text{ for } \frac{H}{B} > 1 \quad (2-3j)$$

where H is equal to the length of the pile above the helical element, L is the pile embedded length, H is depth of helical plate, and ϕ is equal to the angle of internal friction.

For the helical plate situated substantially deeper than its width, the ratio H/B becomes very large and the ratio of B/L becomes equal to one, and the depth factor approaches $\pi/2$. Thus, the bearing capacity for helical plate elements can be given by:

$$q_{ult} = cN'_c + q'(N_q - 1) + 0.5\gamma DN'_\gamma \quad (2-2)$$

$$N'_c = N_c S_c d_c \quad (2-4a)$$

$$N'_q = N_q S_q d_q \quad (2-4b)$$

$$N'_\gamma = N_\gamma S_\gamma d_\gamma \quad (2-4c)$$

where D is the helix diameter, N'_c is the combined cohesion factor, N'_q is the combined surcharge factor, and N'_γ is the combined self-weight term.

In the case of cohesive (fine grained) soils, further simplifications can be made as it is generally assumed that the angle of internal friction is equal to zero for undrained loading conditions. Throughout a series of laboratory tests, Skempton (1951) found that the bearing capacity factors approach the constant values of N'_c equal to nine, N'_q equal to one, and N'_γ equal to zero. In addition, the cohesion term is replaced by the undrained strength (S_u). Thus, the resulting ultimate bearing element capacity is;

$$q_{ult} = 9S_u \quad (2-3)$$

The bearing capacity equation modified for helical plates is then utilized within the individual plate bearing method. The total ultimate pile capacity is then given by the summation of bearing capacities of each individual plate plus the effective shaft resistance over the pile length, i.e.:

$$P_u = \sum q_{ult} A_n + \alpha S_u H(\pi d) \quad (2-4)$$

where d is the diameter of the pile shaft, q_{ult} is the ultimate bearing capacity of the n^{th} helical plate, A_n is equal to the area of the n^{th} helical plate, α is equal to the unit shaft adhesion factor, S_u is undrained shear strength of soil along the shaft and H is equal to the effective (embedded) length of the pile.

2.1.2 Compressive Cylindrical Shear Method

As the spacing to diameter (S/D) ratio of the helices decreases, it becomes more likely that the influence zones of the multiple helical plates will overlap and the encompassed soil mass will form into an adjoined cylindrical failure surface with diameter equal to that of the encompassing helical plates (Narasimha Rao & Prasad, 1993). Thus, the capacity of the pile under compression is equal to the sum of shear resistance along the cylindrical failure surface, adhesion along the shaft and the bearing capacity of the lead helix (Mooney, Clemence, & Adamczak, 1985):

$$P_u = q_{ult}A_1 + S_{uc} (n - 1) s \pi D_{avg} + \alpha S_u H(\pi d) \quad (2-5)$$

where A_1 is the area of the lead helix, S_{uc} is the shear strength of the soil within the cylindrical failure region, H is the length of shaft above the top helix, D_{avg} is equal to the average diameter of the encompassing helical plates, n is the number of helices, α is the adhesion term, and s is the distance between the helices.

2.1.3 Uplift Resistance

For the case of deep installation, the theoretical ultimate capacity of a helical pile is assumed to be equal for both compressive and tensile loading as the load transfer of the helical plates and pile shaft is equal in either case (Ghaly & Clemence, 1998; Mooney, Clemence, & Adamczak, 1985). It is, however, noted that there may be a slight increase in capacity due to the suction/adhesion induced below the pile toe under conditions of uplift. The increase in uplift capacity due to any suction/adhesion is practically neglected as it is considered to be most often negligible and transient, and neglecting offers additional conservatism to the design process. In addition, the self-weight of the pile is also neglected because it is very small compared to the pile ultimate capacity. It should also be noted that the existence of suction/adhesion at the pile toe does not have any effect upon the potential failure mode, i.e. individual plate bearing or cylindrical shear. On the other hand, there is a pronounced difference between uplift and compressive in the case of shallow installations, which should be reflected in theoretical calculation of the pile capacity as will be discussed later.

2.1.4 Shaft Adhesion

The shear resistance of cohesive soil along the pile shaft is evaluated by multiplying the soil adhesion along the shaft (i.e. αS_u) by surface area of the pile shaft. The magnitude of pile shaft resistance is affected by the pile diameter, the pile shaft shape, existing soil conditions, and soil disturbance due to installation. As presented by Ghaly and Clemence (1998), the soil adhesion can be estimated by:

$$q_s = 2/3 S_u \quad (2-6)$$

where S_u is equal to the soil shear strength. It should also be noted that the factor $2/3$ is applied for the case of bare steel in contact with soil and depends upon the material of the pile shaft, thus should be selected appropriately.

Small diameter pile shafts tend to have lower adhesion factors. This is due to the potential soil disturbance during installation. On the other hand, a large diameter pile may attain a large adhesion factor through soil displacement (i.e. increase in soil confinement) and potential soil densification. A change in the state of stress within the soil around the pile shaft can result in a vast change in potential shaft resistance calculations. In certain cases, as in small diameter piles, the shaft resistance may be neglected and/or a small adhesion factor be applied. On the other hand, for the case of large diameter pile shafts, the shaft resistance is significant and should not be neglected.

The shape of the shaft cross-section can also have an effect on the shaft resistance. During installation, a square shaft cross-section has a tendency to create a circular cavity around the shaft. This is caused by the rotation of the larger diagonal dimension causing shaft-to-soil separation, effectively minimizing the mobilized soil resistance along the pile shaft. In addition, during helical pile installation the pile shaft often has a tendency to experience some wobbling along the pile length, which further contributes to shaft soil separation.

The shaft adhesion varies according to the nature of the adjacent soil. For example, the adhesion factor will be reduced for clay soil with high sensitivity whereby its strength could potentially be reduced to its residual strength after pile installation. In general, the applied reduction factor

varies between 0.3 for stiff clay to 0.9 for soft clays (Meyerhof, 1976). The adhesion factor can be estimated based on the soil strength as presented in the Canadian Foundation Engineering Manual (2006), where stiffer soil tends to have lower adhesion factors.

$$\alpha = 0.21 + 0.26 (P_a/S_u) \leq 1 \quad (2-7)$$

where P_a is equal to the atmospheric pressure measured in kPa, and S_u is equal to the undisturbed shear strength of the soil in kPa.

Considering the potential for soil disturbance during installation, the shaft resistance should be applied to an effective shaft length H_{eff} , which is equal to the total shaft height above the top helix minus approximately 1.4 to 2.3 times the diameter of the uppermost helical bearing plate as shown in Figure 2-2 proposed by Rao (1993). In the case of Rao, the effective length of this region was limited under uplift as illustrated.

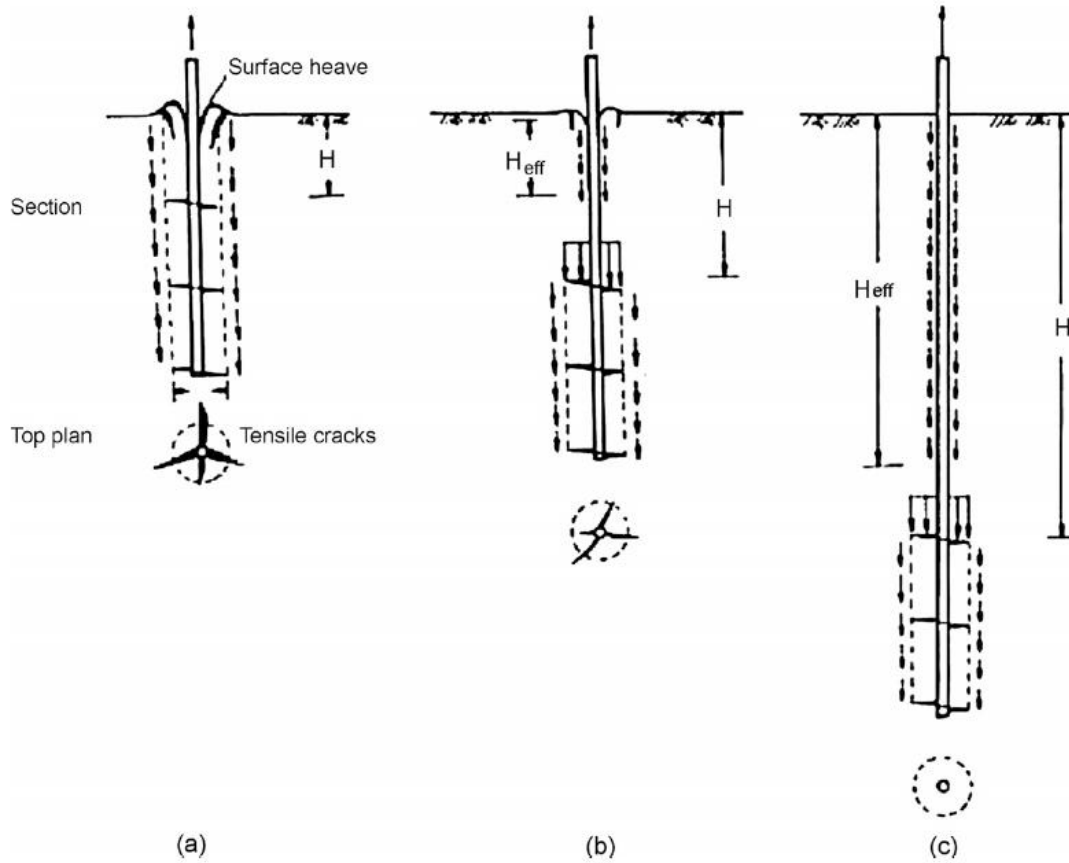


Figure 2-2: Effective Shaft Adhesion a) Shallow Installation b) Transitional Installation c) Deep Installation (Narasimha Rao & Prasad, 1993)

2.1.5 Uplift Capacity Factor N_{cu}

The uplift capacity factor (N_{cu}) is determined by empirical correlations that relate the ratio of depth of embedment to helical plate diameter (H/D). These empirical correlations were established via numerous laboratory and full scale field tests. The factor N_{cu} is similar to the traditional bearing capacity factor N_c and approaches a constant limit of 9 for $(H/D) > 4$. The N_{cu} values can be estimated via the method presented by Meyerhof (1973), i.e:

$$N_{cu} = 1.2 (H / D) \leq 9 \quad (2-8)$$

2.1.6 Geometric Considerations

There are a number of geometric properties that influence the design of a helical pile. These parameters have varying effects on the behavior and capacity of helical piles. These properties include: the diameter of pile shaft, the number, spacing, diameter, pitch and the depth of embedment of the helical plates.

2.1.6.1 Helical Fixation Angle and Pitch

It is generally agreed that in order to produce the least soil disturbance a true helical shape must be provided. This true helical shape includes the angle of fixation whereby the helical plate mates with the pile shaft and the pitch at which the helical plate contours the pile shaft. The pitch is defined as the distance between the top and the bottom of the helical blade measured along the pile shaft. Most commonly used pitch values are 75 mm (3") and 150 mm (6"). Fixation angle sought is typically 90 degree to the pile shaft.

2.1.6.2 Pile Shaft Diameter

The diameter of the pile shaft will have a significant effect on the load carrying capacity of the helical pile. The diameter of the pile shaft has two effects: it increases the surface area for which frictional or adhesion resistance can be mobilized; and increased diameter gives rise to larger displaced soil volume thereby producing localized densification within the immediate vicinity of the installed helical pile as noted in the works conducted by Narasimha Rao (1991).

2.1.6.3 Number of Helical Plates

A helical pile will include from one to four helical plates spaced equally along the lower portion of the pile shaft. It is generally assumed that the increase in the number of plates utilized will result in an increase in capacity, either through bearing or uplift. When the helical pile has a single plate, its capacity will be realized as the result of bearing upon the plate area in addition to the shaft resistance. As additional closely-spaced plates are added, a cylindrical soil mass forms between helices, which creates a larger surface area for the mobilization of either cohesive resistance in the case of fine grained soil or frictional resistance in the case of coarse grained soils. In addition, the weight of the soil contained within this mass can be added to uplift resistance. However, the optimum number of helical plates to maximize capacity is the limit at

which the spacing achieves individual plate bearing. Additional helical plates become ambiguous beyond this limit and have potential to cause elevated soil disruption. However, the addition of helical plates will generally increase the vertical capacity when exposed to either compression or tension forces. This was demonstrated through experimental evidence (Narasimha Rao & Prasad, 1993). When comparing helical pile configurations with two to four plates (all other geometry remaining constant), there was an increase in capacity upwards of 30%.

2.1.6.4 Helices Spacing and Diameter

The spacing between helices is a critical parameter in the development of the cylindrical inter-helical soil mass, i.e. it develops for closely spaced helical plates, and otherwise individual plate bearing behavior occurs. The limiting spacing for individual plate bearing mechanism was explored by Narasimha Rao (1993) for model helical piles installed in cohesive soils with varying S/D ratios. Model piles were installed in clay soils under controlled conditions of varying levels of consolidation. The axial capacity was found to be maximum as (S/D) approached 1.5 the value at which it is assumed a cylindrical shear surface was attained for both compression and tension loading. Narasimha Rao (1993) proposed a correction factor, S_f , for correcting the pile capacity of pile arrangements where (S/D) values are greater than 1.5. i.e;

$$S_f = 1.0 \text{ for } S/D \leq 1.5 \quad (2-9a)$$

$$S_f = 0.863 + 0.069(3.5 - S/D) \text{ for } 1.5 \leq S/D \leq 3.5 \quad (2-11b)$$

$$S_f = 0.700 + 0.148(4.6 - S/D) \text{ for } 3.5 \leq S/D \leq 4.6 \quad (2-11c)$$

where S/D is equal to the spacing between helices divided by radius of the helix, and S_f is the spacing correction factor. With S_f established for (S/D) ratios larger than 1.5, frictional capacities provided by the inter-helical zone can then be calculated and corrected as presented:

$$P_u = S_f(\pi DL)c_u \quad (2-10)$$

where L is equal to the distance between top and bottom helical plates, c_u is equal to the measured undrained shear strength of clay. This correction factor is to be applied to the

calculated capacity assuming that load transfer mechanism follows a cylindrical shear failure surface. The correction factor in essence accounts for a cylindrical shearing surface, which does not fully propagate thus creating a condition where there is partial individual bearing and partial cylindrical shear. It should also be noted that although inter-helical spacing exhibited considerable effects when testing small (model) helical piles in clay, it may not have the same effect for large helical piles tested in the field. The application of these correction factors should therefore be used with caution.

2.1.6.5 Embedment Depth

The ratio of embedment depth to helical plate diameter (H/D) significantly affects the capacity of helical piles. As the lead helix is installed at increasing depths and the ratio of embedment depth to helical diameter increases, three notable changes occur that influence the load carrying capacity of a given pile. First, the weight of the soil above the helix dramatically increases, effectively increasing resistance to uplift forces. Second, the confining pressure upon the shaft increases which increases both compression and uplift resistance. Third, the confining pressure and bearing capacity of the soil beneath the lead helix increase, which increases load carrying capacity of the helical plates.

2.1.6.6 Minimum Uplift Embedment Depth

The available methods for determining the theoretical capacity of helical piles primarily assume that the pile has achieved a deep embedment condition. This assumption is important if the applied force is uplift, and presumes that the mass of the soil above the top most helix is sufficient to mobilize the pullout resistance of the pile-to-soil system. Generally, it is found that the embedment depth to helical diameter ratio required to achieve a deep embedment condition is $H/D > 5$ (Zhang, 1999). If the helical pile is installed near the surface where $H/D \ll 5$, shallow failure response will ensue. Under the shallow embedment condition, the lead helix is exposed to uplift force that activates a wedge-shaped failure surface, extending from the rear most helical plate to the soil surface. This wedge creates a heaving action at the surface at which point there are two potentially limiting mechanisms. First, the heaving of the wedge-shaped failure mass creates tension cracks around the pile shaft and the shaft is effectively removed from behind the wedge-shaped soil mass. Second, the wedge-shaped mass remains affixed to the pile shaft at

which point the wedge-shaped failure no longer mobilizes the shear capacity of the soil and is only contributing to uplift resistance through its dead weight. The minimum depth to prevent the shallow embedment condition is defined as the depth where the weight of a wedge-shaped soil mass is capable of overcoming the ultimate uplift capacity of the shallowest individual helix. This depth is calculated by assuming a conical soil mass created by adjoining the top most helix with a 45 degree line upward to the soil surface and about its shaft. A more rigorous method is proposed by (Perko, 2009), in which a cylindrical integration of soil disks is calculated until the appropriate weight is attained.

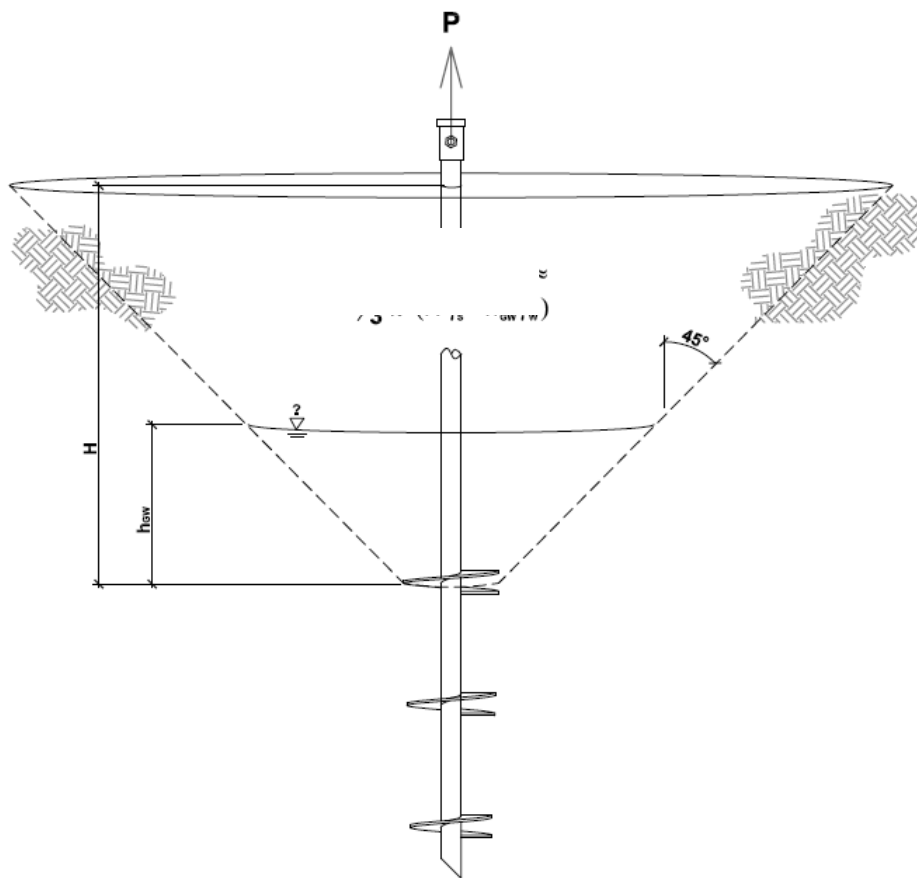


Figure 2-3: Example Influence Cone (Perko, 2009)

$$W = \frac{\pi}{4} \gamma' \int_0^H (D_T + 2z \tan \phi)^2 dz \quad (2-11)$$

where W is the weight of the wedge shaped soil mass, H is equal to the depth to the shallowest helix, z is equal to the distance above the shallowest helix, and γ' is equal to the effective soil unit weight. A alternative version of Equation 2-11 widely used incorporates the ratio H/D also known as N_T (embedment depth to shallowest helix diameter) i.e:

$$W = \frac{\pi}{4} \gamma' D_{T3} (N_T + 2N_{T2} \tan \phi + \frac{4}{3} N_{T3} (\tan \phi)^2)^2 \quad (2-12)$$

Thus, the required minimum depth is found by equating the calculated weight of the mobilized soil mass to the ultimate uplift capacity of the top most helix. This condition varies depending on the soil type located between the top helix and ground surface. The relative minimum embedment ratio varies from 4 in loose soil to 7 in dense soils (Perko, 2009).

The minimum embedment ratio was also investigated by Rao et al (1993) in an experimental program involving small scale model piles installed in cohesive soil. Based on the experimental results, three embedment classifications were established as follows: $(H/D) < 2$ is considered to be shallow; $2 < (H/D) < 4$ is transitional; and $(H/D) > 4$ is considered to be a deep condition. However, Mitsch and Clemence (1985) argued that piles with an embedment ratio of $(H/D) < 5$ follow shallow condition behavior. Regardless of the apparent disagreements on the particular limits of embedment ratio, it is generally agreed upon that the shallow condition of critical importance and that increased embedment under conditions of dense soil is required.

2.2 Empirical Axial Capacity

The ultimate capacity of a helical pile can be approximated using empirical correlations with the results of some field tests such as the standard penetration test (SPT) or the static cone penetration test (CPT). The CPT is suitable for a large range of soils provided adequate pushing force is available for sufficient depth of penetration. Given that the soil investigation program of the current study involved CPT measurements, this method will be considered.

The capacity of the pile can be estimated by (Bustamante & Gianselli, 1982):

$$P_u = \sum_{z=0}^L C q_s \Delta z + A_t q_t \quad (2-13)$$

and estimating the unit base resistance, q_t , and unit shaft resistance, q_s , from

$$q_t = k_c q_{ca} \quad (2-13a)$$

$$q_s = \frac{1}{\alpha} q_c \quad (2-13b)$$

where

q_c = cone penetration resistance (units of stress) from CPT

q_{ca} = equivalent cone penetration resistance below helix/pile toe (average over an a depth equal to 1.5 the helix diameter/pile toe)

k_c = bearing capacity factor based on soil type and pile type (Table 2-1)

α = friction coefficient (Table 2-2)

This approach is based on extensive full scale pile load test data from France (Bustamante & Ganeselli, 1982) and supported by pile load test data in North America (Robertson et al., 1988; Briaud & Tucker, 1988). The scaling effect to account for the difference in size between the cone penetrometer and the pile and the method of installation is accounted for in the selection of k_c and α using Tables 18.3 and 18.4. The method accounts for effects of soil dilation at the pile-soil interface and pile depth and compressibility. It should be used whenever CPT tests are conducted.

Table 2-1: Bearing Capacity Factors, k_c (Canadian Geotechnical Society, 2006)

Soil Type	q_c (MPa)	Factors k_c	
		Group I*	Group II*
Soft clay and mud	< 1	0.4	0.5
Moderately compact clay	1 to 5	0.35	0.45
Silt and loose sand	≤ 5	0.4	0.5
Compact to stiff clay and compact silt	> 5	0.45	0.55
Soft chalk	≤ 5	0.2	0.3
Moderately compact sand and gravel	5 to 12	0.4	0.5
Weathered to fragmented chalk	> 5	0.2	0.4
Compact to very compact sand and gravel	> 12	0.3	0.4

* Note:

- Group I: Plain bored piles, mud bored piles, micro piles (grouted under low pressure), cased bored piles, hollow auger bored piles, piers and barrettes.
- Group II: Cast-in-place screwed piles, driven precast piles, prestressed tubular piles, driven cast piles, jacked metal piles, micropiles (grouted under high pressure with diameters < 250 mm).

Table 2-2: Friction Coefficient, α (Canadian Geotechnical Society, 2006)

Soil Type	q _c (MPa)	Coefficient α				Maximum Limit of q _c (MPa)					
		Category*									
		I		II		I		II		III	
		A	B	A	B	A	B	A	B	A	B
Soft clay and mud	< 1	30	90	90	30	0.015	0.015	0.015	0.015	0.035	-
Moderately compact clay	1-5	40	80	40	80	0.035 (0.08)	0.035 (0.08)	0.035 (0.08)	0.035	0.08	≥ 0.12
Silt and loose sand	≤ 5	60	150	60	120	0.035	0.035	0.035	0.035	0.08	-
Compact to stiff clay and compact silt	> 5	60	120	60	120	0.035 (0.08)	0.035 (0.08)	0.035 (0.08)	0.035	0.08	≥ 0.20
Soft chalk	≤ 5	100	120	100	120	0.035	0.035	0.035	0.035	0.08	-
Moderately compact sand/gravel	5-12	100	200	100	200	0.08 (0.12)	0.035 (0.08)	0.08 (0.12)	0.08	0.12	≥ 0.2
Weathered fragmented chalk	> 5	60	80	60	80	0.12 (0.15)	0.08 (0.12)	0.12 (0.15)	0.12	0.15	≥ 0.2
Compact to very compact sand/gravel	> 12	150	300	150	200	0.12 (0.15)	0.08 (0.12)	0.12 (0.15)	0.12	0.15	≥ 0.2

Note: Bracketed values of maximum limit unit skin friction, q_s , apply to careful execution and minimum disturbance of soil during construction.

* Category:

- IA Plain bored piles, mud bored piles, hollow auger bored piles, micropiles (grouted under low pressure), cast-in-place screwed piles, piers and barrettes.
- IB Cased bored piles, driven piles.
- IIA Driven precast piles, prestressed tubular piles, jacked concrete piles.
- IIB Driven metal piles and jacked metal piles.
- IIIA Driven grouted piles and driven rammed piles.
- IIIB High pressure grouted piles with diameters > 250 mm and micropiles grouted under high pressure.

2.3 Helical Pile Installation Torque

Helical piles are installed by applying torque to the pile head in conjunction with an applied crowd (vertical downward pressure), which enables the helices to “grab” and advance the pile into the soil. The applied torque, in most instances, is provided via a driving head (hydraulically powered rotary motor), which is mounted on either a Boom Truck, Skid Steer or Modified Excavator and is affixed to the pile head during installation. The “crowd” is the vertical pressure applied to the pile head to advance the lead helical section into the soil. Torque motors range in torque output, for example, those produced by Eskridge: the D1000 is rated as approximately 83,000 ft-lbs (112,530 N-m), the D1400, shown in Figure 2-4, is capable of producing approximately 115,000 ft-lbs (155,900 N-m), and custom coupler models can produce torsion as high as 250,000 ft-lbs (338,900 N-m). (Ramsey Industries, 2014)

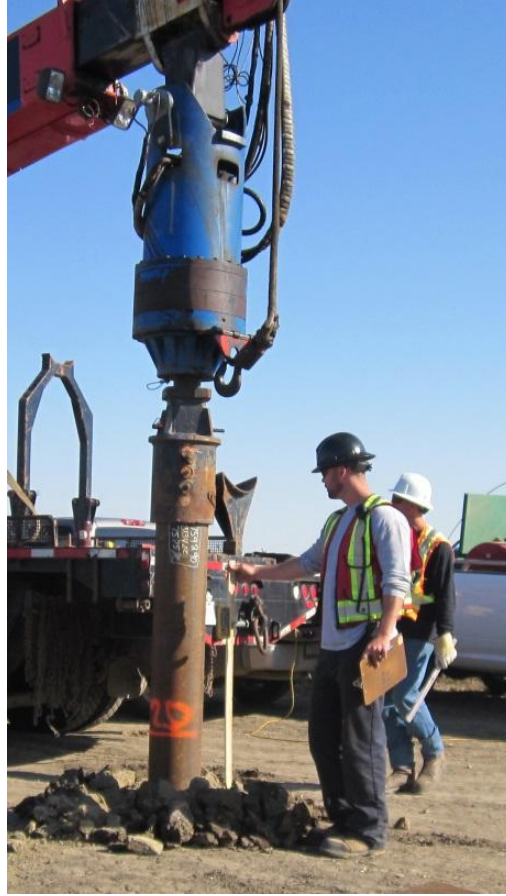


Figure 2-4: Digger 1400 & Boom Truck

The measurement of torque during installation is utilized as a means of quality control/quality assurance and is considered essential to the acceptability of the installed pile. Most commonly, equipment setups enable the measurement of installation torque by monitoring of hydraulic pressures and motor efficiency. Hydraulic pressure gauges and/or electronic pressure transducers are situated in line with the hydraulic system and measure the forward acting pressures, reverse acting pressures and/or differential pressure (forward minus reverse). These pressure measurements are then converted into a torque via calibrated conversion factor based upon the combined hydraulic efficiency of the machine and torque motor, i.e. (Perko, 2009):

$$T = P \times K_p \quad (2-14)$$

where T is equal to the installation torque most commonly in units of kN.m (or ft-lbs), P is equal to the differential hydraulic pressure commonly reported in units of pounds per square inch (psi), and K_p is equal to the calibration factor for the combined hydraulic machine and torque motor.

2.4 Static Pile Load Testing

Static pile load tests are used to evaluate the pile performance under applied loads and determine the pile ultimate capacity, as means for final pile design and for verification of capacity of installed piles. It involves the controlled application of a static load to the head of the installed pile; compression, tension, or lateral loading. The applied force, duration of application, and the resulting displacements are recorded to produce a static load displacement response curve. From this data, the pile performance can be observed, including working load capacity, ultimate load capacity and global stiffness response. (Kyfor, Schnore, Carlo, & Baily, 1992)

2.5 Ultimate Capacity & Load Settlement Interpretation

There are numerous methods for interpreting the ultimate capacity of a helical pile from static load testing results. Most fundamentally, the ultimate capacity of a helical pile is defined as the highest load (either compression or tension) that can be applied before increasing displacement occurs with no noticeable increase in applied load. This is often referred to as a plunging/pullout failure. It should be noted that this definition is concerned with strength only, fundamentally identifying a force at which point there is no remaining resistance. However, plunging failure is often not achieved. While this failure mechanism is often realized in cohesive materials, plunging is more often replaced by progressive strengthening through densification in cohesionless soils. As depicted in Figure 2-5, curves A and B, plunging failure loads can be identified, whereas curve C does not display plunging failure.

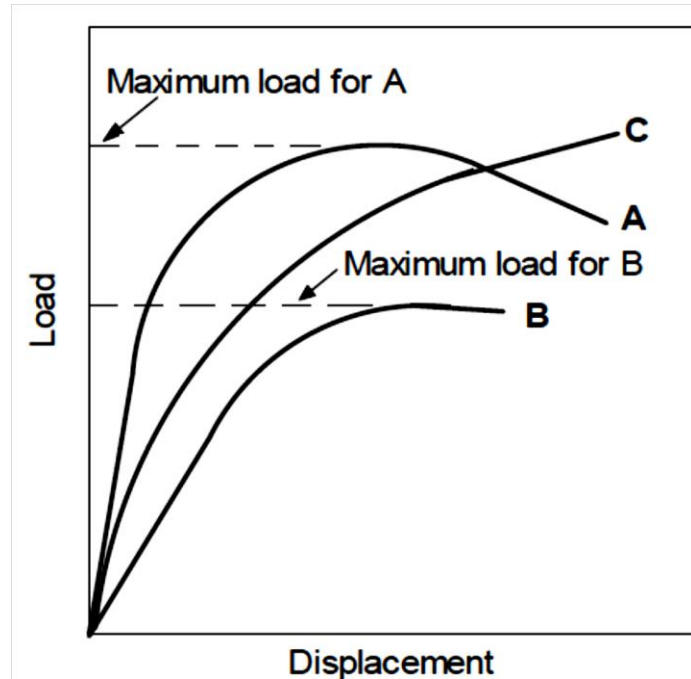


Figure 2-5: Typical Load Displacement Curves (Kulhawy, 2004)

In addition, plunging failure often correlates to a level of settlement, which far exceeds the allowable displacement for the structures. Thus, the identification of a plunging failure may not be entirely useful for appropriate limit state design. Therefore, interpreted failure load criteria are often specified in terms of settlement limits. In this case, the load displacement response curve is used to evaluate the pile performance characteristics and/or interpreted failure load. Three regions can be identified within the load displacement curve for axially loaded piles as shown in Figure 2-6: an initial linear elastic region with high stiffness (large slope), a non-linear region with gradually decreasing stiffness (decreasing slope), and a final linear region with a small residual stiffness (small slope). The initial linear region represents the load being transferred from the pile head down through a combination of shaft friction and helical bearing to the underlying soil. Within this linear region, the global stiffness of the pile-soil system is almost constant. As the load is increased within the transition zone, the shaft resistance approaches its maximum and thereby the load begins to transfer to the soil primarily through helix bearing resulting in nonlinear global stiffness. Eventually, the maximum shaft resistance is reached and the contribution of the bearing resistance increases, approaching its maximum. At this point the ultimate pile capacity is achieved; however, the contribution of the creep displacements to the

pile response may become significant beyond the transition region often producing fluctuating loads. For this reason, most interpreted failure load criteria aim to identify the ultimate load within the non-linear transition region. A suitable interpreted failure load criteria should be capable of identifying lower and upper bounds of the transition zone corresponding to points L_1 and L_2 , respectively, as suggested by Kulhawy (2004) and shown in Figure 2-6. Some of the widely interpreted failure load criteria include; the Fuller and Hoy method (Fuller & Hoy, 1970), the slope and tangent method (Butler & Hoy, 1977), the Davisson's offset method (Davisson, 1973), the O'Neil and Reese method (O'Neill & Reese, 1999), and several slightly modified versions.

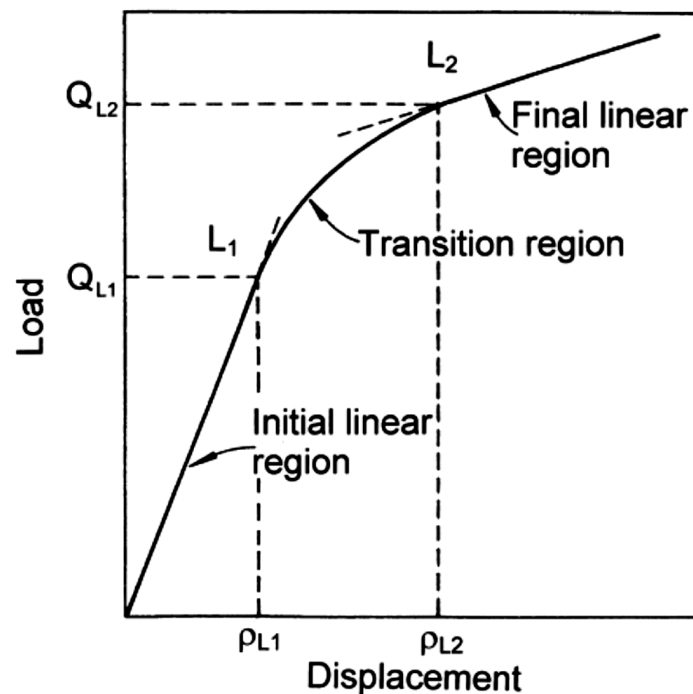


Figure 2-6: Load Displacement Curve Regions (Kulhawy, 2004)

One of the criteria used to define the interpreted ultimate (failure) load was formulated by Fuller and Hoy (1970). In this criterion, the ultimate load corresponds to the point where the slope of the load-displacement curve reaches 0.14 mm/kN (0.05 inches/ton) (Fuller & Hoy, 1970). This point is assumed to be the onset of plunging and its corresponding load is termed as the interpreted ultimate capacity. Another criterion that is widely used to define the ultimate capacity of a pile is the slope and tangent method (Butler & Hoy, 1977). In this case the ultimate capacity

is defined by the intersection of a straight line drawn through the initial linear region and the tangent to the load-displacement curve within the final linear region with slope of 0.14 mm/kN (0.05 inches/ton). This intersection point results in an interpreted failure load and settlement value within the non-linear portion of the load displacement graph (Butler & Hoy, 1977). These two methods are recommended for application along with the Quick Load test procedure (ASTM, 1981).

The offset limit load (Davisson, 1973) is widely used because of its simplicity. In this method, the pile settlement under the ultimate load is given by the summation of the expected elastic deformation of the pile material, a factor related to the pile bearing diameter, and a small offset (Kyfor, Schnore, Carlo, & Baily, 1992), i.e.

$$S_p = \frac{Q \times L}{E_p \times A} + \frac{D}{120} \quad (2-15)$$

where S_p is the total pile head settlement at ultimate loading, Q is the ultimate load, L is the pile length, E_p is Young's Modulus of the pile material, A is the pile effective cross-sectional area, D is the diameter of the pile toe given in mm (equal to the lead helix diameter for helical piles).

This criteria was initially developed to apply specifically to one-foot diameter steel- driven piles. Based on results of conducted load tests, it was determined that failure of these particular piles would occur once the pile is displaced 3.81 mm (0.15 inches). This settlement represented the the pile toe movement required to induce yielding of soil below the pile toe, plus a percentage of the pile diameter (Davisson, 1973). Modifications have since added the elastic shortening of the pile material. However, the Davisson method leads to conservative values of the ultimate loads (Kulhawy & Hirany, 2009). The Davisson criterion is suggested to be used along with the results of the Quick Load test procedure.

O'Neil and Reese (1999) define the ultimate failure limit as the load that produces a settlement equal to 5 % of the diameter of the pile toe, i.e.

$$S_p = 0.05 \times D \quad (2-16)$$

This criterion may however result in excessive settlement for large diameter piles, which would be beyond the non-linear transition region. This method may require recalibration when applied to different pile sizes and configurations.

Livneh and El Naggar (2008) propose and interpreted failure criterion specifically for small diameter helical piles based on the results of an axial load testing program conducted on slender helical piles with a solid square shaft of 44.5 mm and a lead helix diameter ranging from 200 to 300 mm. To ensure the ultimate load falls within the non-linear transition region, the settlement under the ultimate load is given by:

$$S_p = \frac{Q \times L}{E_p \times A} + 0.08 \times D \quad (2-20)$$

For large diameter helical piles, Elkasabgy and El Naggar (2014) revised the Livneh and El Naggar criterion to ensure the ultimate load falls within the nonlinear region i.e.

$$S_p = \frac{Q \times L}{E_p \times A} + 0.035 \times D \quad (2-21)$$

There are a few graphical methods for the interpreted failure load that do not impose a certain settlement limit, such as the Brinch-Hansen Failure Criteria and the Chin Failure Criteria (Perko, 2009). However, the Brinch-Hansen method does not work if a recognizable change in slope is not observed, and the Chin method usually overestimates the ultimate capacity of the pile.

2.6 Capacity to Torque Correlations

The empirical relationship between measured torque during installation and pile capacity has gained a wide acceptance in the helical pile industry in the past few decades as a quality control and assurance method for estimating the general pile capacity. Beginning as a general trade secret formulated through experience, some theoretical models were developed to estimate the torsional resistance of soils to helical pile installation, hence more rational CTC's were proposed. As large capacity helical piles are widely used in today's industrial construction projects, the CTC method has gained more appeal and is associated with more risk.

The work required to install a pile is directly related to the strength of the soil, thus the capacity of the installed pile. Livneh and El Naggar (2008) state that this work is required to overcome the shear strength of the soil and thus is directly related to the pile capacity. Many correlations have been developed with varying accuracy and varying scope for application. One of the earliest attempts to produce an overarching torque factor was carried out by Hoyt and Clemence (1989). It provides results consistent with the limit state theoretical methodologies such as cylindrical shear model and the individual plate bearing model.

2.6.1 Hoyt and Clemence, 1989

The initial work provided by Hoyt and Clemence (1989) produces a simple and elegant relationship that relates the ultimate capacity of the pile P_u to the final installation torque T . The final installation torque is defined as the torque measured over the last one meter of installation depth.

$$P_u = K_t \times T \quad (2-17)$$

The initial formulation of the correlation factor K_t focused on tensile loading (uplift) only. This factor was considered an all-inclusive parameter independent of the number/size/spacing of helical plates and the soil conditions within which the piles were installed. Hoyt and Clemence (1989) analyze 91 tensile load tests at 24 different sites, involving helical pile shaft sizes of 38 mm (1.5 inches) to 89 mm (3.5 inches). Each helical pile had a minimum of two helical plates up to a maximum of 14 whereas the diameter of these plates varied from 152 mm (6 inches) to 508 mm (20 inches).

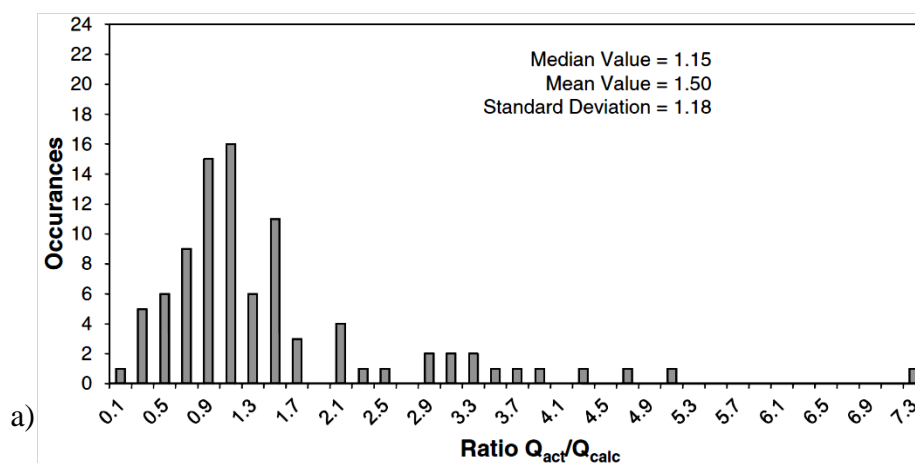
For each pile configuration, the observed ultimate capacity (obtained via load settlement interpretation), the recorded final torque measurement, and theoretically calculated expected ultimate capacity were considered in the analysis. The expected ultimate capacity was evaluated using three methods: the cylindrical shear method, the individual plate bearing method, and the CTC method. The third method, was based upon a K_t factor of 33 m^{-1} (10 ft^{-1}) for all piles with shaft diameters less than 89 mm (3.5 inches), 23 m^{-1} (7 ft^{-1}) for helical piles with 89 mm (3.5 inch) shaft diameter, and 9.8 m^{-1} (3 ft^{-1}) for those with 219 mm (8.63 inch) shaft diameter. All

torque values corresponded to the torque measurements averaged over the final three times the diameter of the largest helix (Hoyt & Clemence, 1989).

The load test was conducted with a strain controlled methodology whereby a final load step was imposed applying approximately 102 mm/min and recoding the resulting load reaction as the failure load. The upper limit of axial capacity for a helical pile was found to be near 775 kN (175,000 lb) with a typical capacity being near 444 kN (100,000 lb).

With this information, the estimated capacity of each method was compared to that of the actual observed capacity. As indicated by the representative histograms in Figure 2-7, the CTC predictions provided the least variance. All three methods showed equal potential for over predicting ultimate capacity.

Hoyt and Clemence emphasize that the major advantage for the CTC confirmation method is that there is no dependence on engineering judgment or variable site/soil properties classification thereby removing a fairly large source of variance and potential error. However, a limitation of the CTC method is that it can only be used after installation and not prior to as a “desk” design. It should be noted that regardless of the methodology, large factors of safety appear to be warranted in all cases considering the potential for over prediction of the pile capacity.



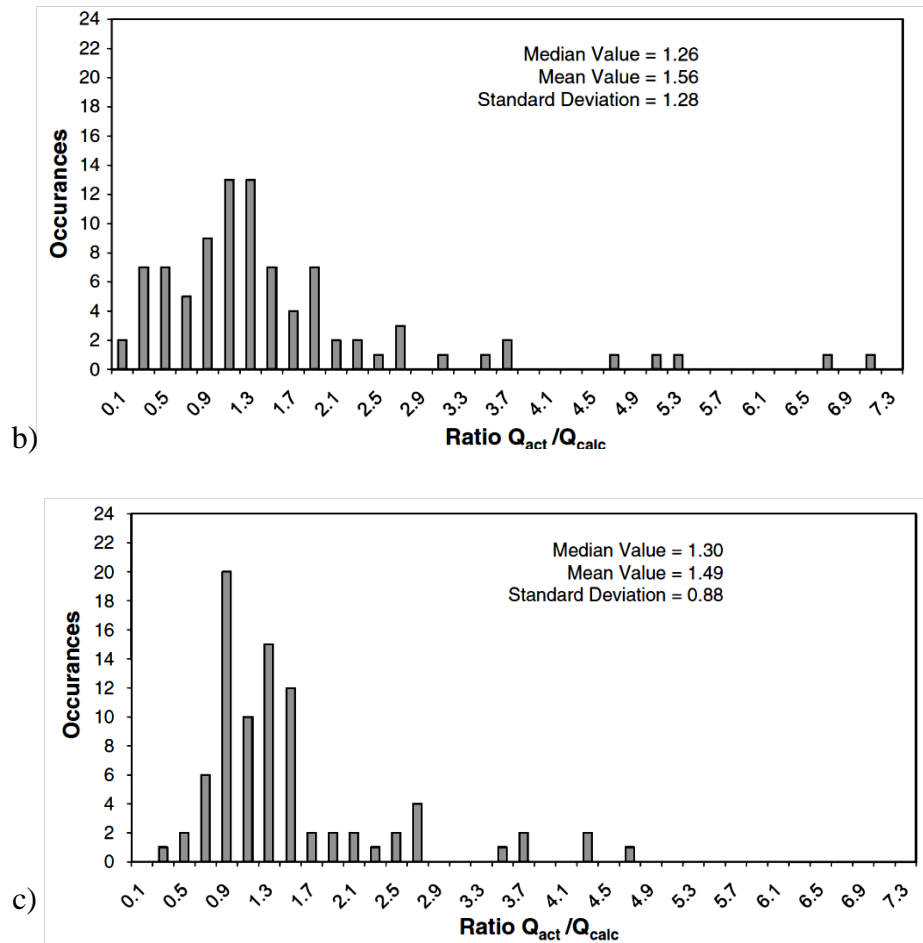


Figure 2-7: Histograms comparing the actual to calculated capacity ratios
Cylindrical shear b) Individual plate bearing c) Torque-to-Capacity

2.6.2 Ghaly and Hanna, 1991

Ghaly and Hanna (1991) compare the experimental and theoretical values of helical pile capacity, and attempt to delineate the main factors affecting the magnitude of installation torque. The study addresses model helical piles of five different configurations installed in a prepared sandy soil in a laboratory testing program.

The number of helices ranged from one to three, while maintaining a constant 10 mm shaft diameter pile. The piles were approximately 1.0 m long and were fully embedded and the installation torque was measured along the entire depth while simultaneously measuring the

internal lateral stresses within the soil itself. They concluded that several factors affect the installation torque. These factors include: general pie configuration (i.e. single helix, multi helix, tapered); shaft diameter; diameter of the upper blade; helix pitch; helix angle; thickness of the helical plates; the shape of leading helical edge (i.e. blunt, tapered, knifed); shape of the pile toe (i.e. flat, tapered, conical); helical manufacturing process (i.e. bolted, welded, cast); and helical pile material surface roughness. These parameters were found to have varying degrees of influence upon the generation of installation torque, and a basic mathematical model was developed as shown in Figure 2-8.

The laboratory test results were used to formulate a non-dimensional CTC. The determined torque factor (F_t) was correlated to the uplift capacity factor (N_{qu}). The torque factors were formulated to account for all parameters that affect the installation torque magnitude, i.e.

$$F_t = \frac{T}{\gamma AHp} \quad N_{qu} = \frac{Q_u}{\gamma AH} \quad (2-18)$$

where T is the installation torque, γ is the unit weight of sand, A is the surface area of the helical plate, H is the installation depth, and p is the anchor pitch.

All experimental data was graphically presented on a semi logarithmic plot revealing a relation between the installation torque and the pile capacity as shown in Figure 2-9a. The resulting relation was determined as:

$$\left[\frac{Q_u}{\gamma A H} \right] = 2 \left[\frac{T}{\gamma A H p} \right]^{1.1} \quad (2-19)$$

The findings of Ghaly and Hanna are similar to those presented by Mitsch and Clemence (1985) and Radhakrishna (1976) as shown in Figure 2-9b.

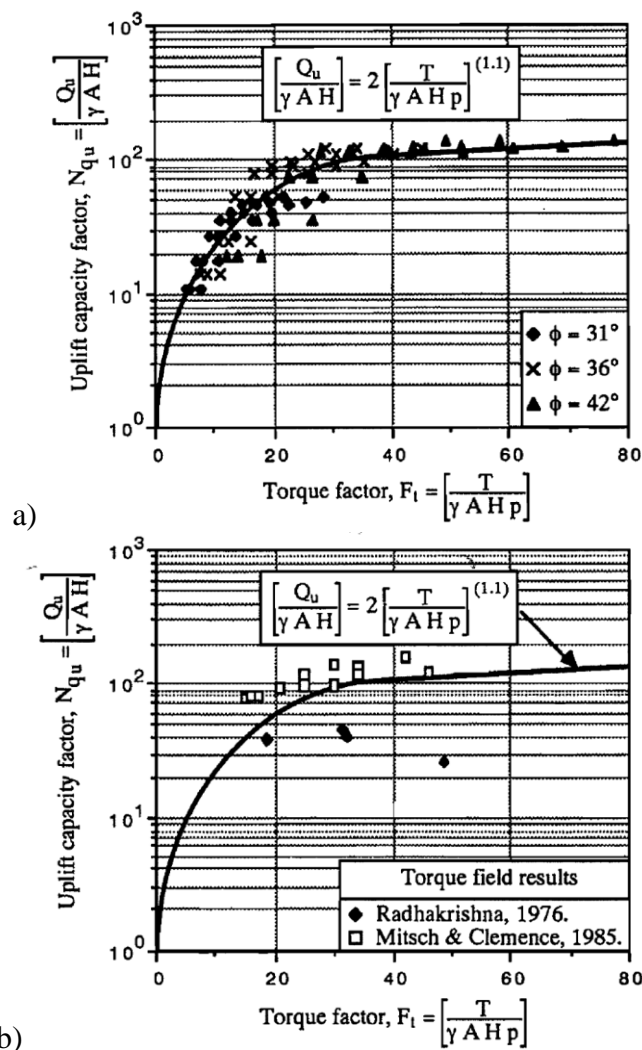


Figure 2-9: Non-dimensional Torque Factor Formulation a) Theoretical formulation b) Experimental data fit (Ghaly & Hanna, 1991)

2.6.3 Zhang, 1999

Zhang (1999) reported an investigation on the load carrying capacity of helical piles installed in both sand and clay soils to establish the shallow and deep conditions. The tested piles consisted of a shaft 219 mm in diameter and helix diameter of 356 mm with a minimum spacing of three times the helix diameter. The test results provided K_t values of $6.8 - 10.7 \text{ m}^{-1}$ for piles installed in clay and K_t values of $4.4 - 10.5 \text{ m}^{-1}$ for piles installed in sand. These results were compared with the CTC relationship provided by Hoyt and Clemence (1989). The results showed that for all piles tested in sand and having achieved a deep condition, the relation was well supported, while those tested in uplift with a shallow condition over predicted the capacity. This finding was expected given the precedence of only utilizing deep condition piles in the original relationship provided by Hoyt and Clemence (1989). Zhang (1999) also details an empirical correlation for estimating the required torque based upon helical plate diameter and soil material. The method relied on the relation between cone tip resistance attained via a CPT test and the installation torque required.

2.6.4 Tappenden, 2007

Tappenden (2007) analyzed 29 axial compressive and tensile load tests on helical piles, including the recorded installation torque values for each pile. The experimental data was used to develop a CTC, which was compared with those by Ghaly and Hanna (1991) and Hoyt and Clemence (1989).

The correlations were based on two separate linear regression plots as shown in Figure 2.10. For piles with shaft diameters of 114 mm, K_t was found to be 16.9 m^{-1} and for the pile with shaft diameters of 140 mm to 406 mm, K_t was 9.19 m^{-1} . These results were compared to that of Ghaly and Hanna's non-dimensional CTC formulation, which consistently overestimated the pile ultimate capacity between in order of 132 to 858% (Figure 2-11) and thus deemed to be inappropriate for full scale helical piles capacity predictions (Tappenden, 2007).

The full scale CTC's provided within Tappenden's work are an example of industry leading research that can be successfully incorporated in design and quality control. The predictions provided by the applied correlations are reasonably accurate and avoid drastic over/under prediction. However it should also be noted that CTC's should not be applied to test piles that are

installed in an over-consolidated desiccated sand material under the shallow conditions as indicated in the data provided by Tappenden.

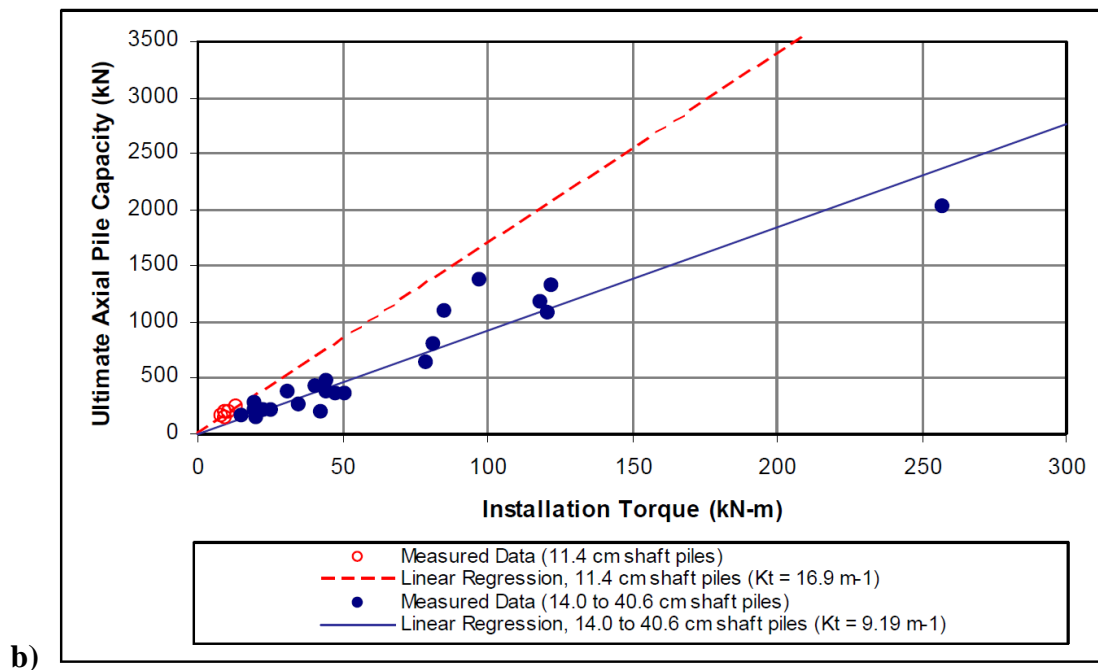
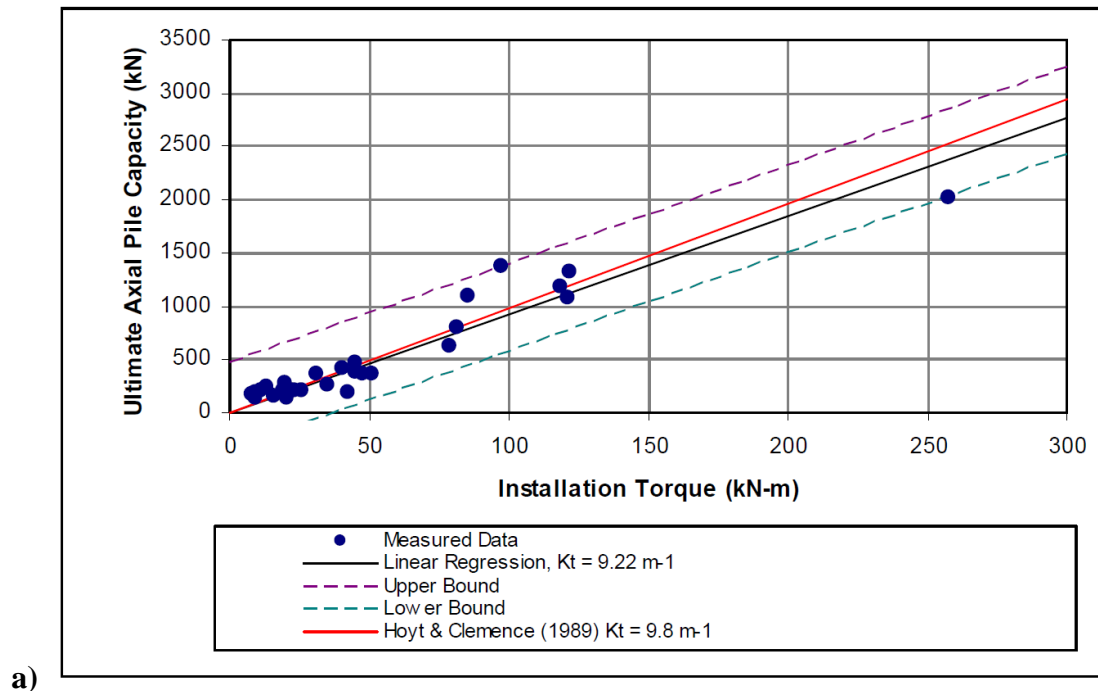


Figure 2-10: a): Axial measured pile capacity and required installation torque; b): Capacity to Torque Correlations based on shaft diameter (Tappenden, 2007)

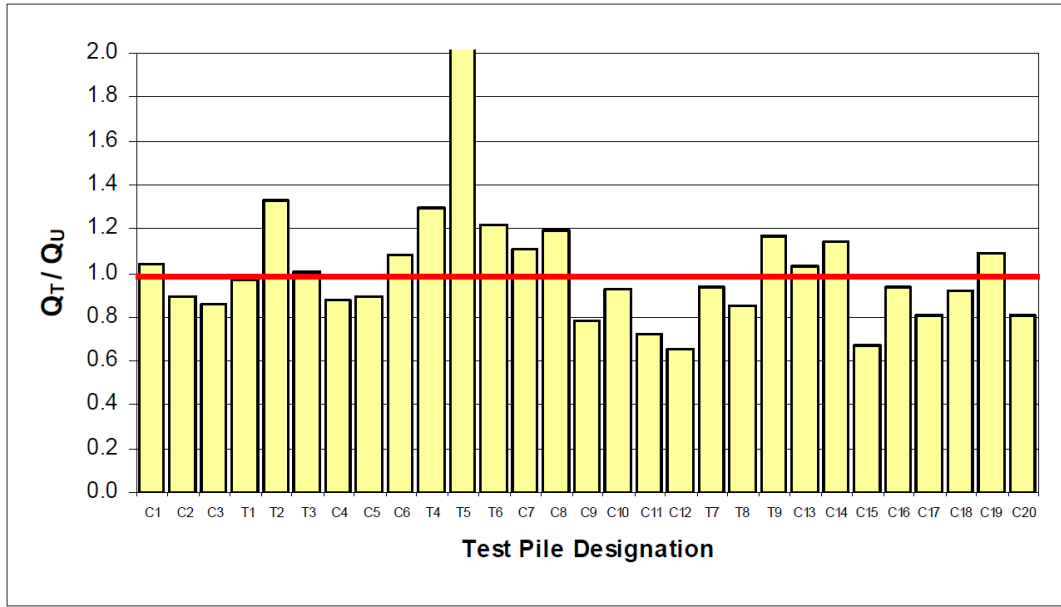


Figure 2-11: Ratios of Predicted Ultimate Capacity, Q_t , to Measured Ultimate Capacity, Q_u , Using Torque Correlations Based on Diameter of Screw pile Shaft

2.6.5 Perko, 2009

Perko (2001) proposed a CTC based on an energy model similar to that used for driven piles. However, the main limitation to the energy model is that it requires numerous parameters, some of which are not easily measurable during pile installation, such as the crowd force (i.e. downward force exerted during pile installation).

Perko (2009) proposed another empirical relation between K_t and the effective shaft diameter (d_{eff}) based on an exponential regression analysis of over 300 load tests in both compression and tension. Among these tests, 239 tests were accompanied by a final installation torque measurement enabling an estimation of the K_t factor, which was established considering the effective diameter of the helical pile (d_{eff}). The data set was graphically analyzed and plotted to produce a line of best fit as shown in Figure 2-12. The empirical equation is expressed as:

$$K_t = \frac{\lambda_k}{d_{eff}^{0.92}} \quad (2-20)$$

where; λ_k is curve fitting factor equal to $1433 \text{ mm}^{0.92}/\text{m}$ ($22 \text{ in}^{0.92}/\text{ft}$).

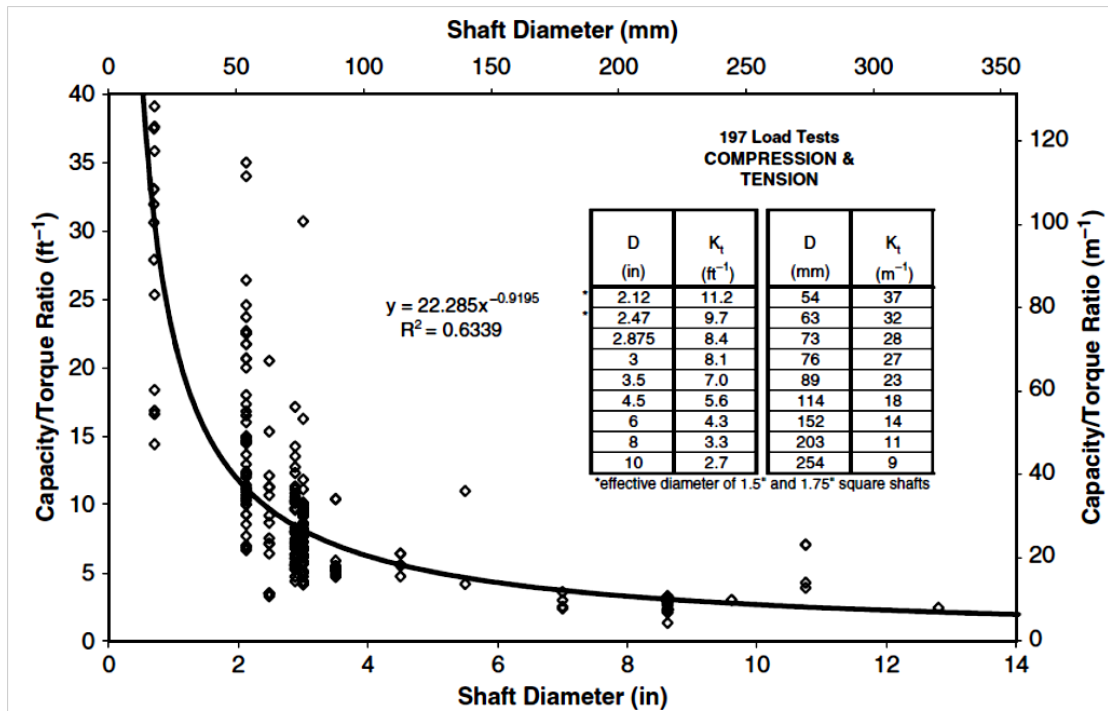


Figure 2-12: Empirical Torque Correlation Line of Best Fit (Perko, 2009)

Torque factors proposed by Perko (i.e. Eq. 2-23) were in good agreement with previous research presented by Hoyt and Clemence (1989), with smaller standard deviation and higher coefficient of determination (R^2) indicating better representation of the tests data. It is interesting to note that the better fit was achieved despite the inclusion of both compression and tension load cases. This may be attributed to considering the effective diameter of the pile shaft in the equation rather than the grouping conducted by Hoyt and Clemence. Another important difference between Perko (2009) and Hoyt and Clemence (1989) analyses is the ultimate capacity criteria that was adopted. Hoyt and Clemence defined the plunging failure load as the load corresponding to a minimum strain rate of 102 mm/min. Perko, on the other hand, utilized the Davisson offset criteria.

Considering compression and tension test data separately, the coefficient of determination increased for tension loading and decreased for compression loading. This was attributed to the fact that compressive capacity is affected by soil strata beneath the embedment depth, which is

not accounted for by the measured installation torque. However, the torque factor for compression was approximately 10% higher than for tension.

Chapter 3

3 Site Investigation & Test Pile Configuration

3.1 Site Location

The test site is located in the small community of Lamont, Alberta, approximately 40 km north east of Edmonton (Figure 3-1), on the far south east corner of the Helical Pier Systems Inc. (HPS) pile manufacturing facility. The soil in the region is generally glacial till, which is predominantly comprised of an unsorted mixture of clay, silt and sand with interlayering of gravels. The thickness of this glacial till is commonly less than 25 m but can be up to 100 m at certain locations (Shetsen, 1990). The test site lies in the area of a stagnation moraine where deposits are described as being of uneven thickness. The local water sorted materials are up to 30m thick with the potential for surface layers to be affected by lake and/or stream erosion (Shetsen, 1990).

A site investigation involving cone penetration test (CPT) soundings was conducted to characterize the interlayering soil layers and establish their shear strength profile. The CPT soundings were advanced in the vicinity of the test piles as will be discussed later. Additional information was gained from two borehole logs corresponding to a location approximately one kilometer from the test site near the intersection of Highway 15 and 29, west of the town of Lamont. These boreholes indicate a very thin top layer of organic soil approximately 0.33 m thick, a second layer of hard clay till continuing to approximately 3.4 m depth, and a third layer of very hard highly weathered, medium plasticity clay shale to a depth of approximately 9 m with no trace of a water table (Tappenden, 2007).

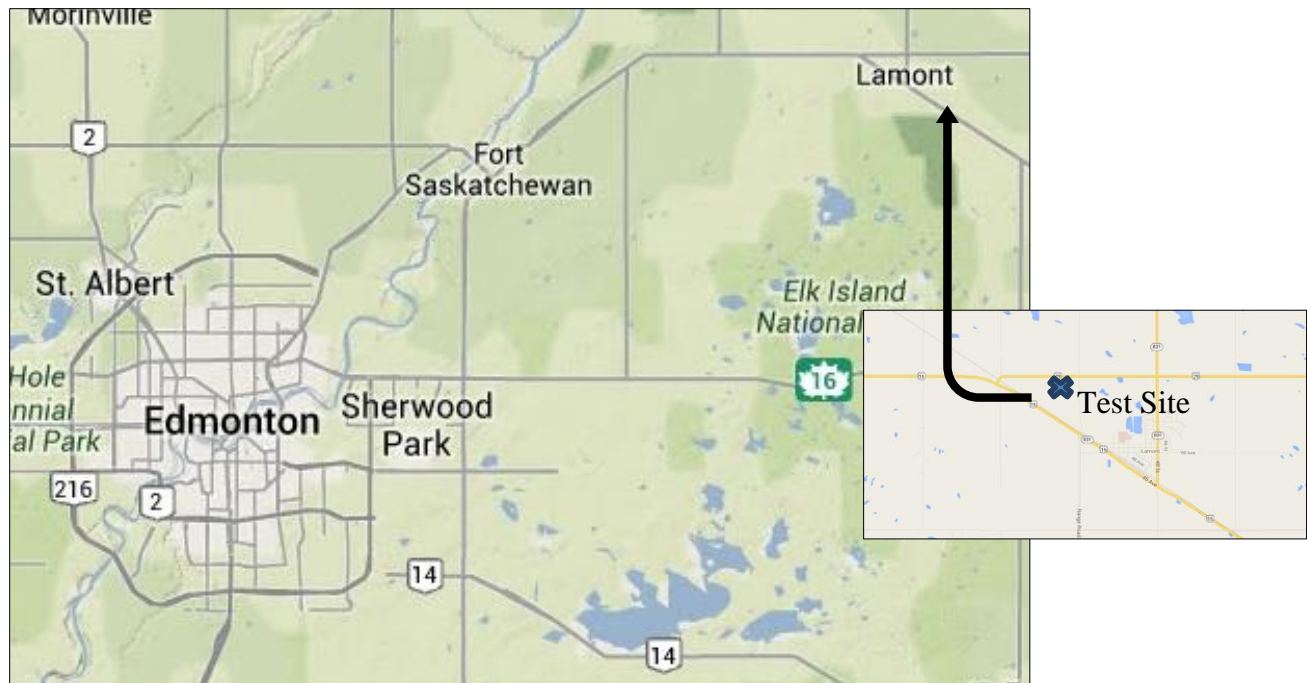


Figure 3-1: Test Site Location

3.2 CPT Testing

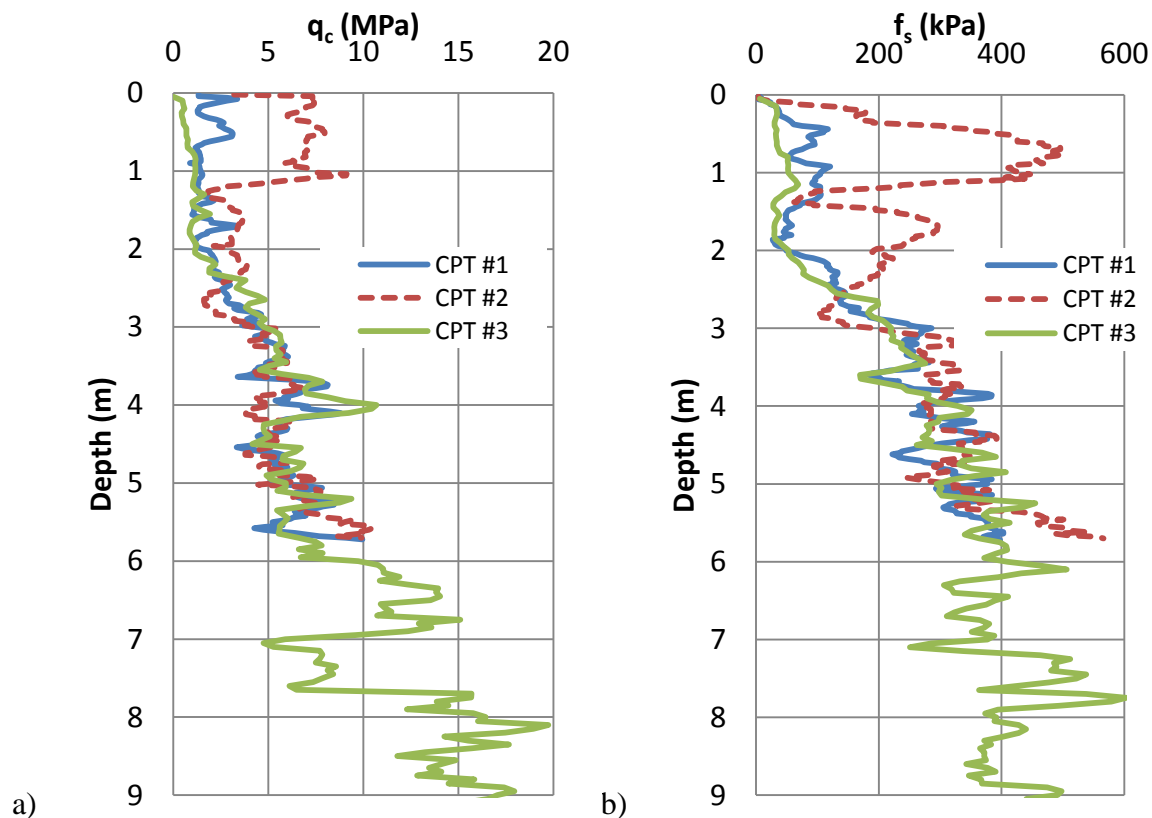
Three CPT soundings were conducted on the site measuring the cone tip resistance (q_c), sleeve friction (f_s), and pore water pressure (u) at regular intervals of 0.02 m. The testing was conducted to a depth of approximately 9 m for one CPT provided by Cone Tech, however, due to hard/stiff soil conditions, the other two CPT tests provided by Sun-Alta Drilling were terminated at approximately 5.7 m because the push rod apparatus was nearing its capacity. All data analysis and interpretation was conducted by the author.

3.2.1 CPT Results

The results from CPT soundings including the cone tip resistance, q_c and sleeve friction, f_s , are presented in Figure 3-2. All three CPT soundings provide consistent results for depths below 2 m from ground surface. In addition, CPT soundings 1 and 3 provide consistent results for the top 2 m, while CPT 2 is somewhat different. It appears that it went through a local pocket of very stiff material or a boulder.

The cone tip resistance values, q_c , ranged from 2 to 10 MPa, whereas sleeve friction values ranged from 30 to 600 kPa. The friction ratio (f_s/q_c) was calculated and is presented in Figure 3-2c. The pore pressure measurements during on shore CPT testing can be inaccurate. The pore pressure sensors mounted on a CPT unit require a stable saturation during measurement, and probing through unsaturated soils can create a suction, which has the potential to remove the saturation within the porous element resulting in unreliable pressure measurements (Robertson, 2009). It seems saturation loss occurred during CPT soundings 1 and 2, thus the results of pore pressure are not presented. CPT sounding 3 on the other hand achieved and maintained saturation and the obtained pore pressure profile is shown in Figure 3-2d.

Considering the test site consists of predominantly stiff over-consolidated clays, the loss of saturation is not unexpected. Additionally, considering the relatively large measured cone tip resistance (ranging from 2 – 10 MPa), the inaccuracy of pore pressure measurements would have little effect when determining the corrected cone resistance values. It is often suggested that uncorrected values for cone tip resistance can be used in scenarios of stiff over-consolidated materials (Robertson , 1990).



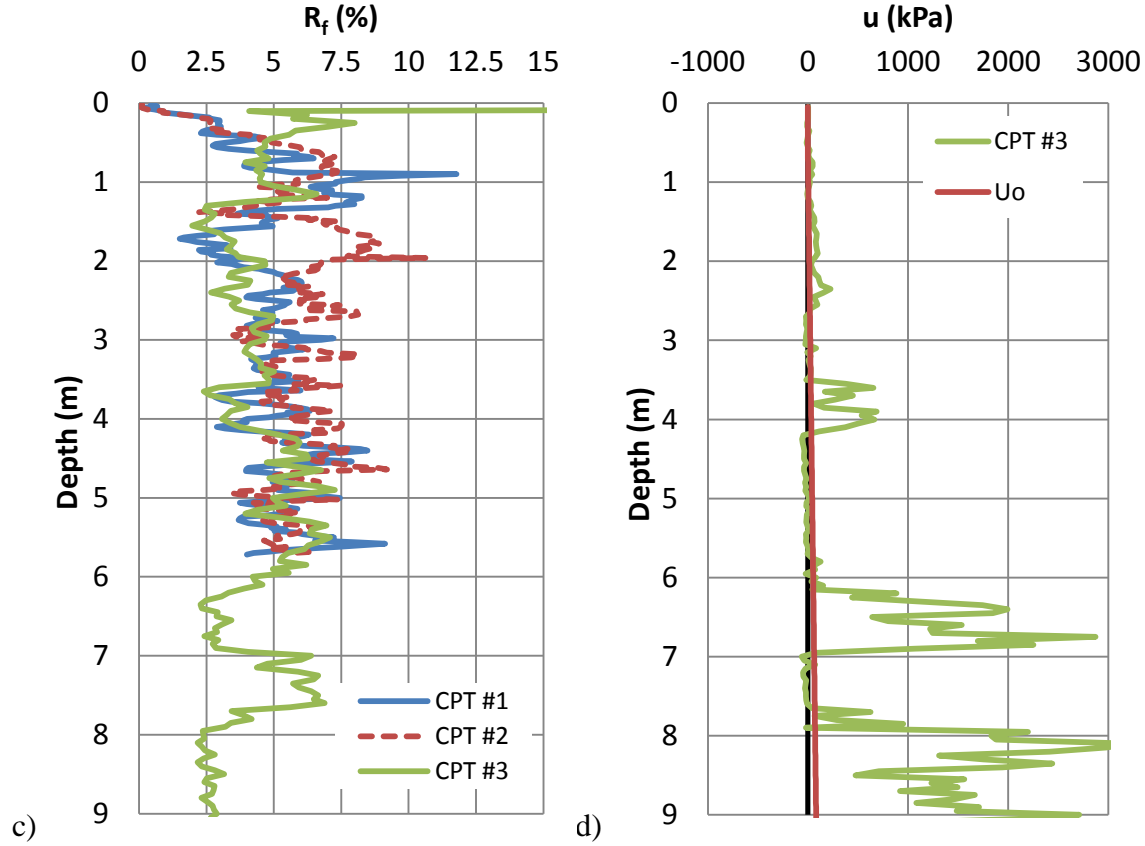


Figure 3-2: CPT – Raw Data: a) Cone tip resistance (q_c); b) Sleeve friction (f_s); c) friction ratio; d) Pore pressure (u_2 & u_o)

3.2.2 Soil Properties

The cone tip resistance (q_c) and the friction ratio (f_s/q_c) values can be used to determine the soil type using the soil behavior type (SBT) chart proposed by Robertson (1990). However, the correlated soil type can be affected by the presence of large in-situ stresses, meaning that the soil type can change depending on the depth of soil. Therefore, it is recommended that the normalized cone tip resistance and friction ratio should be used for classification. The normalized cone tip resistance and friction ratio are given by

$$R_f = \frac{f_s}{q_c} \times 100 \quad (3-1)$$

$$F_r = \frac{f_s}{q_t - \sigma_{vo}} \times 100 \quad (3-2)$$

$$Q_{tn} = \frac{q_t - \sigma_{vo}}{\sigma'_v} \quad (3-3)$$

The corresponding profiles of normalized cone tip resistance and friction ratio are presented in Figure 3-3.

The normalized friction ratio values ranged from 3 to 9% with the exception of the first one meter. The relatively high friction ratio, combined with the high cone tip resistance, indicates that the soil is highly over-consolidated and consists primarily of clay and silt and some sand. The normalized tip resistance and normalized friction ratio are plotted on the SBT chart as shown in Figures 3-4 and 3-5, which indicates that the top 3 m of soil fall within zones 4, 5, 6 (clay, sand, silt mixtures) and the underlying soils fall within zones 11, 12 (very stiff over consolidated fine grained material).

Lunne et al, (1997) provided estimates for the soil unit weight based on the SBT zones as shown in Table 3-1. For the top 3 m of soil (zones 4, 5, 6), the unit weight is 18 kN/m³, and for the underlying soils (zones 11, 12) the unit weight of 21 kN/m³.

Table 3-1: Unit Weight Estimate based on SBT

Zone	Approximate Weight (kN/m ³)	Unit
1	17.5	
2	12.5	
3	17.5	
4	18	
5	18	
6	18	
7	18.5	
8	19	
9	19.5	
10	20	
11	20.5	
12	19	

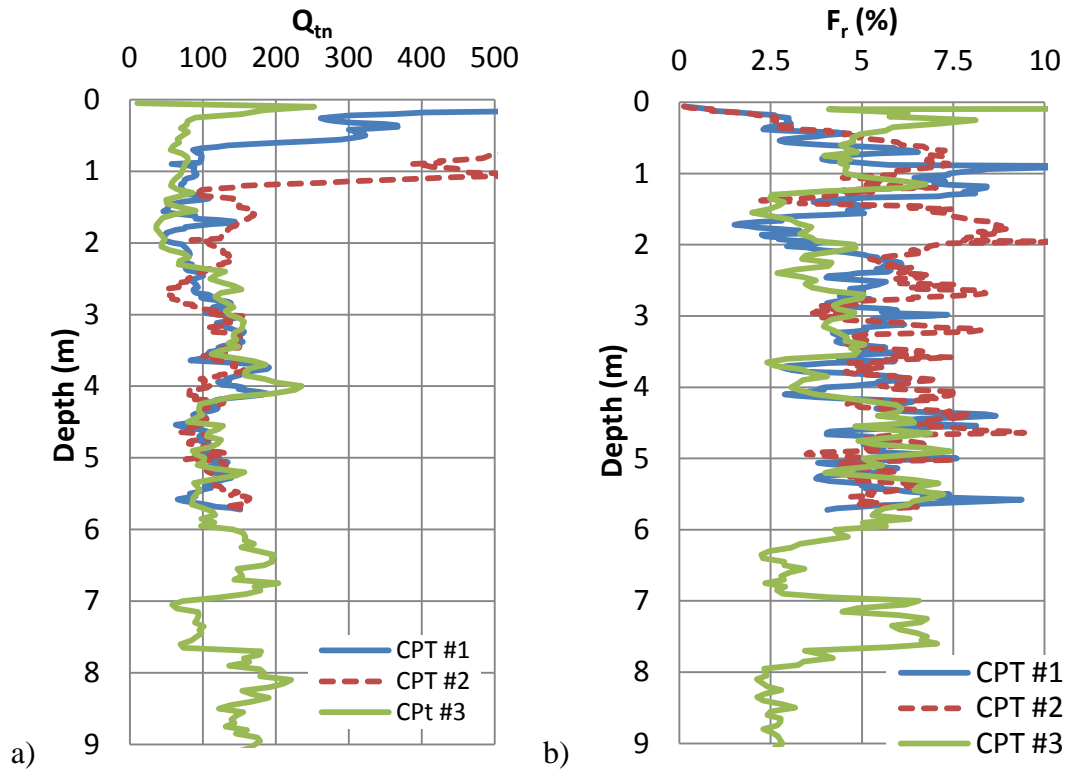


Figure 3-3: a) Normalized tip resistance b) Normalized friction ratio

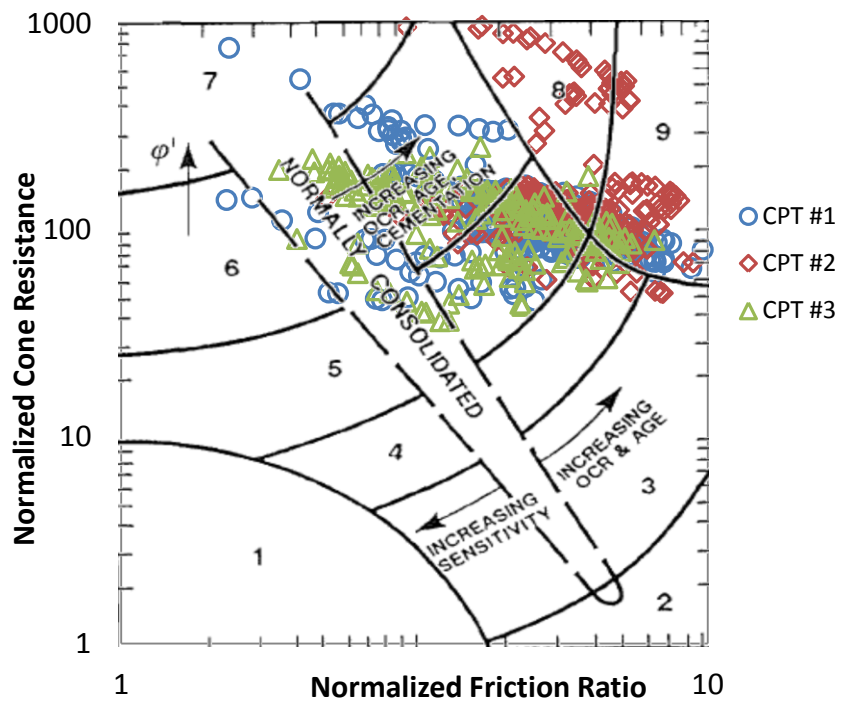


Figure 3-4: SBT chart

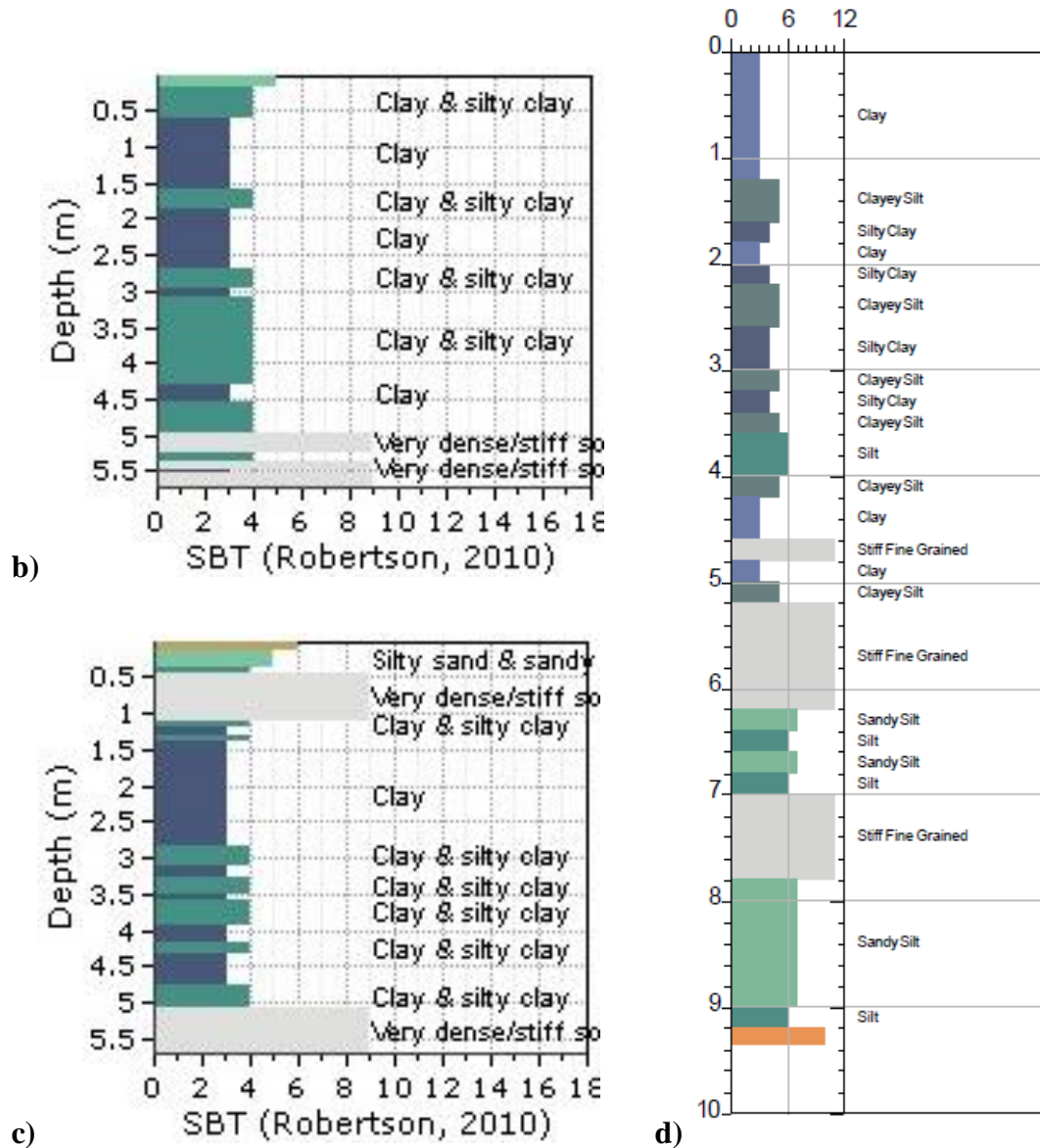


Figure 3-5: SBT; Soil type with for depth a) CPT #1;b) CPT #2; and c)C PT #3

The undrained shear strength (S_u) of the soil can be estimated using the cone tip resistance following different approaches (Lunne, Robertson, & Powell, 1997). It can be estimated using the total cone resistance, i.e.

$$S_u = \frac{q_c - \sigma_{vo}}{N_k} \quad (3-4)$$

where q_c is the total cone resistance, σ_{vo} is the total in-situ vertical stress, and N_k represents the cone factor.

It can also be estimated using the effective cone tip resistance,

$$S_u = \frac{q_e}{N_k} = \frac{q_t - u_2}{N_k} \quad (3-5)$$

or using the excess pore pressure measurements,

$$S_u = \frac{\Delta u}{N_{\Delta u}} \quad (3-6)$$

Considering the potential inaccuracy of pore pressure measurements taken during the CPT soundings, the total cone resistance method is used as presented in Equation

$$S_u = \frac{q_c - \sigma_{vo}}{N_k} \quad (3-4)$$

Meigh (1987) reported that the typical cone factor for glacial clays ranges from 14 to 22 with an average of 18. These values were empirically correlated to the shear strength values obtained via large scale plate bearing tests. The effects of overconsolidation (OCR) and plasticity index (I_p) were also considered in the analysis. He reported proportional relationships for both parameters with the cone factor. Lunne et al. (1997) analyzed large amounts of testing data and suggested that, generally, cone factors range from 15 to 20. Considering the elevated friction ratios and the associated near-site borehole logs, it is assumed that an appropriate estimation of N_k is 18.

OCR can also be used to provide an estimate of the undrained shear strength. OCR can be estimated by:

$$OCR = 0.33 \left(\frac{q_t - \sigma_{vo}}{\sigma'_v} \right) \quad (3-7)$$

The variation of OCR with depth is shown in Figure 3-6. As can be noted from Figure 3-6, OCR for the top 1.0 m exceeds 40 and ranges between 10 and 20 for soil below 1.0 m, suggesting a highly over-consolidated soil profile; i.e., overconsolidated clay till underlain by heavily overconsolidated weathered clay shale.

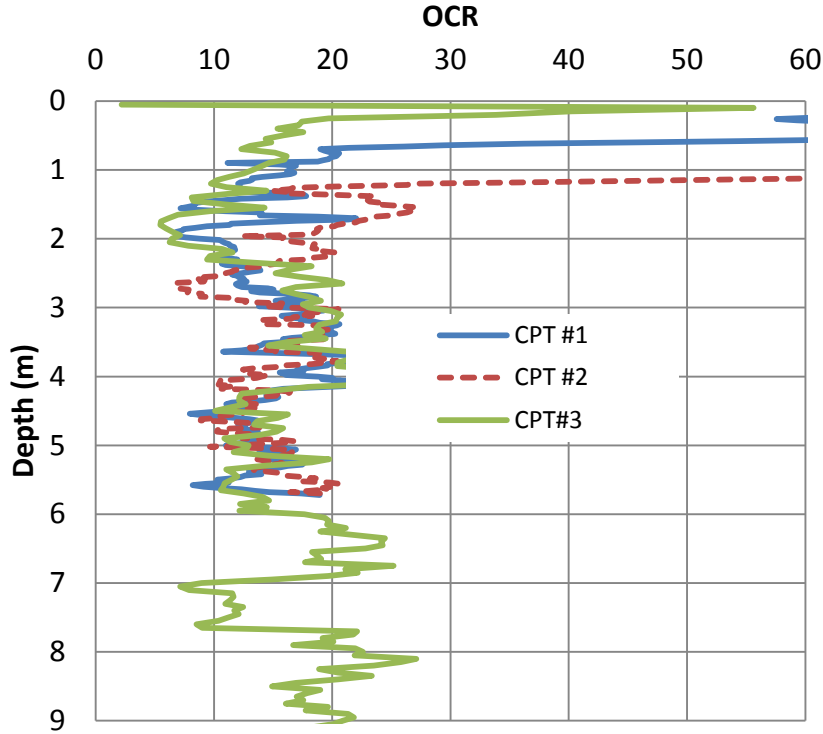


Figure 3-6: Estimated OCR profiles

The undrained shear strength can be correlated to OCR according to the simplified critical state soil mechanics model (Transportation Research Board, 2007), i.e.:

$$S_u = 0.22 (OCR)^{0.8} (\sigma'_v) \quad (3-8)$$

The estimated undrained shear strength profiles calculated using Equations 3-4 and 3-8 are provided in Figure 3-7.

The undrained shear strength evaluated based on the total cone tip resistance varies from 100 kPa at 1.0 m depth gradually increasing to approximately 900 kPa at 9.0 m depth. On the other hand, the undrained shear strength estimated based on OCR values varies from approximately 20 kPa at 1.0 m to approximately 250 kPa at 9.0 m depth. The average undrained shear strength was determined considering all CPT data. In addition, it is assumed that the remolded shear strength is equal to the lesser of the already estimated shear strength and the measured sleeve friction. Both peak and remolded shear strength profiles are shown in Figure 3-7. The peak and remolded

shear strength values used for further analysis are presented in Table 3-2 as averaged within one meter intervals; i.e 0 to 1 meters, 1 to 2 meters etc..

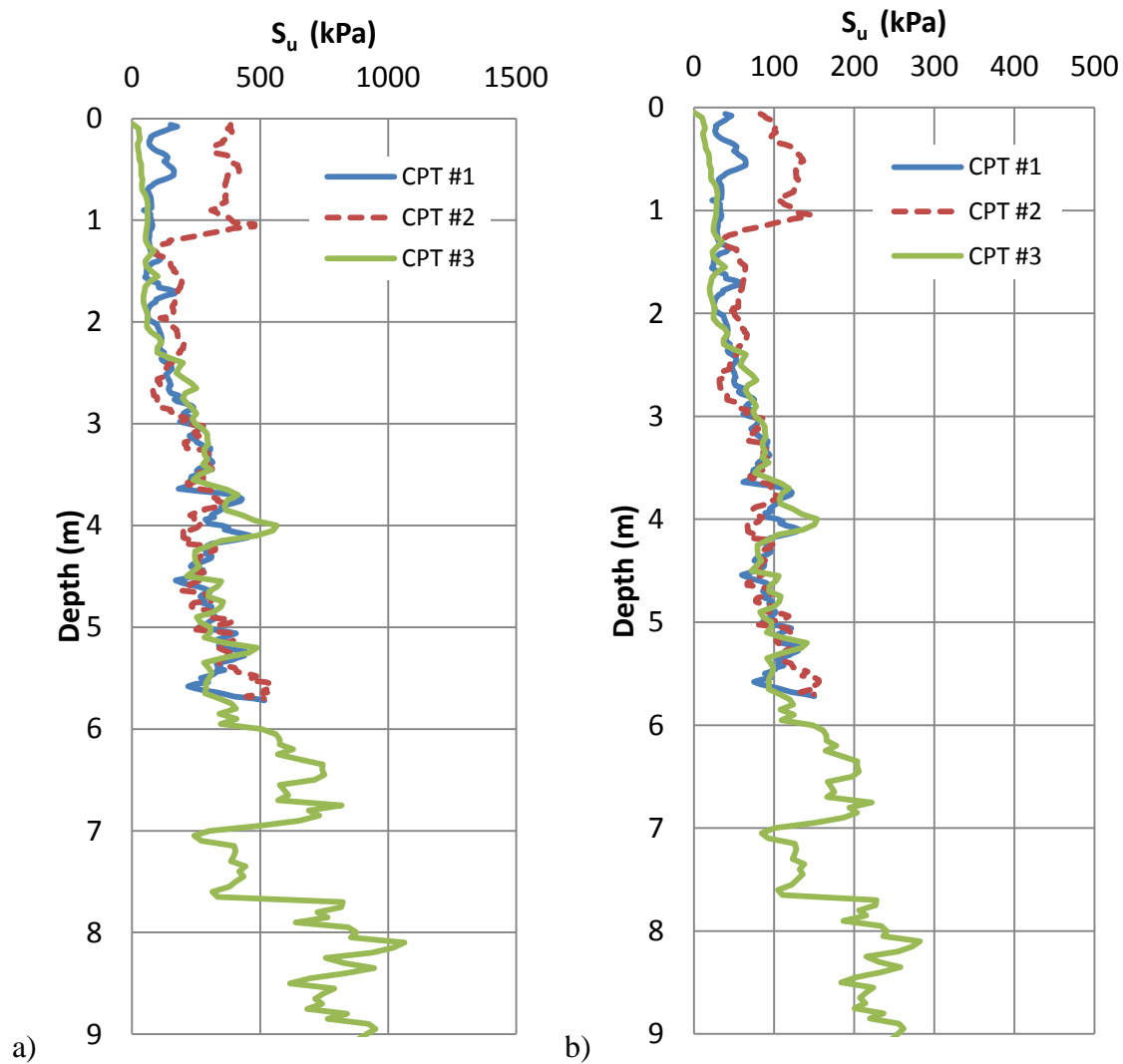


Figure 3-7: Undrained shear strength S_u estimated from: a) N_k ; b) OCR

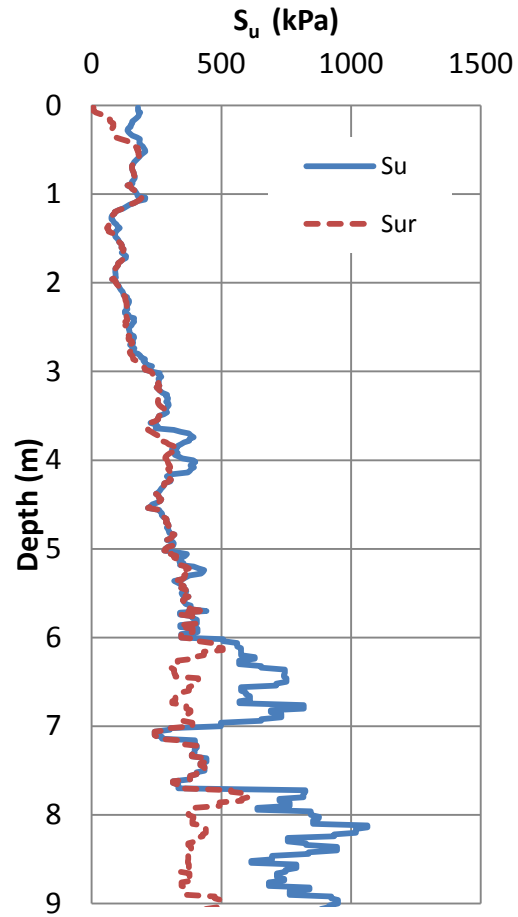


Figure 3-8: Design Shear Strength Peak (S_{up}) and Remolded (S_{ur})

Table 3-2: Peak shear strength (S_{up}) and remolded shear strength (S_{ur}) values averaged over 1 m intervals.

Depth (m)	S_{ur} (kPa)	S_{up} (kPa)
1	83.4	112.6
2	70.3	73.7
3	96.5	104.1
4	175.4	199.8
5	238.8	246.6
6	249.3	421.8
7	267.8	332.2
8	264.1	552.2
9	307.2	597.8

3.3 Test Pile Configurations & Instrumentation

Five different pile configurations were chosen to enable evaluating the influence of pile diameter and helical plates' configuration on the installation torque and the ultimate load carrying capacity. Each pile configuration was tested in both compression and tension (uplift), with the exception of the 10-3/4" diameter pile configurations.

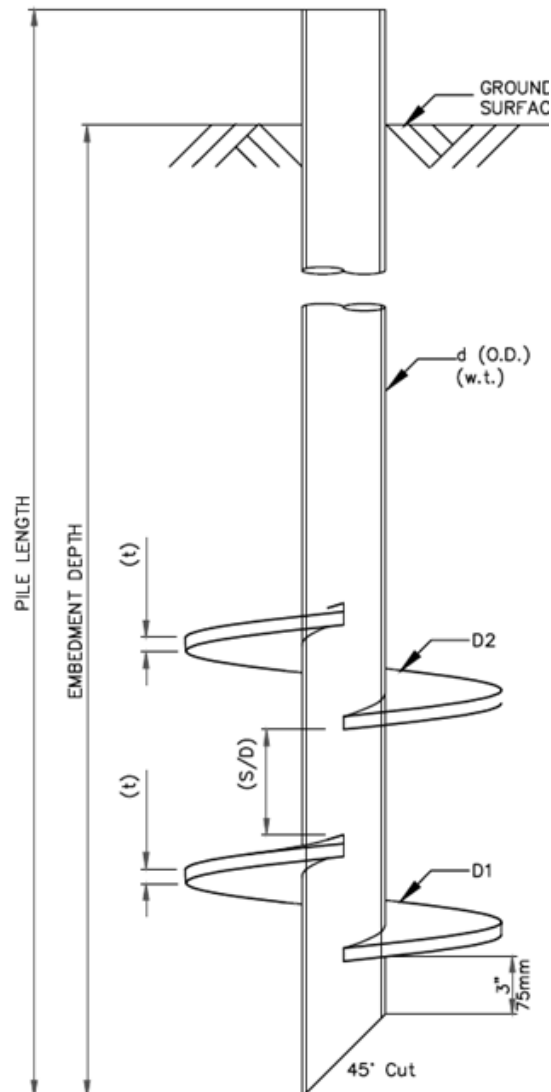
Prior to installation, all test and reaction piles were marked along their length in order to indicate embedment depth every 300 mm (one foot). These markings were utilized to provide manual recording of depth with time coinciding with installation torque measurements. In addition, selected pile configurations were instrumented with strain gauges installed at different locations along their length. The readings of the strain gauges were used to evaluate the load transfer mechanism present during static load testing.

3.3.1 Pile Configurations

Pile configurations utilized in the testing program are detailed in

Table 3-3. Pile IDs include a letter, a number then a letter. The first letter denotes the loading mode, whereby "C" refers to compressive loading, "T" refers to tension (uplift) loading, and "RP" refers to a pile utilized as a reaction pile within the loading test setup. The number, 6, 8 or 10, refers to the pile diameter, namely 6-5/8" (168.3 mm), 8-5/8" (219.1 mm) and 10-3/4" (273 mm), respectively. These diameters are some of the most commonly used sizes of large capacity helical piles. The last letter is either an "S" or a "D", which refers to a single helix or double helices, respectively.

The helix diameter was approximately three times the pile diameter, i.e., the 168.3, 219.1, and 273 mm pile were fitted with 457.2, 609.6 and 762 mm helical plates, respectively. For piles with double helices, the inter-helix spacing was equal to three times the helix diameter. A schematic drawing of the test pile configurations is provided in Figure 3-9.



Helical Pile Schedule

HELICAL PILE TYPE	SHAFT DIA. (O.D.) (d) (in)	PILE WALL THICKNESS (w.t.) (in)	HELIX DIA. (D1) (in)	HELIX DIA. (D2) (in)	PITCH (P) (in)	HELIX THK. (t) (in)	PILE LENGTH (ft)	INTER HELICAL SPACING RATIO (S/D) (in)	EMBEDMENT DEPTH (ft)
RP 1-7	10 3/4	0.365	30	NA	6	3/4	25	NA	20.5
C/T 6S	6 5/8	0.280	18	NA	6	3/4	25	NA	24
C/T 6D	6 5/8	0.280	18	18	6	3/4	25	54	24
C/T 8S	8 5/8	0.322	24	NA	6	3/4	25	NA	22
C/T 8D	8 5/8	0.322	24	24	6	3/4	25	72	22
C/T 10S	10 3/4	0.365	30	NA	6	3/4	25	NA	20.5
C/T 10D	10 3/4	0.365	30	30	6	3/4	25	90	21.5

Figure 3-9: Test Pile Drawing

Table 3-3: Pile Configuration and Testing Summary

Pile ID	<u>Pile Shaft</u>		<u>Helix</u>				Spacing Ratio (S/D)	Axial Testing	Load	Strain Gauge
	Length (m)	Embedment (m)	Diameter (m)	No. of Helices	Diameter (m)					
C6S	7.62	6.858	0.1683	1	0.4572	-		Compression		YES
T6S	7.62	6.858	0.1683	1	0.4572	-		Tension		NO
C6D	7.62	6.858	0.1683	2	0.4572	3		Compression		NO
T6D	7.62	6.858	0.1683	2	0.4572	3		Tension		NO
C8S	7.62	6.858	0.2191	1	0.6096	-		Compression		YES
T8S	7.62	6.858	0.2191	1	0.6096	-		Tension		YES
C8D	7.62	6.858	0.2191	2	0.6096	3		Compression		YES
T8D	7.62	6.858	0.2191	2	0.6096	3		Tension		YES
C10S	7.62	6.248	0.273	1	0.762	-		Compression		YES
C10D	7.62	6.248	0.273	2	0.762	3		Compression		YES
RP1-8	7.62	6.248	0.273	1	0.762	-		NA		NO

3.3.2 Strain Gauge Installation

Some of the test piles were instrumented with axial strain gauges attached to their exterior walls. For single helix piles, strain gauges were attached at three locations along the pile shaft. For double helix piles, strain gauges were attached at five locations along the pile shaft. Two quarter-bridge strain gauges were attached at each location. Strain gauge readings during the load tests were used to determine the load transferred to the soil through the pile shaft and the helices. To measure the load transferred through the shaft, strain gauges were installed at the mid-point between the pile head at the top helical plate and the mid-point between the two helices. To measure the helical plates' loads, strain gauges were installed approximately 75 mm above and 75 mm below each helix.

The strain gauges were CEA-06-250UN-350 general purpose strain gauges applied in quarter-bridge arrangements, which were installed diametrically opposite and arranged longitudinally in line along the pile shaft. All lead wires were fished from the gauge location through small holes in the shaft near the installed locations and up through the center of the pile terminating at the pile head where they were connection to a data acquisition module. As shown in Figure 3-10, each gauge location was prepared by sanding the exterior wall of the pile to enable complete and

even adhesion of the gauge to the pile surface. Once gauges were installed and lead wires were connected, the strain gauge and its connection were treated with a surface sealant to protect it from moisture. After all adhesives and sealants were cured, the entire quarter bridge circuit was tested for voltage leaks and baseline resistance. Once proper working order was established, the entire gauge location was then covered with a layer 15 mm thick of ceramic epoxy (Nordbak Pneu-Wear produced by Loctite intended for high abrasive environments), which was then covered with tapered edges.



a)



b)

Figure 3-10: a) Double Helix Instrumented Pile with Installed Strain Gauges b) Double Helix Instrumented Pile Strain Gauges Coated in Protective Epoxy

3.3.3 Installation Procedure & Layout

All test and reaction piles were spaced centre-to-centre at 2.743 m (9 feet) in a semi grid formation as shown in Figure 3-11. All 168.3 and 219.1 mm diameter test piles were arranged to have two-reaction pile loading system. The 273 mm diameter piles were arranged to have four-reaction pile loading system. The reaction piles (RP) were arranged to be utilized in testing multiple piles as shown in Figure 3-11.

The spacing between a reaction pile and a test pile of 168.3 mm diameter was 2.134 m (7 ft), corresponding to 4.7 times the diameter of the largest helix between the edge of the helices. The spacing between a reaction pile and a test pile of 219.1 mm diameter was 2.134 m (7 ft), corresponding to 3.5 times the diameter of the largest helix between the edge of the helices. The spacing between a reaction pile and a test pile for the 273 mm diameter pile was 3.1 m (10.17 feet), corresponding to a ratio of 4.1 times the diameter of the largest helix between the edge of the helical plates.

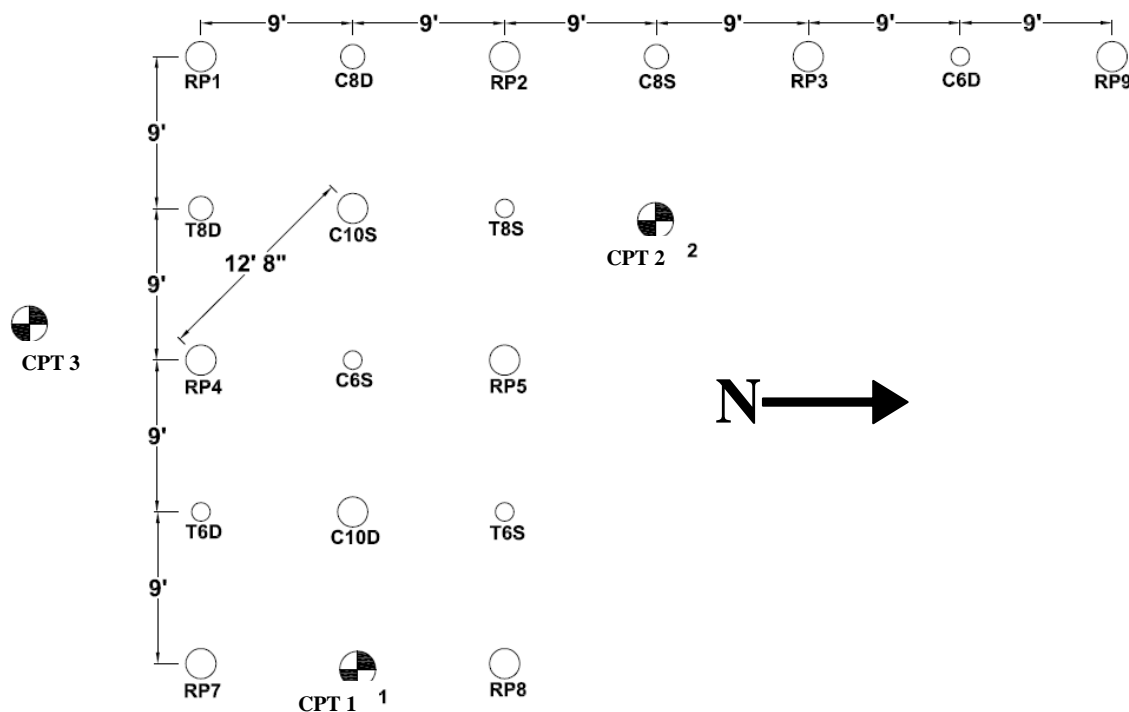


Figure 3-11: Lamont Test Site Layout – Pile Locations & CPT Soundings

Chapter 4

4 Installation Torque

Installation torque applied to a helical pile is required to overcome the soil resistance as the pile advances into the soil. As the embedded surface area of the installed pile increases so does the soil resistance and the required installation torque. The rate of change in required installation torque depends on the change in soil strength/stiffness.

The-current-state-of-practice is to install helical piles with a hydraulic powered rotational drive head. First, the helical pile is affixed to the drive head; a vertical pressure (crowd) is applied to advance the lead helical plate into the soil; and finally, torque is applied sufficient enough to engage the pitch of the helical plates within the soil thereby producing an advancing force effectively pulling the pile into the soil.

Installation torque is most commonly measured by recording the hydraulic pressure in line with the rotary hydraulic drive head. This measured pressure is either a direct forward acting pressure or, in some cases, a differential pressure (forward minus reverse). Pressure readings are commonly recorded as pounds per square inch (psi), and are then converted to an effective applied torque via an efficiency factor, K , provided by the manufacturer of the drive head. Torque measurement can be conducted at intervals throughout the installation process to produce the profile of torque with depth. The final torque and/or the average torque measured over a distance equal to 3 times the diameter of the largest helix (i.e. last 3D) is usually recorded and used as quality control via CTC.

4.1 Measurement of installation parameters

Field installations of all test and reaction piles within this study were conducted with the use of a boom truck and a 156 kN-m (115,000 ft-lb) capacity hydraulic torque drive head (two speed Digger 1400 produced by Eskridge Inc.) as shown in Figure 2-4.



Figure 4-1: Boom Truck & Digger 1400

During installation, measurements were made to accurately monitor the rate and magnitude of applied forces. The differential hydraulic pressure was measured by means of pressure transducers mounted in line with the forward and reverse hydraulic lines powering the drive head. Mechanical torque and vertical crowd were monitored via a load cell referred to as the “Torque Pin” mounted at the juncture between the drive head and the boom truck dog-bone. The installation rate was captured via a proximity sensor mounted near the tool of the drive head. Lastly, the embedment depth was recorded manually through the visual inspection of depth markings on the exterior pile wall. All data was recorded with a data acquisition system connected to a computer; and all manual observations were recorded referencing their specific real time.

4.1.1 Torque Pin

The Torque Pin is a load cell that can take accurate strain measurements, which are then calibrated to provide force readings. It was located within the joint connecting the boom truck dog-bone to the drive head, along two precise shear planes. The measurement of forces at these precise intersections enables the determination of the torque through the coupling of the horizontally oriented shear forces, and the determination of crowd, through the coupling of the vertically oriented shear forces.

The load cell is constructed such that it takes four separate temperature-independent strain measurements. To provide redundancy, two identical pairs of strain gauges are used to provide clear indication of potential errors during measurement. It is designed to provide clear signal transmission despite the electrically ‘noisy environment’. Force measurements were taken once every second throughout the duration of installation.

To calibrate the torque pin readings, a calibration test bench was constructed as shown in Figure 4-2. This calibration table consisted of two hydraulic pistons and a fixed central section. The hydraulic pistons were controlled via data acquisition system connected to a computer. In order to effectively calibrate the torque pin, it was fixed similar to its alignment within the boom truck and drive head unit. During calibration, a maximum torque of 190 kN-m and force of 550 kN were applied, which corresponded to approximately 120% of the expected capacity of the drive head and boom truck torque and crowd loading limits, respectively. The applied forces were controlled by increasing the hydraulic pressure within the piston chamber at intervals of approximately 345 kPa (50 psi). The calibration testing was thus conducted by increasing the hydraulic pressures while measuring the signal in pulse position modulation (ppm) provided by the torque pin and zeroing the reading offset. The results of this calibration test are presented in Figure 4-3 and Figure 4-4. A linear regression was applied to the recorded data to provide an accurate linear fit with coefficient of determination (R^2) values of 0.9967 for the torque sensor measurements and 0.9951 for the crowd sensor measurements. This indicated the accuracy of the instrument. It should be noted that it was more difficult to control the hydraulic pressure below 670-1340 kPa (100-200 psi), and consequently, the lower end of the calibration near zero load was difficult to establish accurately.

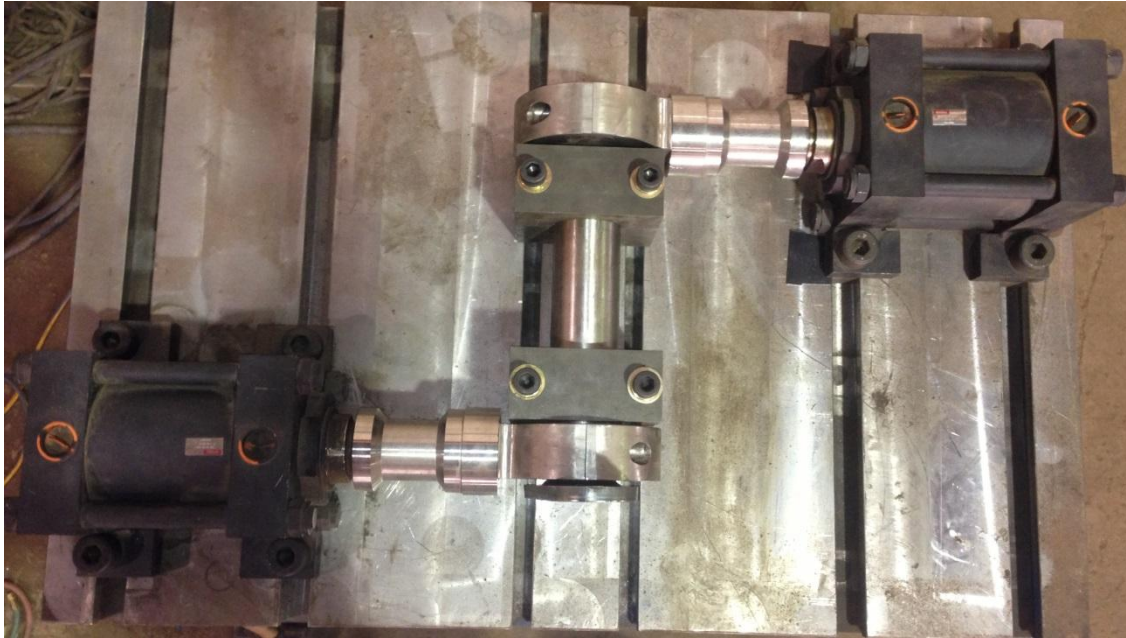


Figure 4-2: Torque Pin Calibration Table

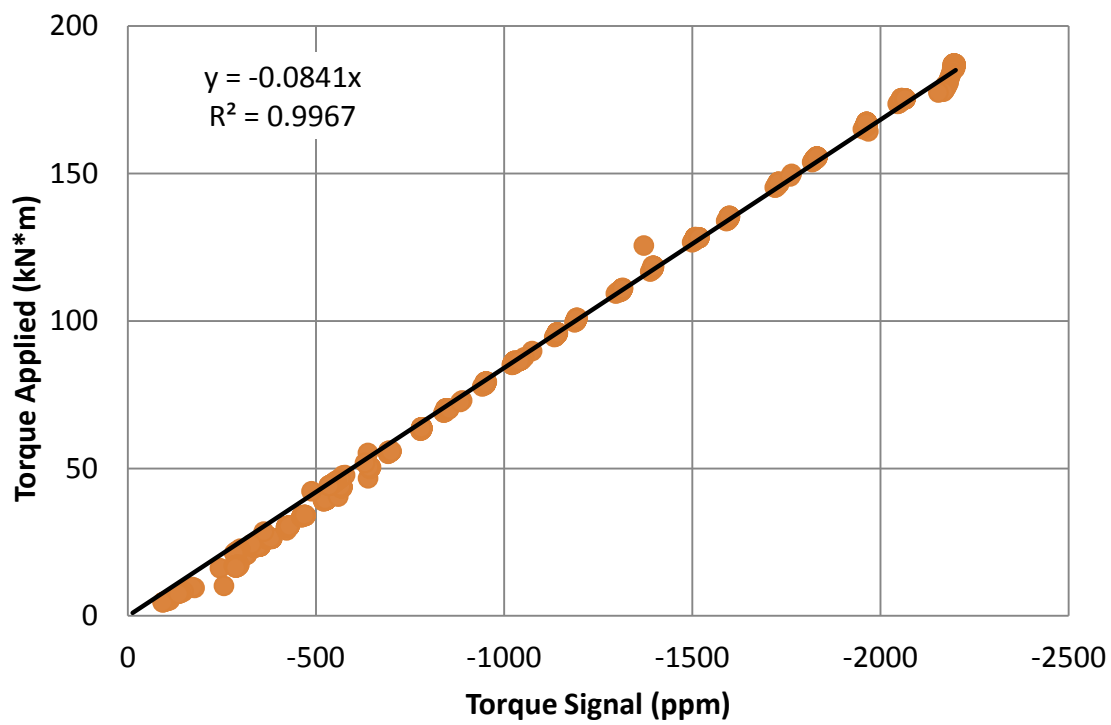


Figure 4-3: Torque Sensors Calibration

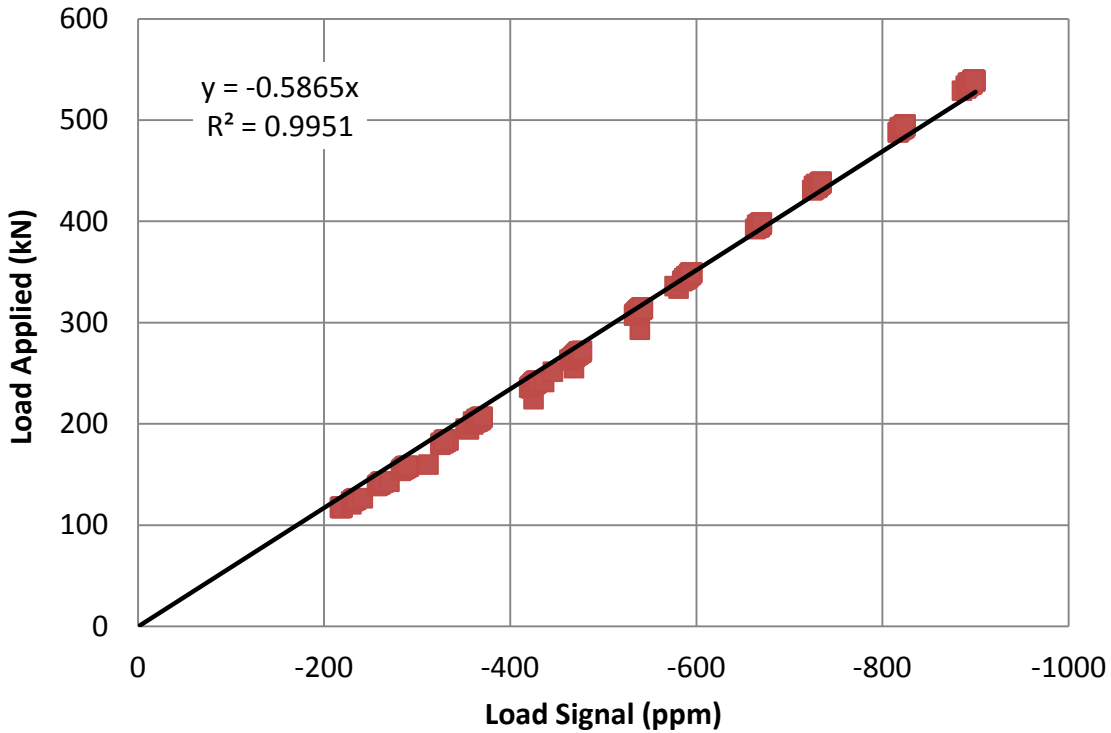


Figure 4-4: Load Sensors Calibration

4.1.2 Hydraulic Pressure

The hydraulic system was monitored in conjunction with force measurements taken through the torque pin. Forward and reverse pressure lines were equipped with a set of pressure transducers located at the farthest end of the boom nearest the drive head. This minimized potential effects of frictional losses over the length of the hydraulic hosing as shown in Figure 4-5.



Figure 4-5: Hydraulic Pressure Transducer

Every drive head and hydraulic machine combination must be accompanied by a calibration specification sheet that details the efficiency of the equipment to produce a working torque. Conversion from the differential pressure to an applied working torque is conducted via a predetermined efficiency factor, K , which for the Eskridge motor shown is equal to 8.46 at low speed and 23.00 at high speeds. Therefore, the measured torque according to pressure measurements is:

$$T (ft * lbs) = P (psi) * K \quad (4-1)$$

where P is the pressure hydraulic differential.

It should be noted that the efficiency of the drive head/hydraulic machine, and hence the efficiency factor can change significantly during the service life of the drive head. For the results shown herein, all installation torque measurements calculated via the conversion of hydraulic

pressure to torque were conducted with a K factor equal to 23. This value was confirmed through data analysis after installation as will be discussed.

4.1.3 Installation Rate

The rate of installation was effectively recorded through the combined use of two sets of data. A proximity sensor, as shown in Figure 4-6, was attached near the kelley of the drive head where the helical pile is fixed for installation. The proximity sensor provided a continuous count in real time of each quarter turn as the drive head rotated and advanced the pile into the ground.



Figure 4-6: Installation Rate Measurement

The installation rate was also evaluated through marking the shafts of all installed piles at 0.3 m (1.0 ft) intervals and monitoring their advance into the ground. As each mark passed the original ground surface, the real time was recorded to provide the time required to install each 0.3 m of the pile. The installation rate was then established assuming constant rate within each 0.3 m.

The real time manual depth recordings and rotational counts, the torque, crowd, and pressure data were fit to a depth profile. The pile installation torque profile consists of all data measured at a rate of one recording per second.

4.2 Torque Measurement Sensitivity

4.2.1 Effects of Crowd on Installation Torque Generation

The vertical force applied during the rotation of a helical pile increases the soil resistance to the advancing pile and hence increases the required installation torque. To account for this effect, Perko (2001) included crowd in his theoretical energy-based model to predict the installation torque. Similarly, Rogers (2012) introduced a factor K_{ht} , defined as the ratio of the horizontal force divided by the vertical force utilized, when determining the torque required to rotate a pile against the soil-pile skin friction or adhesion forces. However, Sakr (2013) neglected the down pressure forces (crowd) during installation in his model as he deemed it to be negligible.

The measured crowd and installation torque profiles collected in the current study are presented in Figures 4-7 to 4-9. Inspecting the results in these figures confirms that there is a positive relation between the installation torque and the measured crowd. As the vertical crowd increased, so did the required installation torque. However, it should be noted that it is a regular practice for helical pile installation crews to apply increased downward pressure in situations of hard installation conditions to avoid auguring and causing soil disruption. Thus, the relation between the crowd and installation torque is operator-dependent rather than depending only on a soil resistance response.

To investigate the relation between the installation torque and crowd, all the corresponding values acquired during installation are plotted as dots in Figure 4-10. Inspecting the results in Figure 4-10 reveals that both the crowd and installation torque increased with depth. It is noted that the torque increased approximately proportional to the crowd with a lower bound rate equal to $0.133 \frac{kN-m}{kN}$. This indicates that one of two scenarios exists; the application of increased crowd results in an increase in torque through a normal force and friction force relation, or as the soil resistance increases the operator responds by increasing crowd. The data acquired within his study is insufficient to determine with surety the existing scenario; however it is clear that a relation exists.

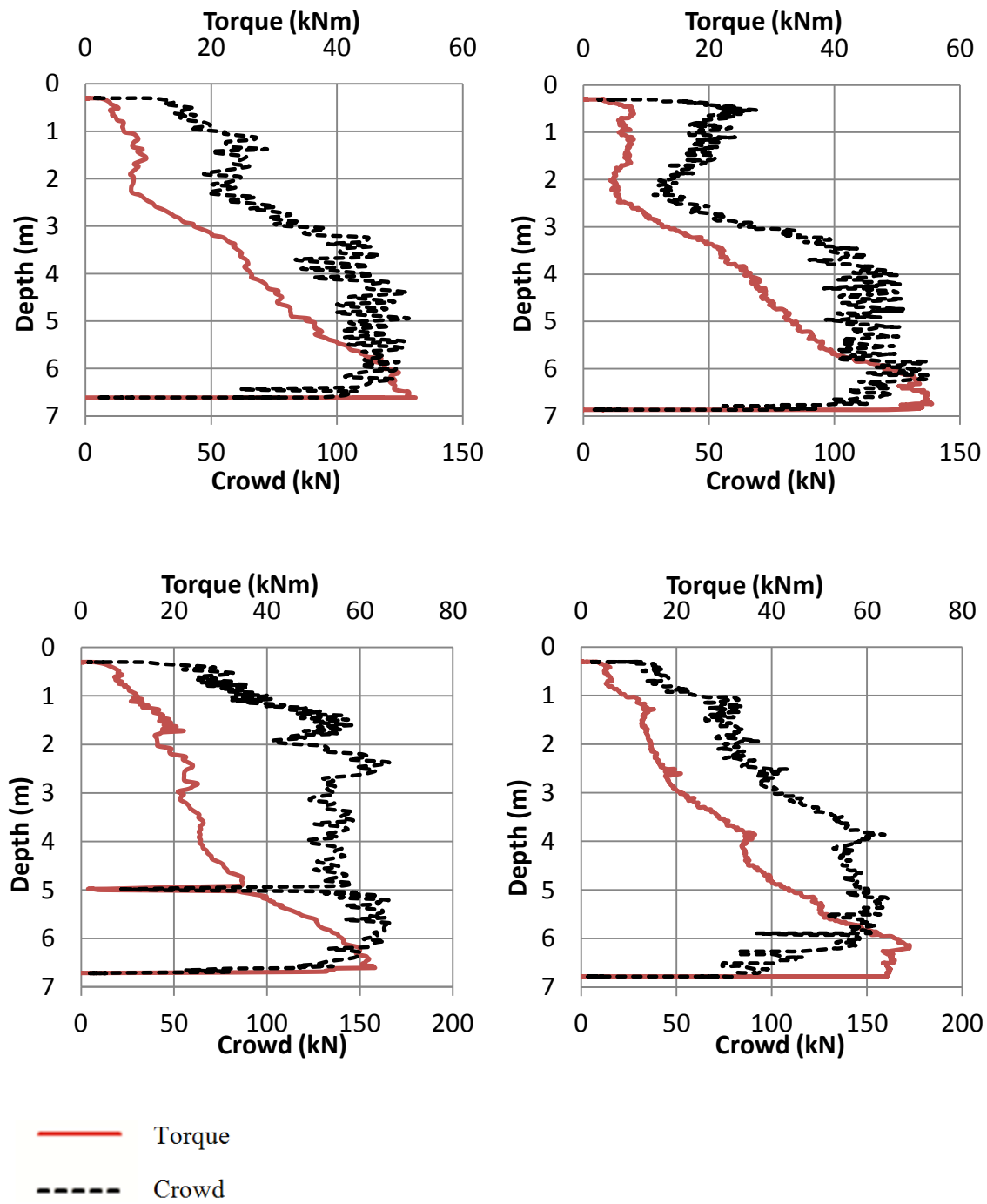


Figure 4-7: Install force profiles for 179 mm pile: a) C6S; b) T6S; c) C6D; and d) T6D

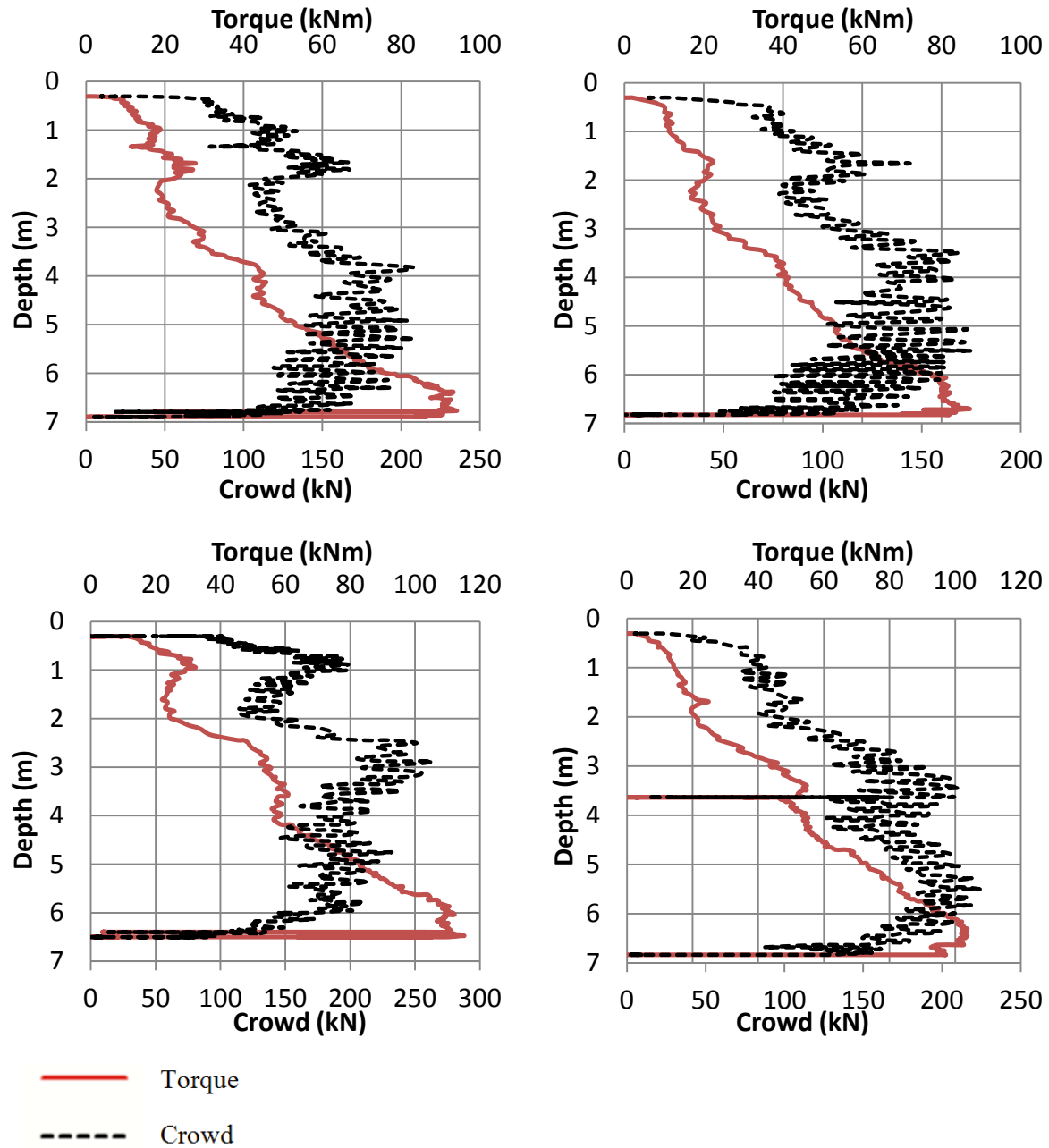


Figure 4-8: Install force profile for 219 mm pile a) C8S; b) T8S; c) C8D; and d)T8D

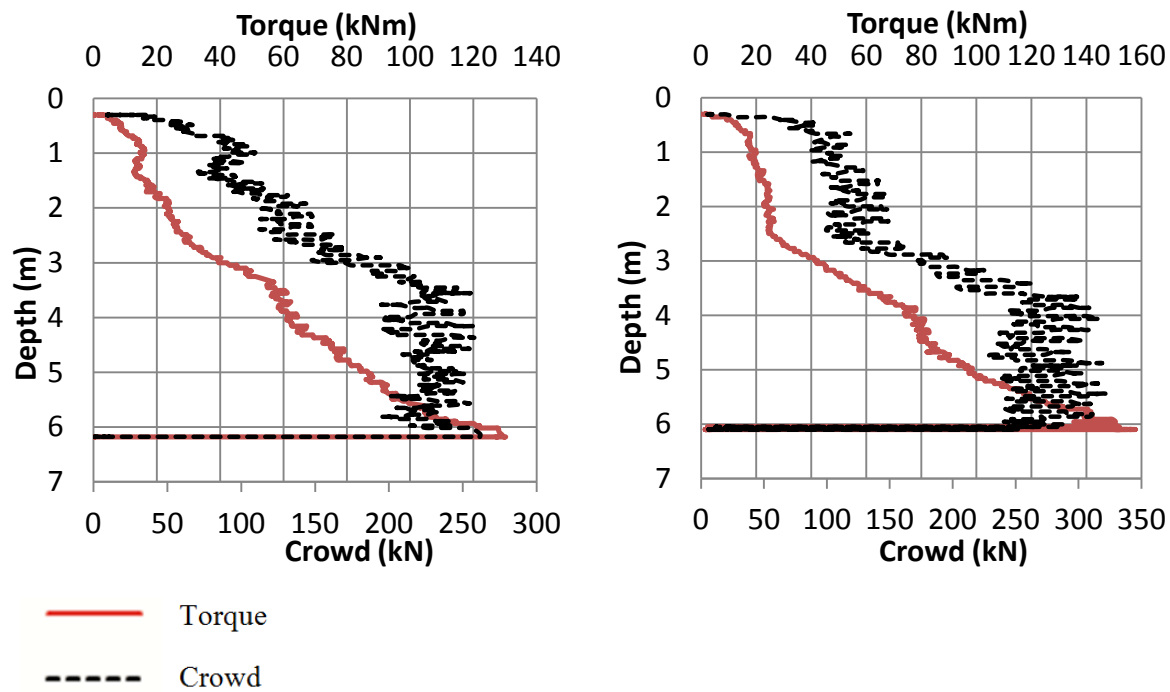


Figure 4-9: Install Force Profile for 273 mm pile a) C10S; and b) C10D

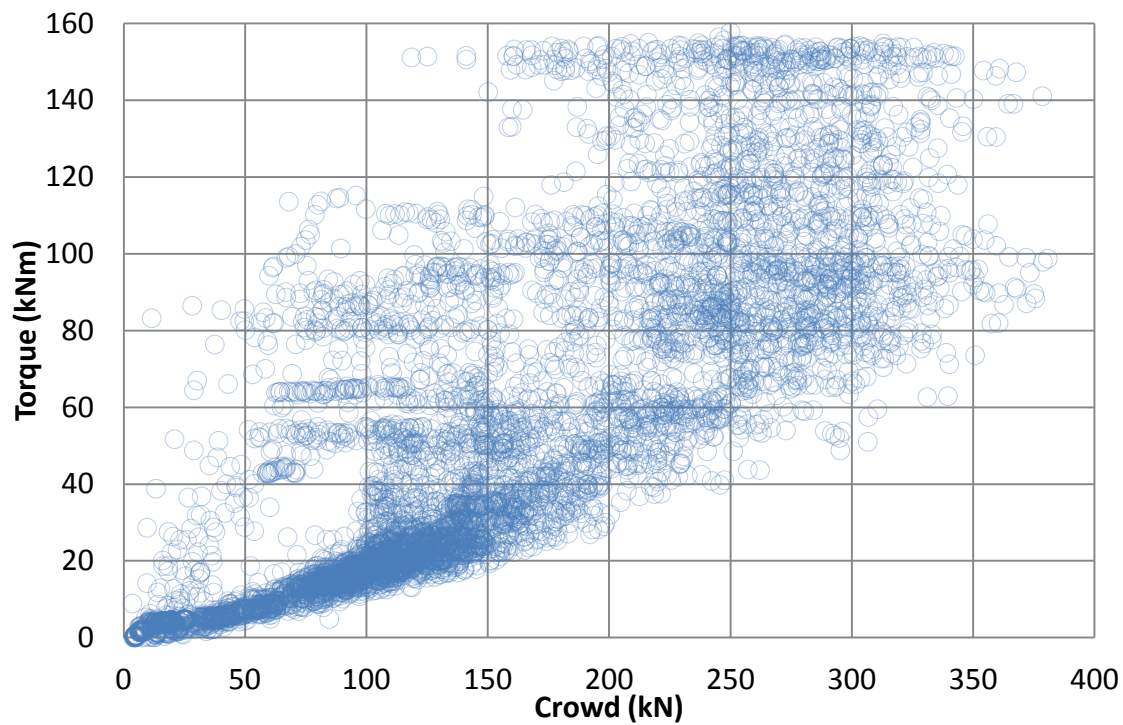


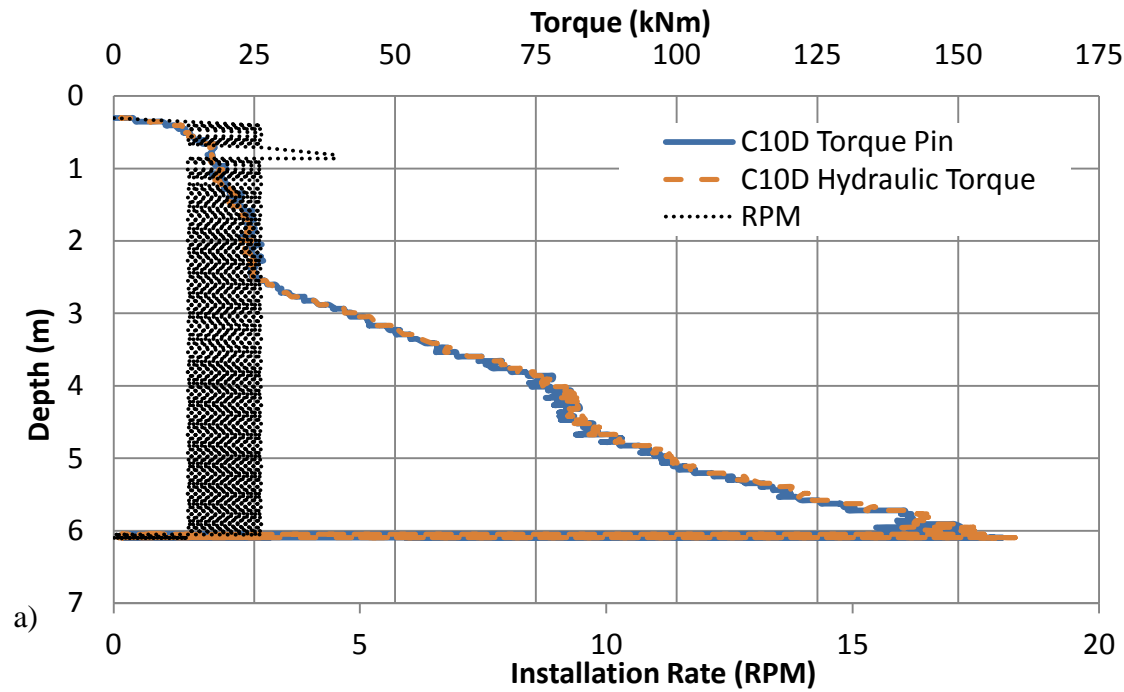
Figure 4-10: Crowd vs Torque Relationship

4.2.2 Hydraulic Versus Mechanical Torque Measurements

Accurate final torque measurements, usually recorded as the average torque for the last one meter of installation, or 3D, and necessary for empirical evaluation of the pile capacity. The conventional method for measuring installation torque used in the helical piling industry involves taking measurements from a calibrated hydraulic pressure dial gage mounted in line with the forward pressure (or forward and reverse) of the drive head. When taking a torque measurement, it is necessary to slow the rotational speed of the drive head (i.e. maintain a low idle) to induce a consistent torque when recording the pressure reading. At elevated speeds, the high-flow hydraulic conditions have a tendency to create a bouncing dial reading and potentially elevated pressure readings not consistent with the true applied torque (Bradka & Kasprick, 2013; Perko, 2009). On the other hand, mechanical torque measurement (e.g. torque pin) is not affected by the rotational speed. The instrumented torque pin measures strains in the pin material and provides a signal calibrated to torque forces. The efficiencies of the motor and hydraulic system are bypassed and only the resulting applied force is measured and recorded.

To evaluate the effect of the rotational speed of the hydraulically calculated torque, the hydraulically calculated and mechanically measured installation torque profiles are compared in Figure 4-11 for three different rotational speed conditions. It should be noted that the pressure measurements were converted to torque with $k = 23$. Figure 4-11a shows that the hydraulic and mechanical torque measurements for C10D were almost identical for the case of low rotational speed (3-5). On the other hand, Figure 4-11b shows that for pile C6S, which was installed at high rotational speed of 15-20 rpm, the hydraulically measured torque was drastically different both in magnitude and profile from the mechanically measured torque. To further elucidate this point, Pile T8D was installed using different rotational speeds as shown in Figure 4-11c. The torque profiles presented in Figure 4-11c confirm the variation of the hydraulically measured torque with the installation rotational speed. Initially, the rotational speed was approximately 20 rpm and the hydraulically measured torque was vastly different from the mechanically measured torque. In two intervals during T8D installation, at depths of approximately 3.6 m and 6 m, the installation rate was decreased from 15-20 RPM to approximately 5-6 RPM. At these intervals, the hydraulically measured torque was in good agreement with the mechanically measured torque.

This clearly demonstrates the sensitivity of the hydraulically measured torque to the installation speed and the stability of the mechanically measured torque (torque pin). For this reason, the installation torque depth profiles used in the analysis in the following consist of torque measured via the torque pin only.



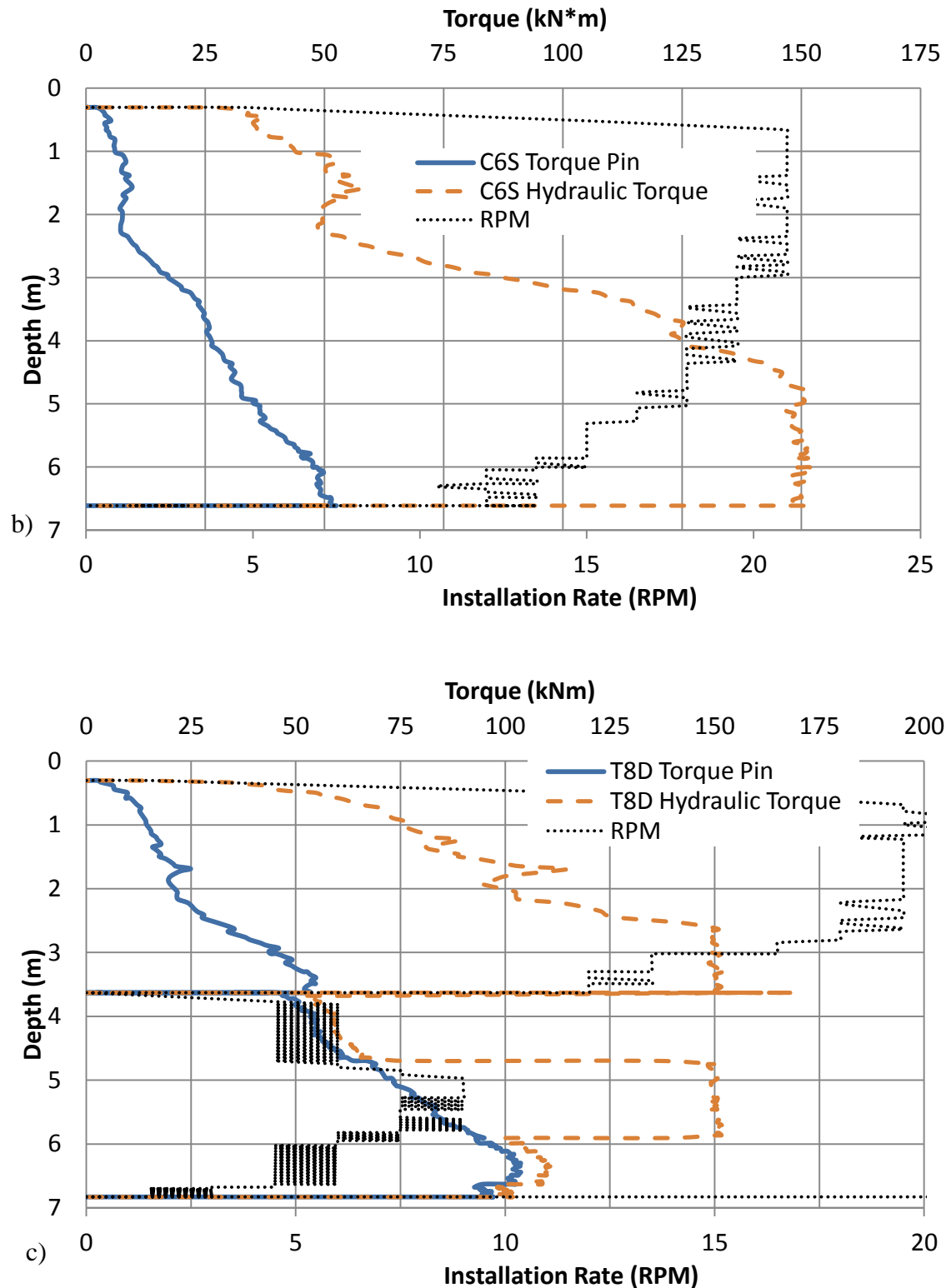


Figure 4-11: Hydraulic and mechanical torque: a) measured at low RPM for C10D; b) measured at high RPM for C6S; and c) measured at variable RPM for T8D

4.2.3 Effects of Installation Rate on Torque

During installation of helical piles, it is recommended to advance the pile into the soil at a minimum rate of 80% of the blade pitch during each revolution (Perko, 2009). If the pile cannot be advanced into the soil, auguring occurs, which significantly disturbs the surrounding soil. The installation torque reduces as the helical plates pass through remolded soil with reduced strength. Thus, the ‘capacity to torque’ correlation factor established from the reduced installation torque may not correlate well with the pile capacity. Extensive auguring may also cause disturbance around the helical plate, and hence, significant displacement would be required to mobilize any bearing/shaft friction resistance within the affected area (Perko, 2009).

The commonly used rotational speed of installation (25-30 rpm) enables continuous smooth installation, while allowing the operator to react to changing installation conditions. However, this high rotational speed compromises the accuracy of hydraulically measured torque. In most cases, the rotational speed is reduced to stabilize the hydraulic system and facilitate an accurate hydraulic torque reading (Bradka & Kasprick, 2013). On the other hand, changes in the rotational speed do not alter the torque pin readings. Given that the readings from the torque pin and the hydraulic system matched well when the rotational speed was ≤ 5 rpm, it is recommended to maintain the rotational speed at 5 rpm while taking the torque reading to ensure its accuracy.

It is necessary to investigate the potential effects of installation rotational speed on the accuracy of the hydraulic torque measurement when installing helical piles in other soil conditions. This investigation can also provide valuable insights as to soil disturbance due to the installation rate. For example, the installation rate may reduce the strength of cohesive soil to its residual value, which will consequently affect the required torque.

4.3 Installation Torque Results

Livneh and El Nagggar (2008) stated that the installation torque is a measure of the energy required to overcome the shear strength of the soil and hence is directly related to the soil shear strength and the pile capacity. The installation torque depends on the embedded surface area of the pile (Sakr, 2013; Perko, 2001; Rogers, 2012). Thus, it is expected that installation torque increases as the depth increases, especially for piles installed in soil whose strength increases

with depth. The rate of increase in installation torque would correspond to the pile surface area embedded in the soil and the change in soil strength.

The torque depth profiles constructed for all test and reaction piles installed at the Lamont site were consistent with reliable readings and repeatable results. All piles displayed similar trends of generally increasing torque with depth. This is evident from Figure 4-13, which compares the installation torque profiles for all reaction piles, consisting of 273.0 diameter pipe and single 762 mm helix. Similarly, Figure 4-14, Figure 4-15 and Figure 4-15 compare the torque profiles for all 168.6, 219.1 and 273.0 mm diameter tests piles (both single and double helices). These figures confirm that all piles with the same geometry displayed similar torque profiles. It is also noted that the double helix piles generated larger final torque compared to single helix piles. This confirms that the second helix increases the installation torque.

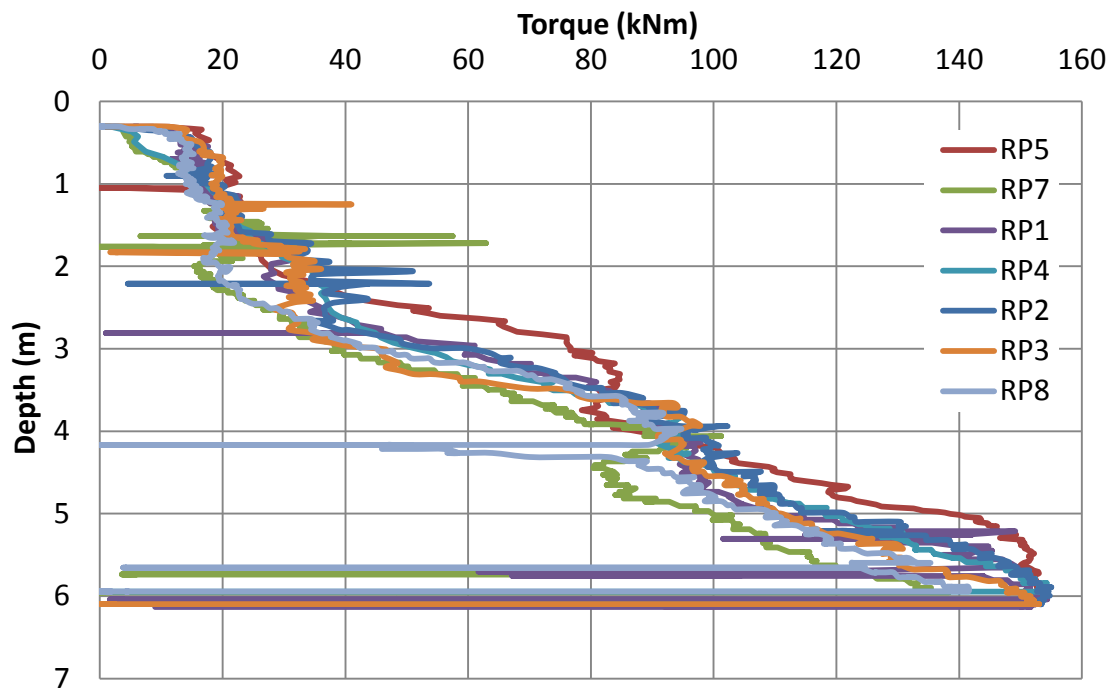


Figure 4-12: Torque Profile for Reaction Piles (RP1-8)

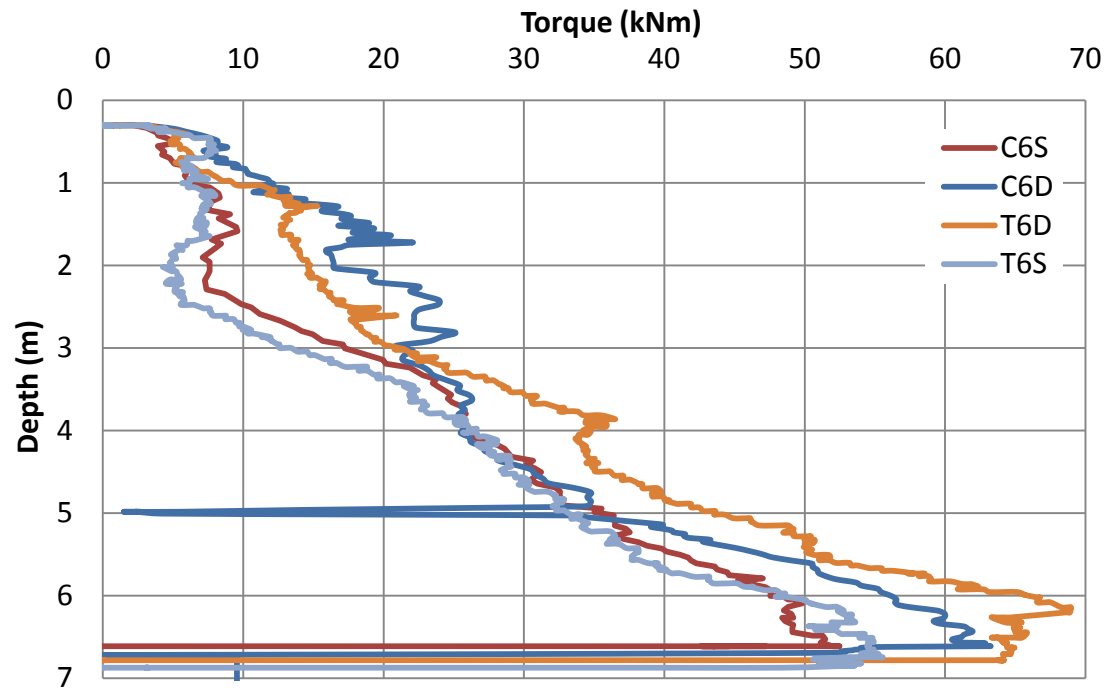


Figure 4-13: Torque Profile for Test Piles; C6D, T6D, C6S, T6S

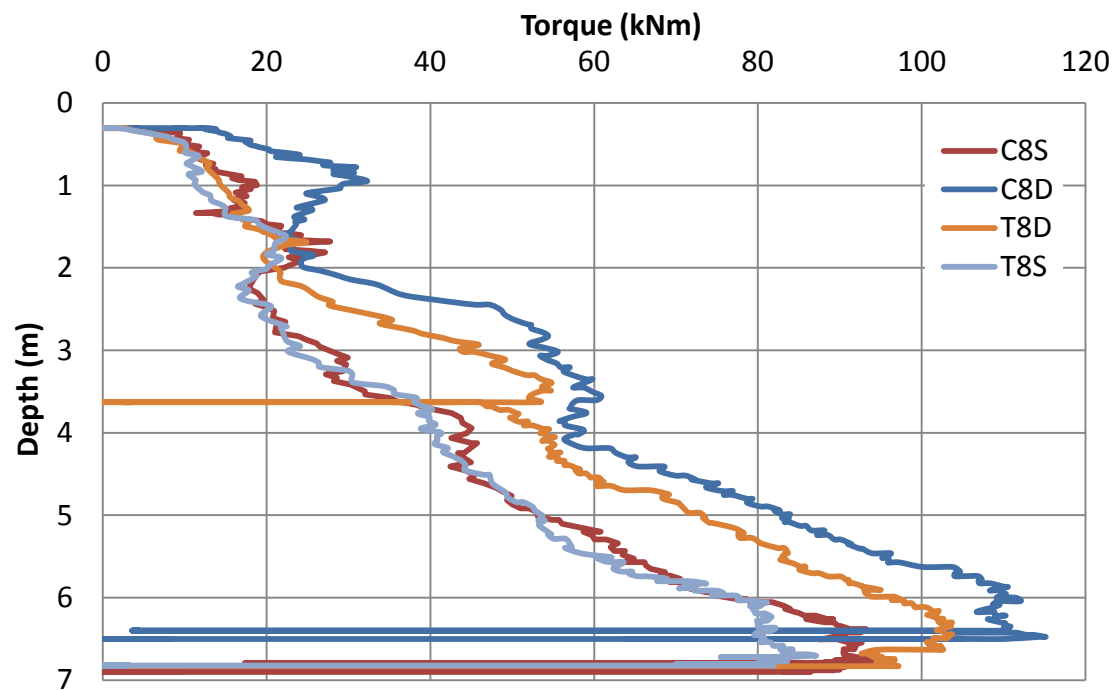


Figure 4-14: Torque Profiles for Test Piles; C8D, T8D, C8S, T8S

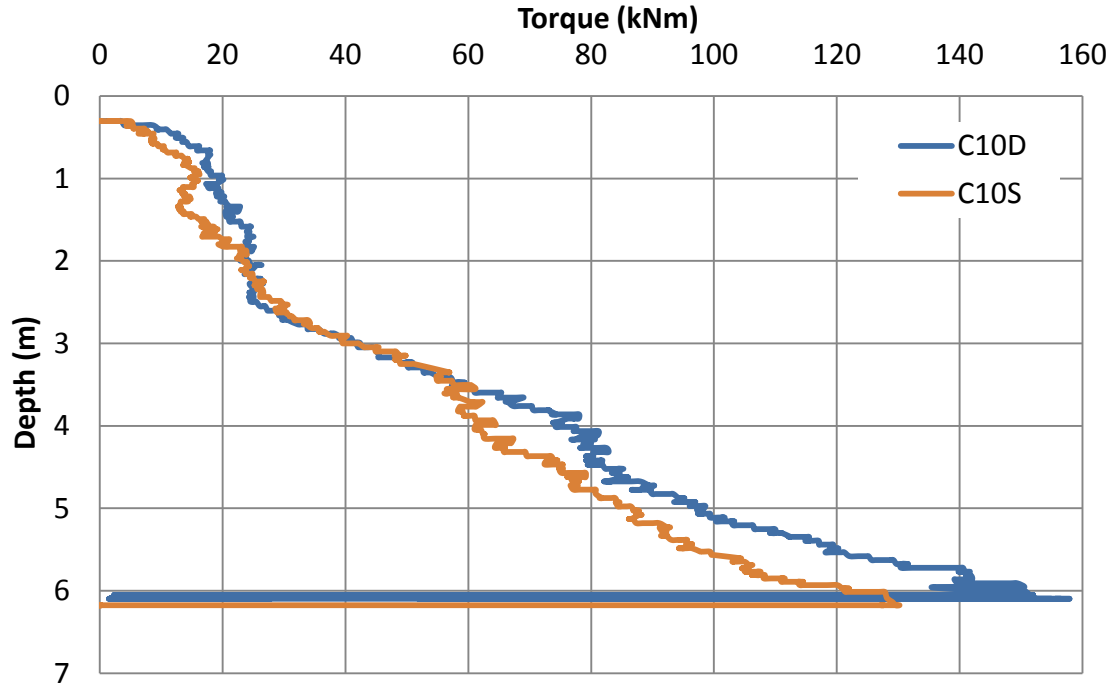


Figure 4-15: Torque Depth Profile Test Piles; C10S, C10D

In order to investigate the effect of the pile diameter on the installation torque, the torque profiles for piles with different diameters are presented in Figure 4-16 and Figure 4-17 for single and double helix piles, respectively. It is clearly evident that the increase in pile pipe diameter has a more significant effect on the required installation torque than that of the second helix. For example, inspecting Figures 4-16 and 4-17, the addition of second helix resulted in an increase of the final torque by 5 - 10 kNm, whereas the increase in the pile diameter from 168.6 to 219.1 mm (and from 219.1 to 273.0 mm) increased the installation torque by 20 - 30 kNm. This confirms that the installation torque is proportional to the total pile embedded surface area and the soil shear strength.

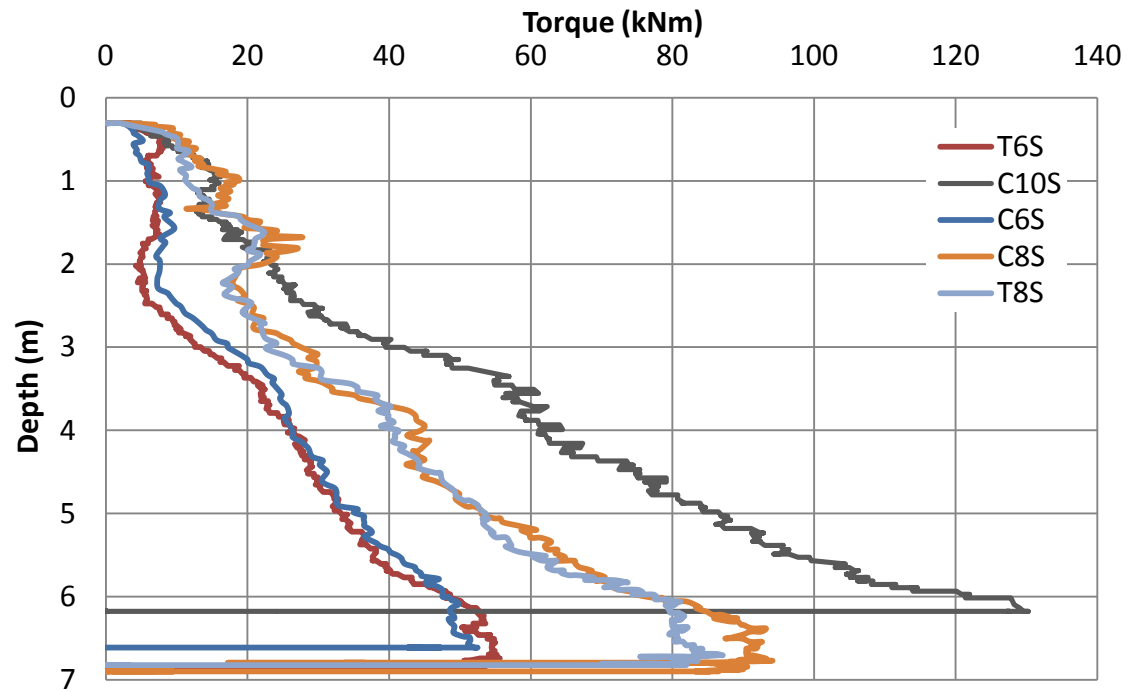


Figure 4-16: Torque Depth Profile for Single Helix Piles

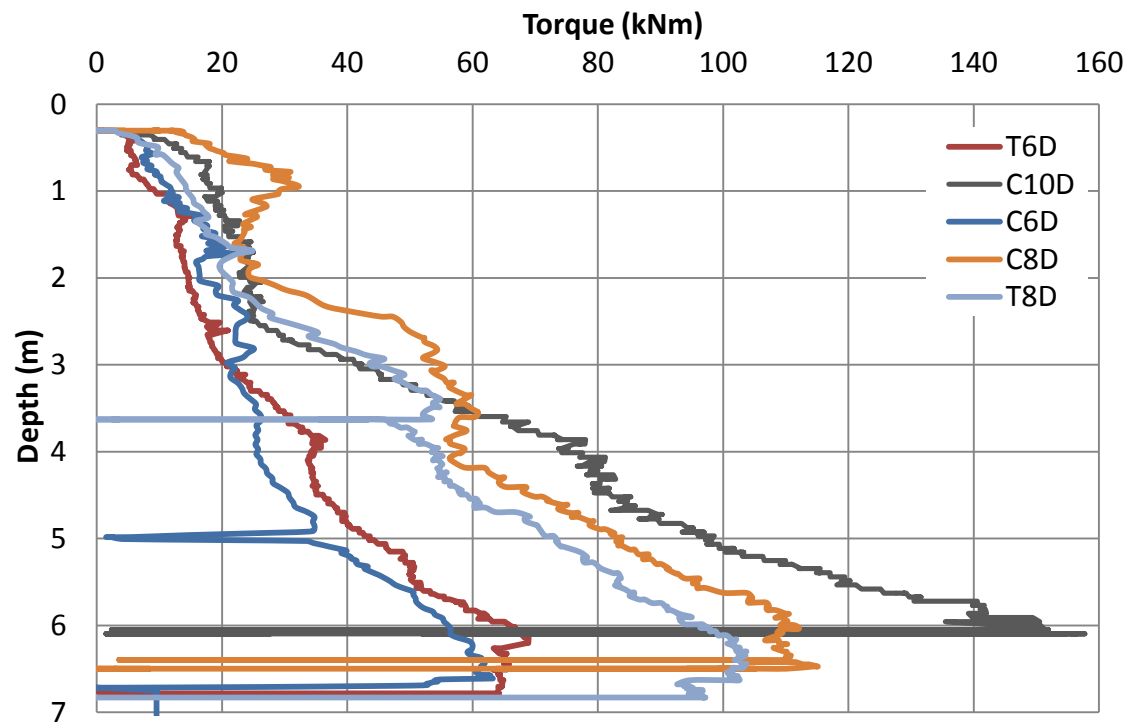


Figure 4-17: Torque Depth Profile for Double Helix Piles

4.4 Average and Final Installation Torque

Three recordings of installation torque were evaluated as follows: an overall average torque weighted over the entire embedment depth; an average torque weighted over the last installed depth equal to 3D; and the final maximum installation torque measured at final embedment. The final torque and the torque averaged over the last 3D exhibited similar trends; i.e. they increased as the embedded area of the pile increased. The difference between the two values increased as the diameter of the pile/helix increased. On the other hand, the overall average torque values were less consistent and thus deemed inappropriate for correlation with pile capacity. Final install torque measurement has a tendency to include short spikes not indicative of the major soil strata relied upon for bearing at the lead helix. Therefore, the average torque weighted over the last installed depth equal to 3D, presented in Figure 4-18, are utilized to establish the CTC factors within this study.

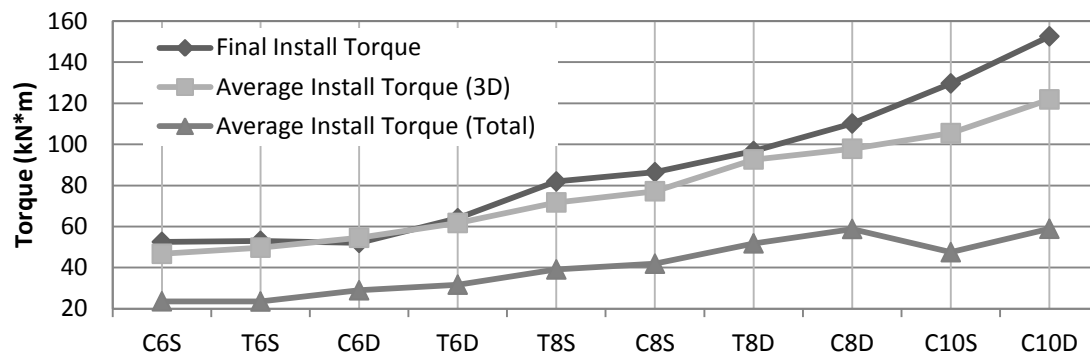


Figure 4-18: Average and Final Installation Torque

4.5 Installation Torque Prediction

Several researchers proposed theoretical models to estimate torque factors for helical piles installed in different types of soils (e.g. Ghaly and Hanna, 1991; Perko, 2001; and Sakr, 2013). These models assume that all forces are transmitted and/or generated by the interaction of the embedded area of the pile and the soil. However, they differ in how the vertical crowd is

considered. Some models assume it contributes to torque generation, while others do not. The models also differ with regard to the assumption related to the shear plane between the advancing helical plate and the surrounding soil.

A simplified theoretical model is employed in this study to predict the variation of the installation torque with depth. It assumes that as the helical pile advances into the soil, the shearing plane is located along the surface areas of the pile shaft and helical plates. Thus, there is no cylindrical shear surface surrounding the helical plates. In addition, it assumes the crowd force is applied consistently (i.e. no excessive crowd applied), hence they have insignificant effect on installation torque.

In this theoretical model, the installation torque is based on the summation of the contribution of soil shear resistance over the pile embedded area, i.e.:

$$T_{total}(z) = t_{shaft}(z) + t_{lead\ helix}(z) + t_{rear\ helix}(z) \quad (4-2)$$

where, $t_{shaft}(z)$ is the torque due to soil resistance along the embedded pile shaft, $t_{lead\ helix}(z)$ is the torque due to soil resistance along the lead helix and $t_{rear\ helix}(z)$ is torque due to soil resistance along the rear helix. These torque contributions may be given by:

$$t_{shaft}(z) = \sum_0^z z\pi \frac{d_o^2}{2} \alpha S_u(z) dz \quad (4-3)$$

$$t_{lead\ helix}(z) = \sum_0^z A_{h1} \alpha \bar{S}_u(z - l_1) R_{gh1} dz \quad (4-4)$$

$$t_{rear\ helix}(z) = \sum_0^z A_{h2} \alpha \bar{S}_u(z - l_1 - p - s) R_{gh2} dz \quad (4-5)$$

where

$$A_{h1} = \frac{\pi}{2} (D_1^2 - d_o^2) \quad A_{h2} = \frac{\pi}{2} (D_2^2 - d_o^2) \quad P_s = z\pi \frac{d_o^2}{2} \quad (4-6)$$

in which, A_{h1} is the area of the lead helix, A_{h2} is the area of the rear helix, d_o is the outer diameter of the pile shaft, l_1 is the distance from the toe to the lead helix, p is the pitch of the

helix, s is the spacing between lead and rear helix, $R_{gh\#}$ is the radius of gyration of the helical plate, S_u is the undrained shear strength at a depth z in meters, \bar{S}_u is the average undrained shear strength calculated over a depth equal to the pitch of the helical plate, and dz is equal to the depth increment. Substituting Equations 4-3, 4-4 and 4-5 into Equation 4-2, the final installation torque for each embedment depth is given by:

$$T_{total}(z) = \sum_0^z (A_{h1} \alpha \bar{S}_u(z - l_1) + A_{h2} \alpha \bar{S}_u(z - l_1 - p - s)) R_g + z \pi \frac{d_o^2}{2} \alpha S_u(z) dz \quad (4-7)$$

Employing Equation 4-7, the installation torque is calculated over depth steps of 0.02 m (the smallest increment enabled by the CPT data acquisition). The lead and rear helix torque contributions were calculated using the peak undrained shear strength of the soil, while the pile shaft torque contribution was calculated employing the remolded undrained shear strength of the soil. These assumptions reflect the advancing path of a helical pile during installation. The soil along the pile shaft is assumed to experience maximum shearing/disturbance due to the passage of the helical plates as well as the advancing shaft, thereby most likely will exhibit residual shear strength. On the other hand, the lead helix will penetrate/shear an undisturbed path throughout installation until final embedment is reached. The rear-most helix can be assumed to take one of two possible paths: follow the lead helix through an existing failure plane, and hence experience remolded soil resistance; or introduce a new path through undisturbed soil. It is assumed here to follow a unique path not previously taken by the lead helix; i.e. it experiences peak soil shear strength.

Figure 4-19 to Figure 4-24 present the predicted installation torque profiles for the six helical pile configurations tested in this study, along with the measured torque data. It is noted that the predicted torque profiles agree well with the measured installation torque. This excellent agreement indicates that this simple torque prediction model, if calibrated with additional site experimentation and site exploration, can provide an additional quality assurance and quality control element for helical piles. Further research efforts toward gathering data sets for different soil types and pile configurations would be valuable.

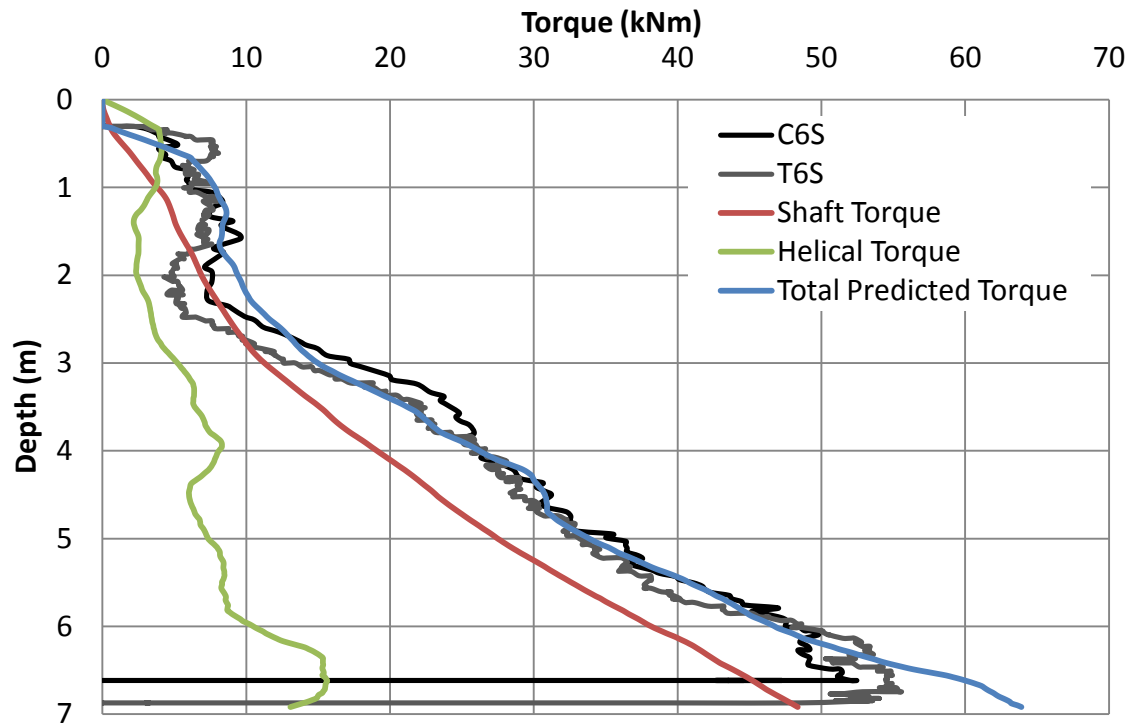


Figure 4-19: 168.6 mm Diameter Pile with Single Helix Torque Prediction

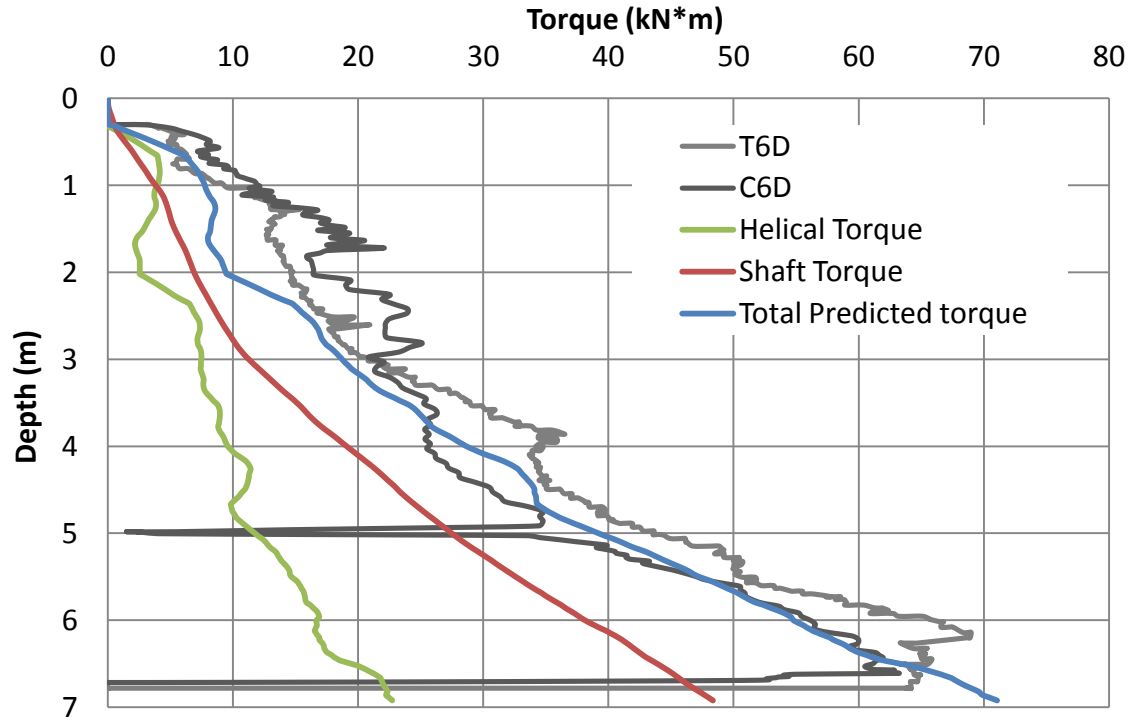


Figure 4-20: 168.3 mm Diameter Pile with Double Helix Torque Prediction

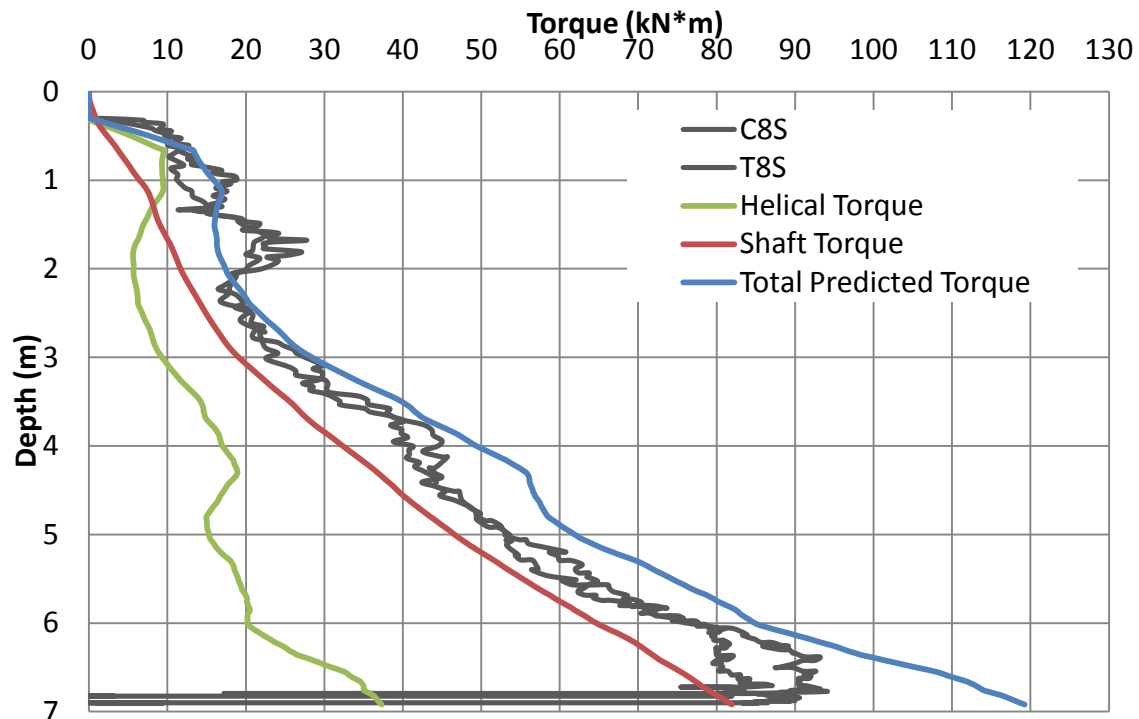


Figure 4-21: 219 mm Diameter Pile with Single Helix Torque Prediction

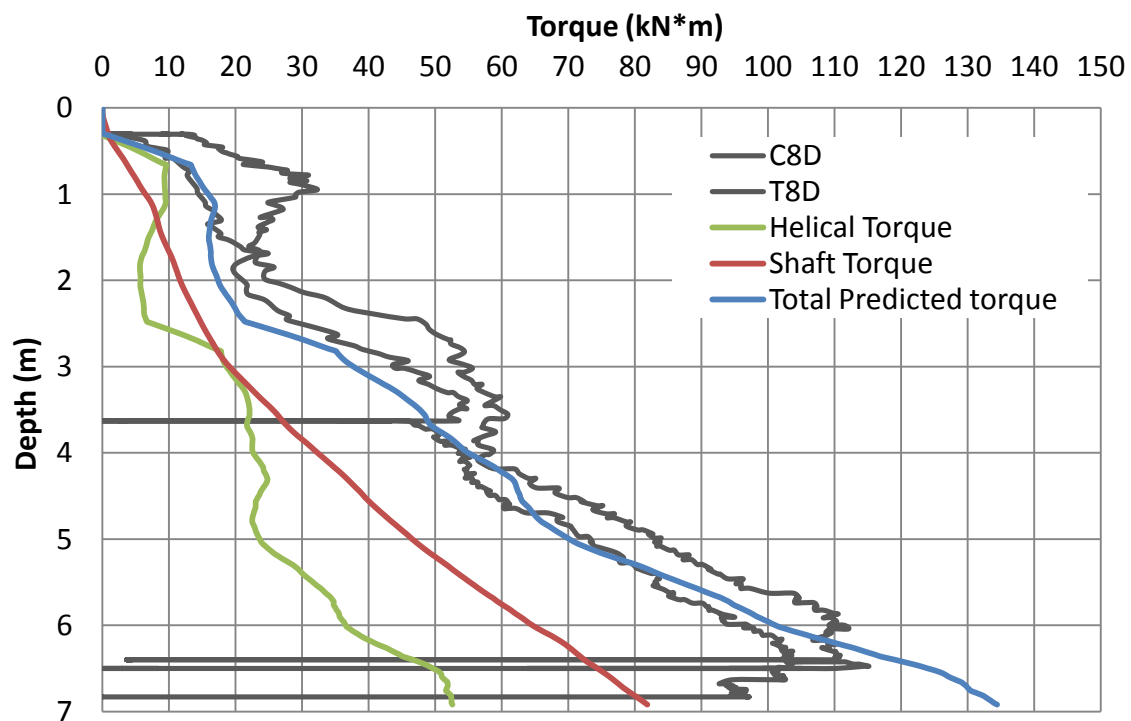


Figure 4-22: 219 mm Diameter Pile with Double Helix Torque Prediction

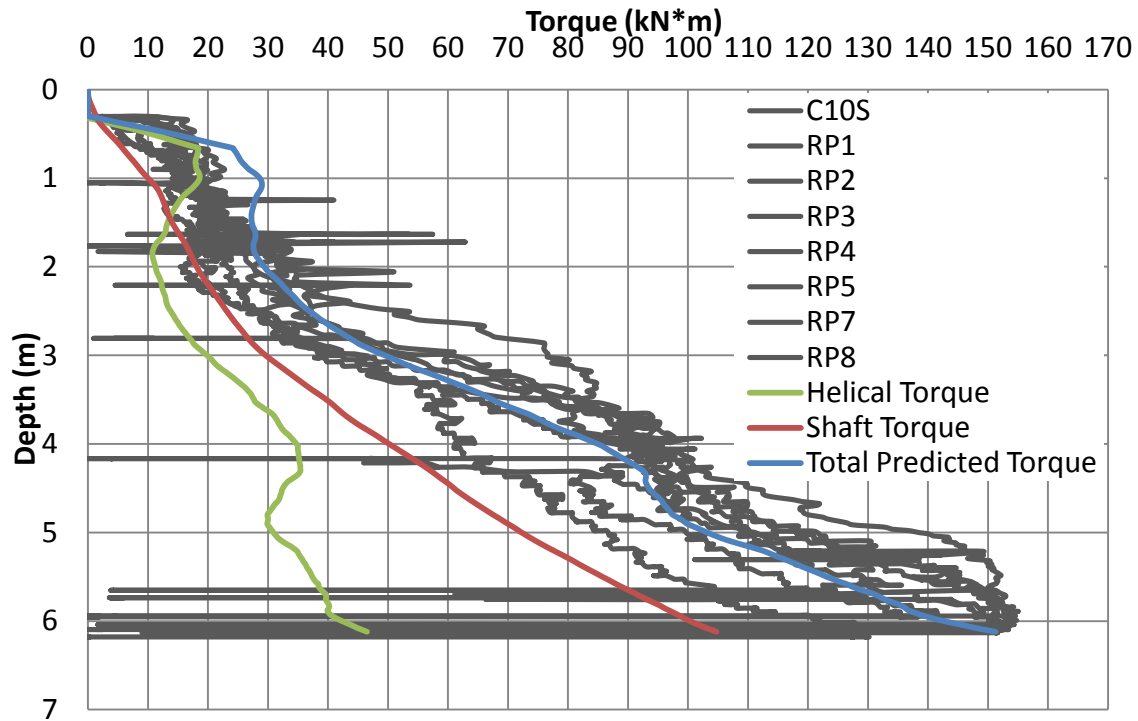


Figure 4-23: 273 mm Diameter Pile with single Helix Torque Prediction

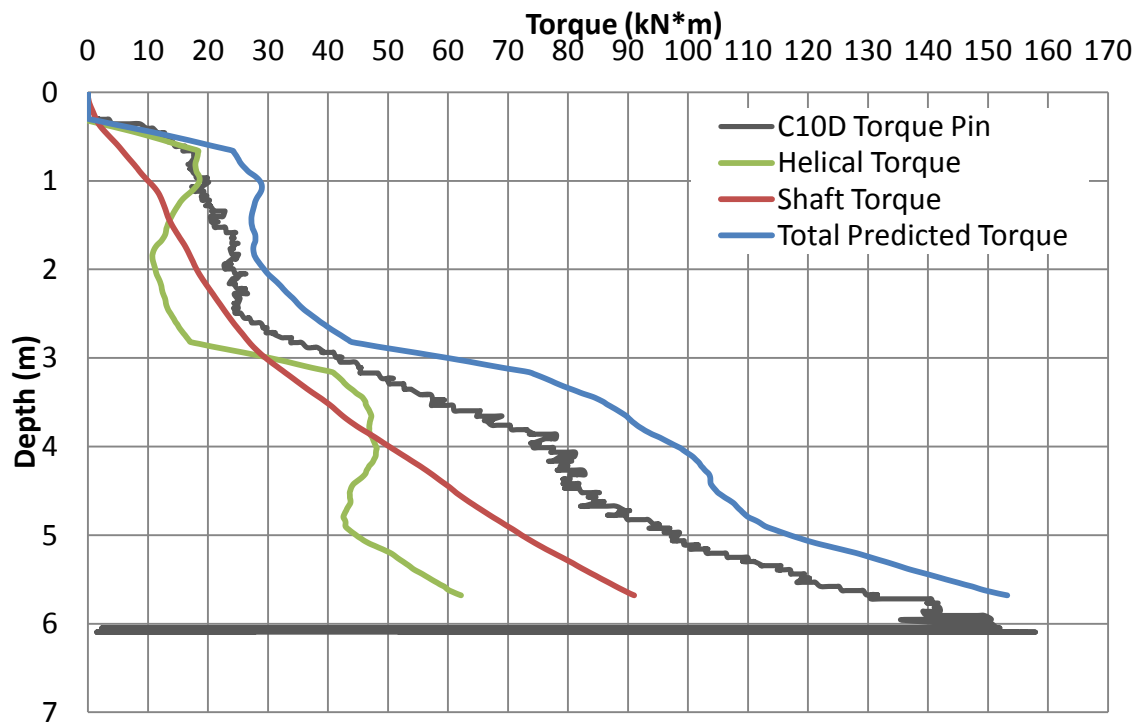


Figure 4-24: 273 mm Diameter Pile with Double helix Torque Prediction

Chapter 5

5 Axial Pile Load Tests

The experimental investigation comprised six compression and four tension load tests. The load tests were conducted as per applicable ASTM standard procedures. The compression or tension loads were applied to the pile head while simultaneously monitoring the pile movement. In addition, seven of the test piles were instrumented with strain gauges to enable observations of load transfer mechanisms.

5.1 Setup & Layout

The test site layout was configured to minimize the required number of reaction piles. For all 168.6 and 219.1 mm diameter piles, a system of two reaction piles and a single reaction beam was used. In the case of the 273.0 mm test piles, a four-reaction pile arrangement was employed. The layout of the installed test and reaction piles are as per Figure 3-11, where all pile spacing is a minimum of 2.7 m center-to-center.

The compressive and tension loads were applied by using a hydraulic jack with maximum capacity of 2,530 kN. A pneumatic pump was utilized to control the load increment. The load was measured employing two methods: using a calibrated load cell with a maximum capacity of 4,000 kN situated between the reaction beam and the hydraulic jack; and using a pressure transducer with a maximum capacity of 2,530 kN, which was mounted in line with the hydraulic jack. Figure 5-1 shows the arrangements for the hydraulic jack and load cell arrangements for both the compression and uplift loading, while Figure 5-2 demonstrates the 2-pile and 4-pile reaction frame arrangements.

Both vertical and horizontal pile head movements were monitored during loading. Two linear variable displacement transducers (LVDT's) were utilized to measure the vertical settlement of the piles. The LVDTs were mounted on the pile head, diametrically opposite each other, and were bearing against stationary independent reference steel beams. Three manual gauges were similarly mounted to the pile head to provide redundancy. In addition, two manual gauges were arranged orthogonally to one another in the horizontal plane to measure the lateral movement of

the pile head. The LVDTs and manual gauges provided accurate measurement to the nearest 0.0254 mm. The LVDTs arrangement and the reference beams are shown in Figure 5-1. All load test data, with the exception of pile strain gauge readings, were recorded at one second intervals via the data acquisition module Graphtec midi logger GL200A shown in Figure 5-3.



Figure 5-1: Loading Setup a) Compression b) Tension

a)



b)



Figure 5-2: Reaction Setup a) Two Reaction Pile Setup b) Four Reaction Pile Setup



Figure 5-3: Data Acquisition System

5.2 Procedure

A quick maintained load procedure was implemented in the pile load tests. The load was applied in increments of 50 kN (5 % of the anticipated failure load). For each load increment, the load was maintained at an almost constant level for 5 minutes, as set out in ASTM D1143 (2007). Once the rate of pile head movement increased and failure was approached, or the testing apparatus was at its limit, the final load increment was maintained for a period of 10 minutes. Following the maximum applied load, the load was removed in approximately 200 kN increments while maintaining each increment for 5 minutes. The final unloading of the pile head was monitored for an additional 10 minutes.

5.3 Pile Load Test Results

The results from the axial pile load testing program are presented herein in terms of load-settlement curves and load transfer diagrams. The load-settlement curves are interpreted to determine the ultimate pile capacity values. The determined pile capacity values are then used, along with average installation torque measured over a depth of the last three times the largest helical diameter, to establish a Capacity to Torque Correlation (CTC) factor that can be used for the prediction of the ultimate pile capacity.

5.4 Interpreted Ultimate Capacity

All static axial load tests were conducted according to the quick maintained load test procedure and, as such, appropriate interpretation methodologies were employed. Four methods were utilized for interpreting the tests results to determine the interpreted ultimate pile capacity, including: the Davisson's offset method (Davisson, 1973); the method proposed by Elkasabgy and El Naggar (2015), which defines the ultimate load as the load corresponding to net settlement equal to 8% of the largest helix diameter; the method proposed by Fuller and Hoy (1970); and the plunging failure (if occurred) taken as the maximum load occurring.

5.5 Load Test Results

The load test results will be discussed first in terms of the load-settlement curves and the interpretation of the ultimate load carrying capacity of the test piles.

5.5.1 Compressive Load Tests

Figure 5-4 presents the load-settlement curve for Pile C6S. It exhibits a typical plunging failure with a failure load of 644 kN, which occurred at a settlements of 25 mm. The other interpreted failure criteria produced interpreted ultimate load varying from 430 to 630 kN, with Davisson' criterion providing the lowest value while Elkasabgy and El Naggar was the closest to the failure load. These loads corresponded to settlements varying from 7.2 mm to 19.3 mm. Similarly, Figure 5-5 presents the load-settlement curves for Pile C6D. It clearly demonstrates that the pile experienced plunging failure, which occurred at 1144 kN with a settlement of 27.4 mm. The other failure criteria predicted ultimate load capacity varying from 896 kN to 1090 kN, with Davisson' criterion providing the lowest value while Elkasabgy and El Naggar was the closest to

the failure load. The corresponding settlement values varied between 12.6 and 27.0 mm. It should also be noted that the capacity of the double helix pile C6D is much higher than the capacity of the single helix pile C6S.

Piles C8S and C8D exhibited the same trends as can be noted from the results presented in Figures 5-6 and 5-7. They experienced plunging failure at 1064 and 1516 kN, respectively, which occurred at settlements of 39.4 and 34 mm. Similarly, the interpreted failure criteria provided lower loads corresponding to lower settlement; the interpreted ultimate load using the Elkasabgy and El Naggar criterion was the closest to the actual failure load and the Davisson's criterion provided the lowest capacity. Figures 5-8 and 5-9 present the results for piles C10S and C10D, respectively. Both piles exhibited plunging failure, with failure loads 1445 kN and 1822 kN. It is also noted that both piles experienced significant creep settlement. As can be noted from the figures, the onset of failure occurred at 58.0 mm and 85.1 mm, respectively, but the creep settlement reached 77.3 and more than 100mm. The load test was finally stopped due to the excessive displacement that exceeded the capacity of the loading system.

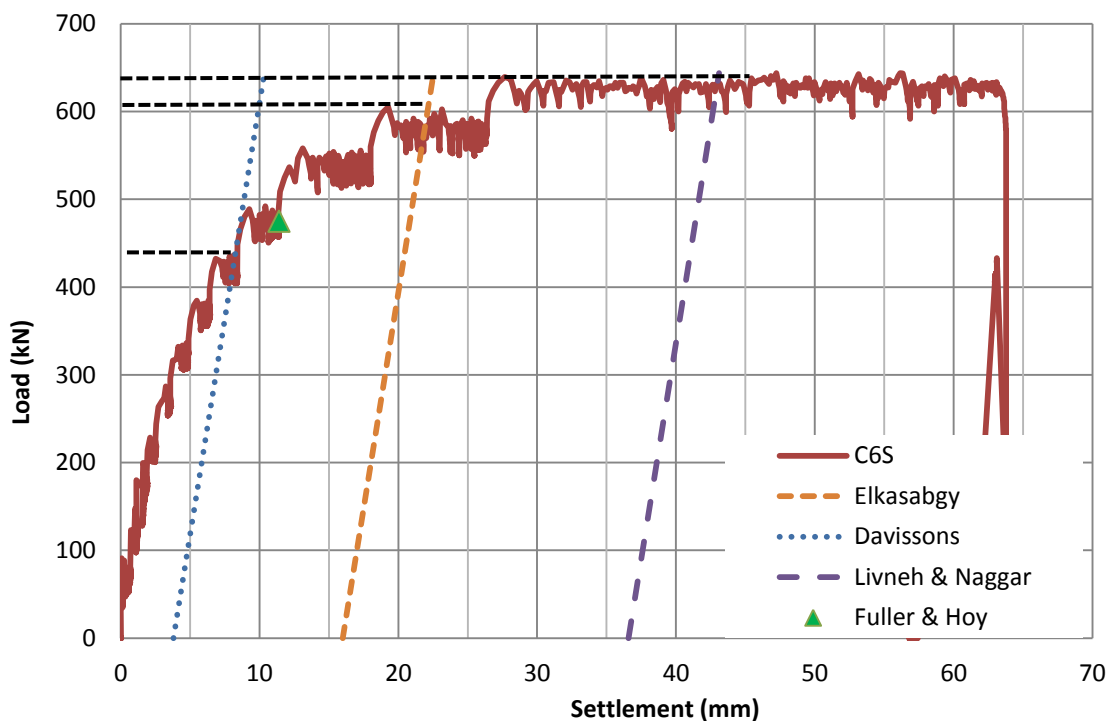


Figure 5-4: Load Settlement Curve for Test Pile C6S

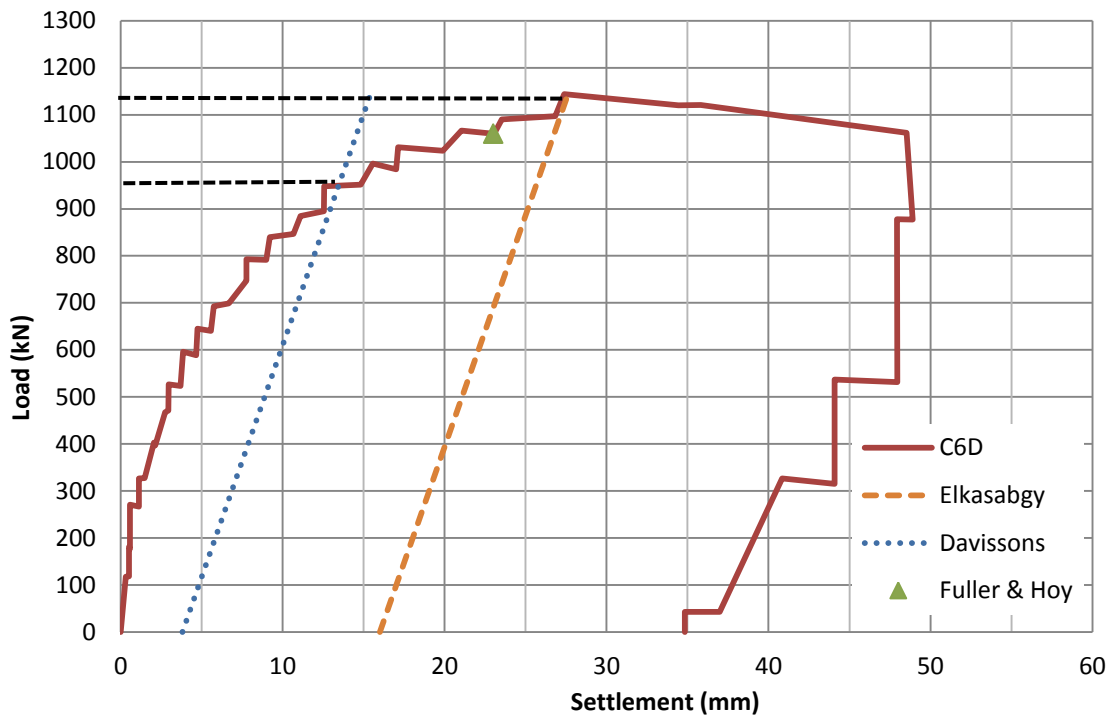


Figure 5-5: Load Settlement Curve for Test Pile C6D

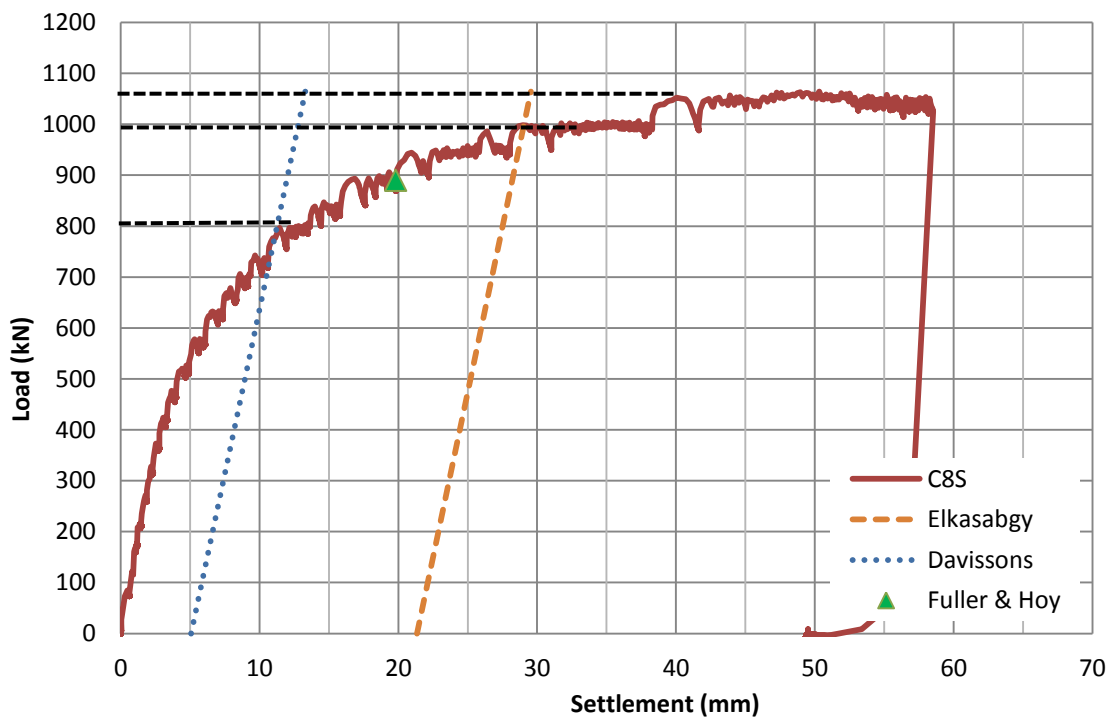


Figure 5-6: Load Settlement Curve for Test Pile C8S

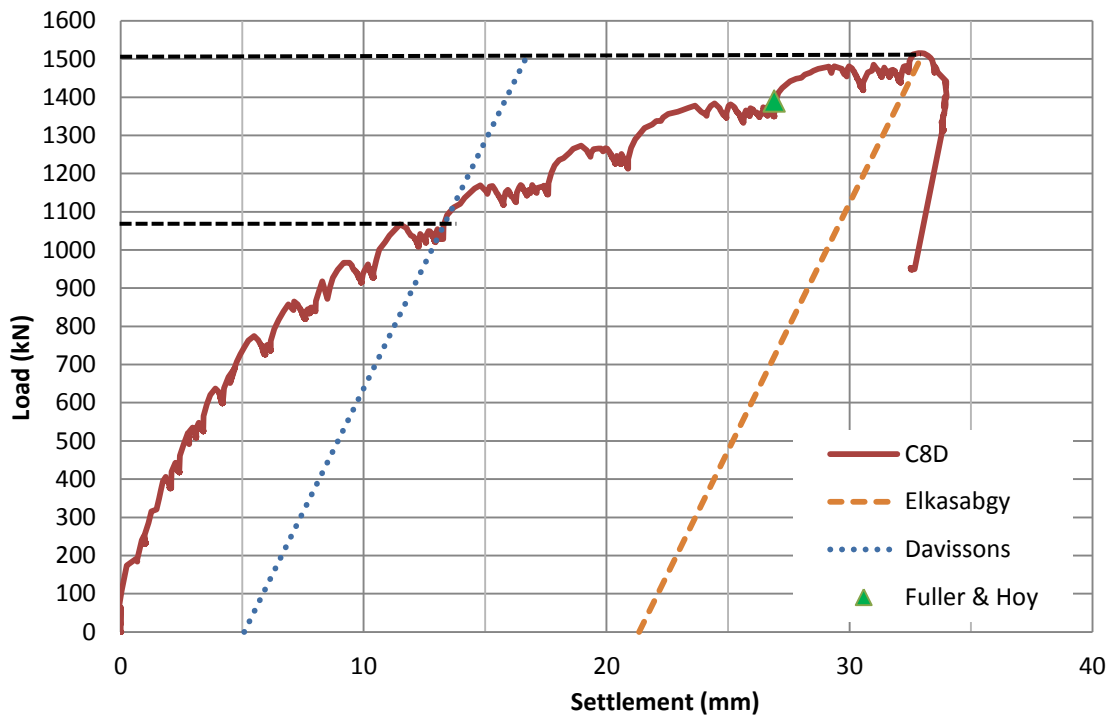


Figure 5-7: Load Settlement Curve for Test Pile C8D

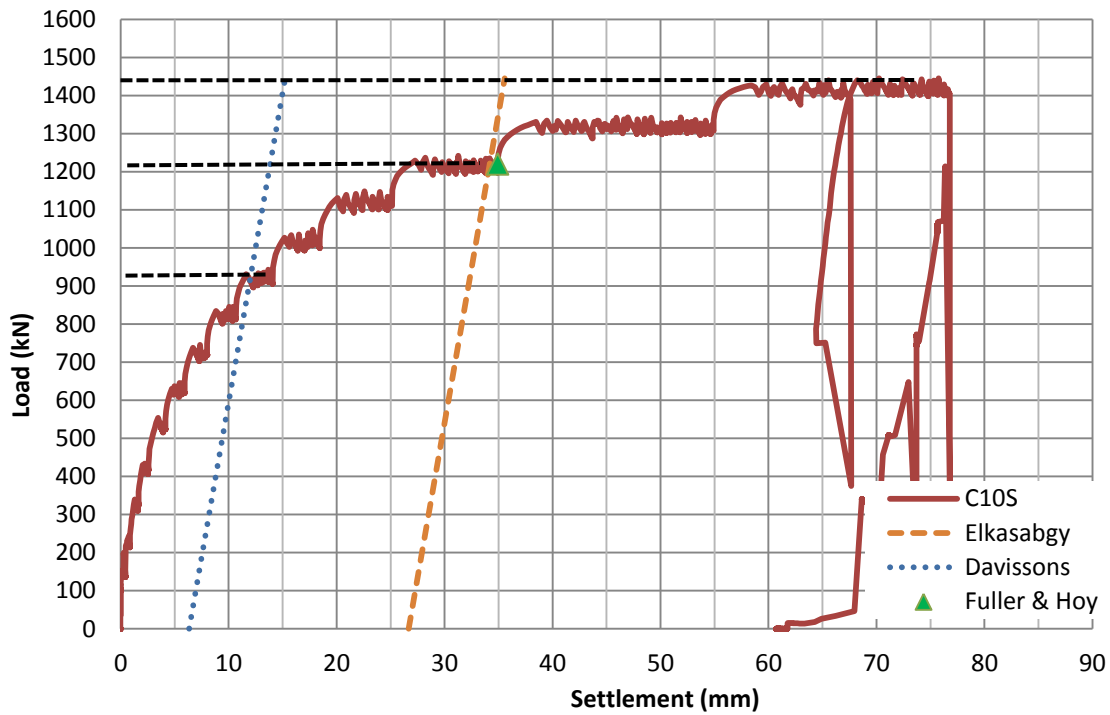


Figure 5-8: Load Settlement Curve for Test Pile C10S

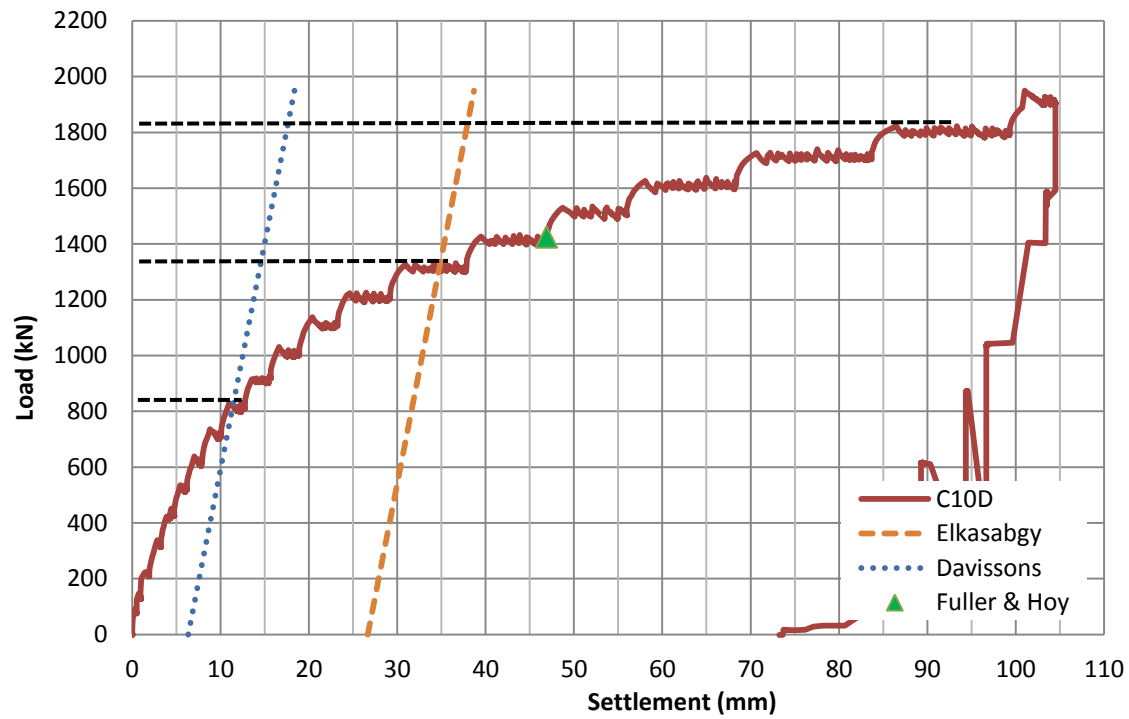


Figure 5-9: Load Settlement Curve for Test Pile C10D

5.5.2 Uplift Load Tests

Figure 5-10 shows the load-displacement of Pile T6S, which exhibited clear failure with a quickly terminating non-linear transition region. Failure occurred at 870 kN, while the interpreted ultimate capacities ranged between 720 and 837 kN, which occurred at displacements of 10.7 - 31.7 mm. Similarly, Pile T6D displayed recognizable failure as shown in Figure 5-11 with failure load of 982 kN. The interpreted ultimate capacities ranged between 870 – 982 kN, and the corresponding displacements ranged between 15.4 and 22.5 mm. Figures 5-12 and 5-13 present the results for piles T8S and T8D. Again, they show the same trends with failure loads of 1100 and 1380 kN, while the interpreted ultimate capacity varied from 970 to 1020 for T8S and from 1053 to 1276 kN. It is noted from the tension load tests that failure occurred at relatively smaller displacements. Consequently, the interpreted failure loads were much closer to the actual failure loads.

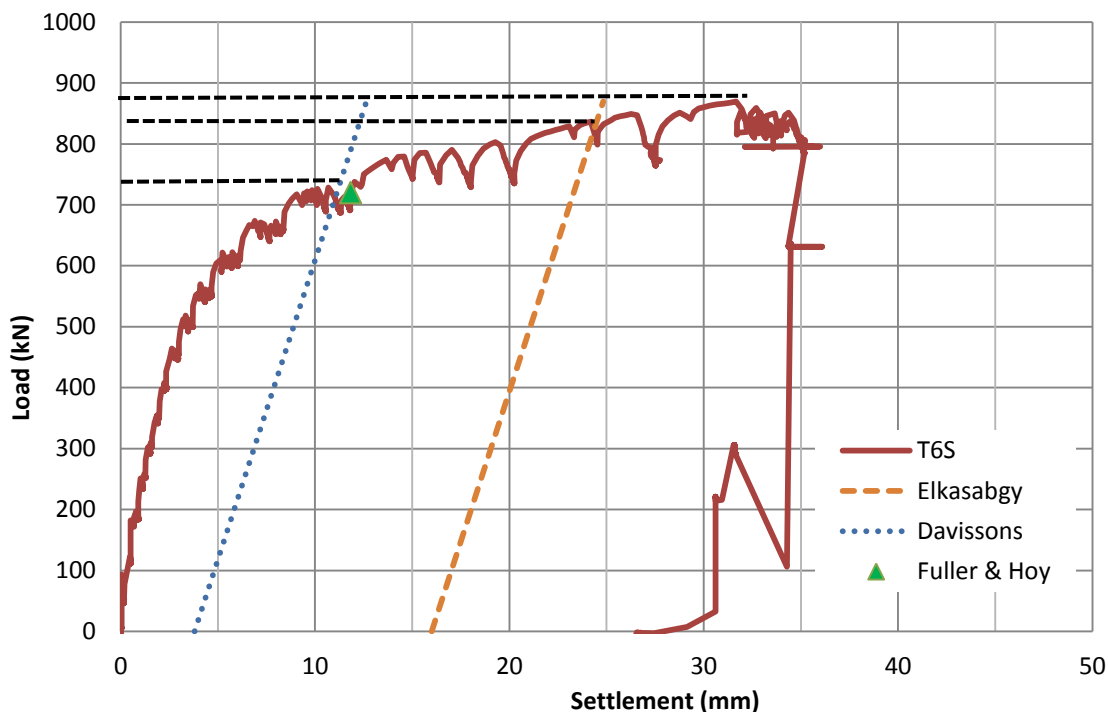


Figure 5-10: Load Settlement Graph Test Pile T6S

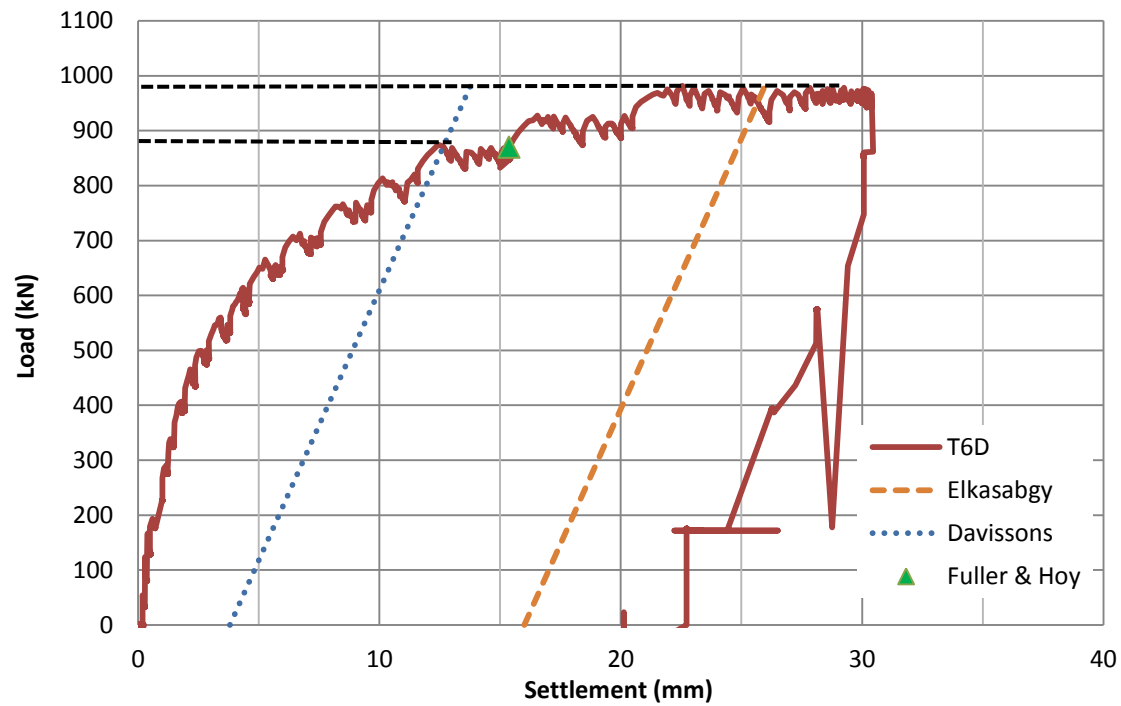


Figure 5-11: Load Settlement Curve for Test Pile T6D

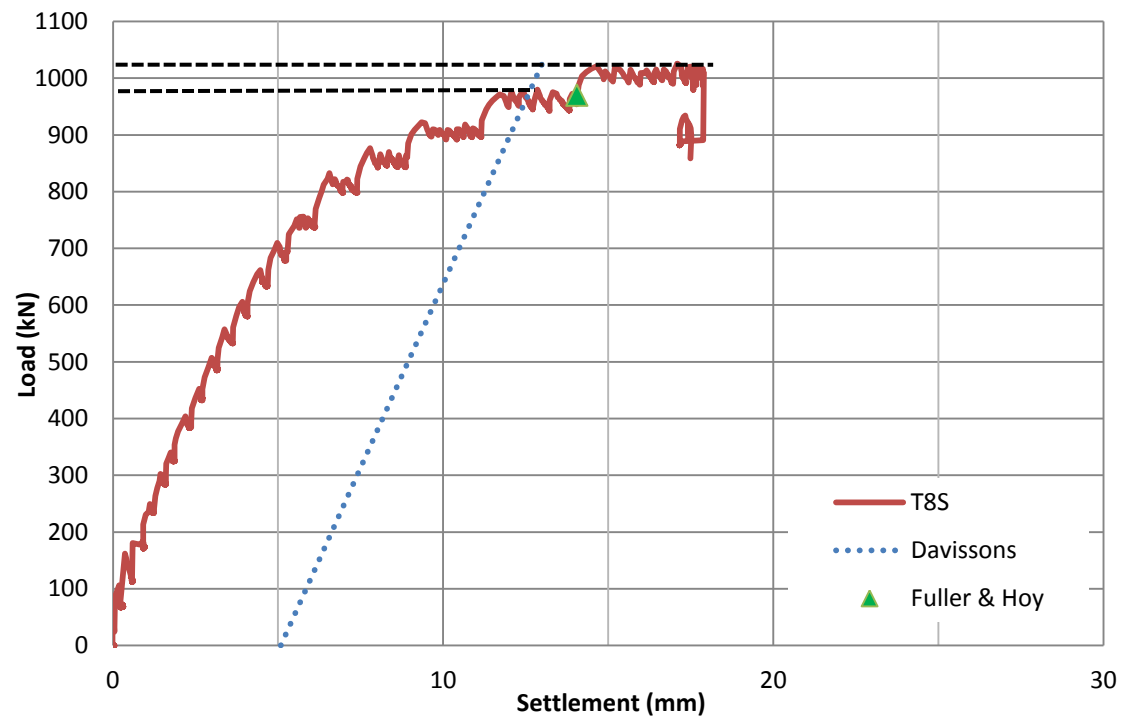


Figure 5-12: Load Settlement Curve for Test Pile T8S

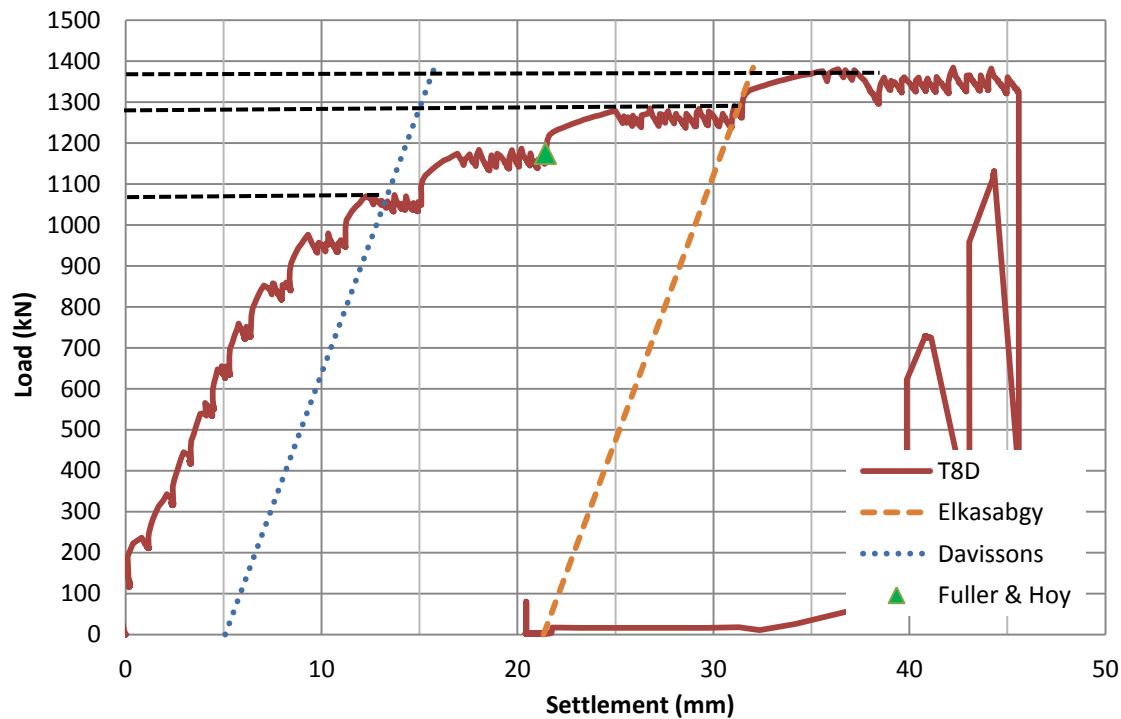


Figure 5-13: Load Settlement Curve for Test Pile T8D

5.5.3 Comparison of interpreted failure load criteria

The ultimate capacity of all tested piles determined from the different interpreted failure criteria are summarized in Figure 5-14 and in Table 5-1. As can be noted from the table and the figure, the ultimate capacity determined by the method proposed by Elkasabgy and El Naggar (2015) provided the closest capacity values to the plunging failure load, while the Davisson method provided the most conservative. In addition, the Fuller and Hoy (1970) method provided reasonable estimates of the pile ultimate load capacity.

It is also noted from Table 5-1 that the pile settlement corresponding to the plunging failure load ranged from 15 to 85 mm. In many cases, the capacity of the loading system and/or the range of settlement measurement devices do not allow the loading to proceed up to such large settlement. Therefore, the plunging failure may not be attained in many practical test setups. On the other hand, the settlement for the Elkasabgy and El Naggar and Fuller and Hoy criteria ranged from 19 to 34 and 11 to 46 mm, respectively. Thus, the interpreted failure criteria proposed by Elkasabgy

and El Naggar and Fuller and Hoy appear to be more appropriate for the determination of the capacity of large diameter helical piles. It is noted that the Fuller and Hoy criterion produces a more conservative estimate of the ultimate pile capacity, but it is based on the actual pile performance during the pile load test and not just the pile geometrical properties.

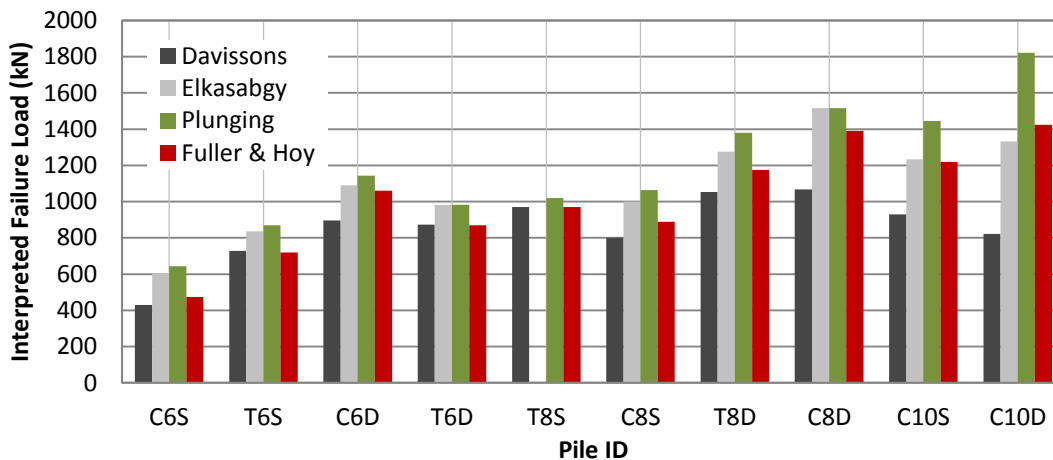


Figure 5-14: Comparison of Ultimate Failure Load from Different Criteria

Table 5-1: Ultimate capacity of tested piles

Pile ID	Average Install Torque - 3D (kNm)	Davisson		Elkasabgy & El Naggar		Plunging		Fuller & Hoy	
		Load (kN)	Set (mm)	Load (kN)	Set (mm)	Load (kN)	Set (mm)	Load (kN)	Set (mm)
C6S	46.7	430	7.2	605	19.3	644	25	475	11.4
C6D	54.5	896	12.6	1090	23.5	1144	27.4	1060	23
C8S	77.14	800	11.3	1000	29.1	1064	39.4	890	19.8
C8D	97.8	1067	11.5	1516	34	1516	34	1390	26.9
C10S	105.4	930	11.6	1233	34.1	1445	58	1220	34.9
C10D	121.8	822	11.3	1332	31.2	1822	85.1	1425	46.9
T6S	49.7	728	10.7	837	24.2	870	31.7	720	11.8
T6D	61.7	874	12.43	982	22.5	982	22.5	870	15.4
T8S	71.7	971	11.7	-	-	1020	15.2	970	14.1
T8D	92.6	1053	13.1	1276	31.32	1380	35.8	1175	21.4

5.6 Capacity-Torque-Correlations

Undoubtedly, plunging failure is universally accepted method to determine the pile ultimate capacity. However, as discussed above, plunging failure may not be attained because of test setup limitations and/or significant creep displacement of the test pile. In this case, it is necessary to select a suitable interpreted failure criterion for determining the pile ultimate capacity values to be used to establish CTC factors. An interpreted failure criterion that utilizes a suitable settlement tolerance (e.g. Elkasabgy and El Naggar) may be employed. However, settlement criteria may not always be valid for varying pile geometry. Alternatively, criteria based on the actual pile performance during the load test are applicable to different pile geometry (e.g. Fuller and Hoy), and may be more appropriate for varying soil conditions.

5.6.1 CTC factors

The ultimate capacity of the tested piles determined from the plunging failure and the interpreted failure criteria were used to evaluate the CTC factors. The calculated values are presented in Table 5-2. It can be noted from Table 5-2 that the CTC factors varied from 6.7 to 16.4 for Davisson, 13.0 to 21.0 for Elkasabgy and El Naggar, 13.8 to 21.0 for Plunging, and 10.2 to 19.4 for Fuller and Hoy criteria. It is also noted that the CTC factors for double helix piles were slightly higher than those for the single helix piles for the same pile diameter. Finally, there is no significant difference between the CTC factors for piles in tension versus compression, perhaps because all tension piles were installed under deep embedment condition.

Given the closeness of the pile ultimate capacity and CTC factors determined using the Fuller and Hoy with those obtained from the plunging failure, it is suggested to use the Fuller and Hoy criterion to establish the pile capacity values from the load test data. These ultimate capacity values are then used to establish the CTC factors.

Table 5-2: Summary of correlation of torque to capacity factors

Pile ID	Average Install Torque - 3D (kN*m)	Davisson		Elkasabgy & El Naggar		Plunging		Fuller & Hoy	
		Load (kN)	K_t (m^{-1})	Load (kN)	K_t (m^{-1})	Load (kN)	K_t (m^{-1})	Load (kN)	K_t (m^{-1})
C6S	46.7	430	9.2	605	13.0	644	13.8	475	10.2
C6D	54.5	896	16.4	1090	20.0	1144	21.0	1060	19.4
C8S	77.14	800	10.4	1000	13.0	1064	13.8	890	11.5
C8D	97.8	1067	10.9	1516	15.5	1516	15.5	1390	14.2
C10S	105.4	930	8.8	1233	11.7	1445	13.7	1220	11.6
C10D	121.8	822	6.7	1332	10.9	1822	15.0	1425	11.7
T6S	49.7	728	14.6	837	16.8	870	17.5	720	14.5
T6D	61.7	874	14.2	982	15.9	982	15.9	870	14.1
T8S	71.7	971	13.5	-	-	1020	14.2	970	13.5
T8D	92.6	1053	11.4	1276	13.8	1380	14.9	1175	12.7

5.6.2 Capacity-Torque-Correlation Curve Fitting

The existing CTC formulations were developed based on investigations of large data sets that include the ultimate capacity of helical piles and their installation torque over the last 3D. These formulations either established a constant CTC factor (e.g. Hoyt and Clemence), or developed a CTC factor as a function of the pile diameter (e.g. Perko, 2009).

5.6.3 Evaluation of Capacity to Torque Correlation Factors

The CTC data obtained in this study is based on all tension and compressive interpreted failure loads determined using the Fuller & Hoy criterion and the torque measured over the last 3D. In addition, these results are augmented by the pile ultimate capacity and installation torque values reported by Tappenen (2007) for large diameter helical piles installed in similar soil profile (i.e. sand/glacial till). This helped increase the data set used to establish a suitable CTC relation for helical piles installed in glacial tills.

Figure 5-15 presents the CTC factors established by directly correlating the pile capacity to its installation torque. The obtained CTC factor, $K_t = 10.3$ has a coefficient of determination of 0.8379. This CTC factor appears to give slightly conservative predictions of helical piles installed in glacial till but perhaps appropriate for sandy soils.

Figure 5-16 presents the direct capacity to torque factors plotted vs the pile diameter, and the curve fitting of the data used the pile diameter as a fitting parameter. The lines of best fit for glacial till, sand, and all data compiled are used to establish a CTC relationship incorporating the pile diameter as a fitting parameter. For the purpose of comparison, the CTC relationship provided by Perko (2009) is plotted in Figure 5-16. It is observed from the figure that there is close agreement between the best fit for all data and Perko (2009), especially for larger diameter piles. This agreement suggests that the Perko relationship can be used to predict the capacity of helical piles in different types of soils.

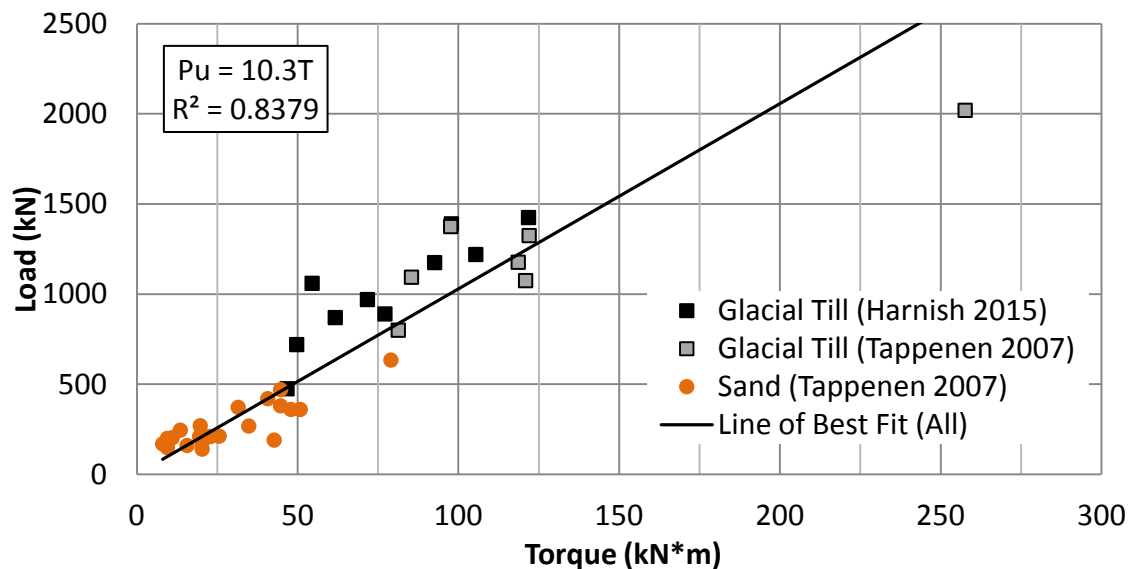


Figure 5-15: Direct Torque –to –Capacity Correlation

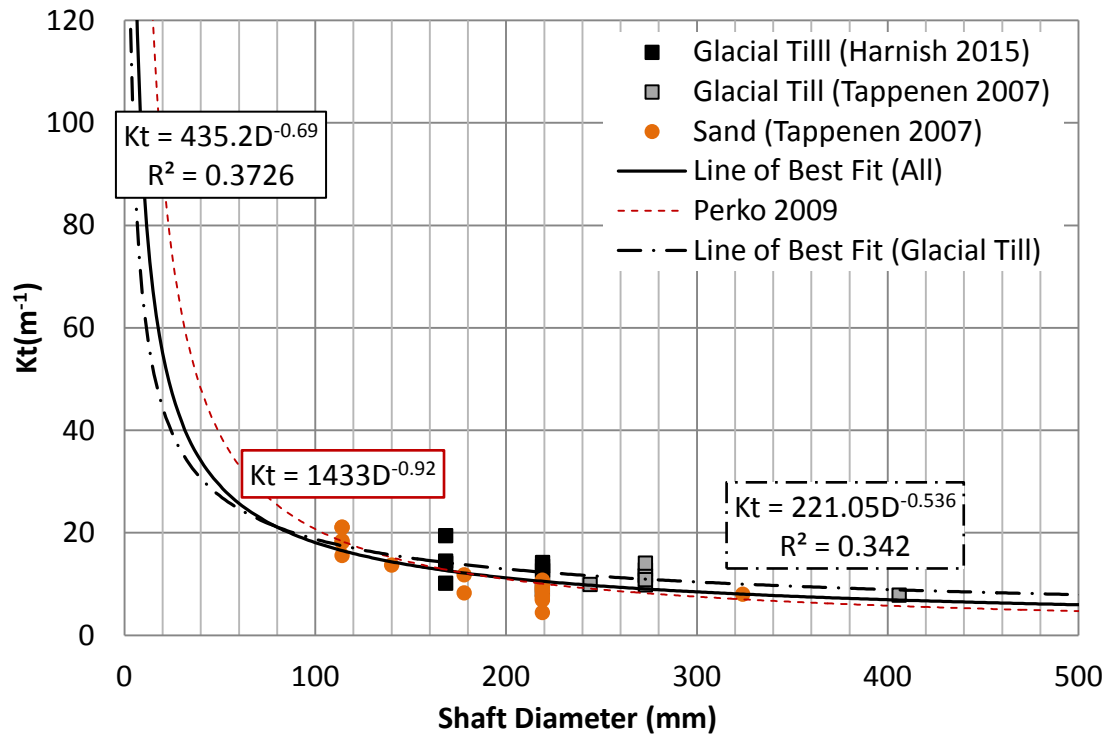


Figure 5-16: Torque to Capacity vs Shaft Diameter

5.6.4 Proposed Capacity to Torque Correlation Using Pile Embedded Area

The main limiting factor of the above formulations is that they do not account fully for the helical pile configuration (i.e. pile diameter, helix diameter, number of helices). Utilizing the total embedded pile area as a fitting parameter would enable incorporating the pile diameter, number and diameter of helices, and depth of installation in curve fitting. Therefore, the use of pile embedded area as a curve fitting parameter in establishing CTC relationship is explored herein. This offers the option to subtract the surface area of the pile embedded within expected zones of very soft layers, which can even enhance the accuracy of CTC relationship.

Figure 5-17 shows the CTC factors plotted against the pile embedded area. The data is curve fitted considering the pile embedded area as a fitting parameter. Two best fit lines are attempted, one to fit all data and one to fit only glacial till data. As can be observed from Figure 5-17, the equation obtained curve fitting all data underestimates K_t for all the glacial till data points. On the other hand, as expected, the equation obtained by curve fitting only the glacial data

represents the glacial till data points reasonably well. Accordingly, it is suggested to use the equation that represents the CTC factor for helical piles installed in glacial till, i.e.

$$K_t = 27.64A_e^{-0.5} \quad (5-1)$$

where K_t (m^{-1}) is the torque to capacity factor, and A_e (m^2) is the total embedded area. It should be noted that Equation 5-1 is developed using a limited data set. It is recommended that additional work be done to expand the data set through testing additional pile configurations as well as soil type.

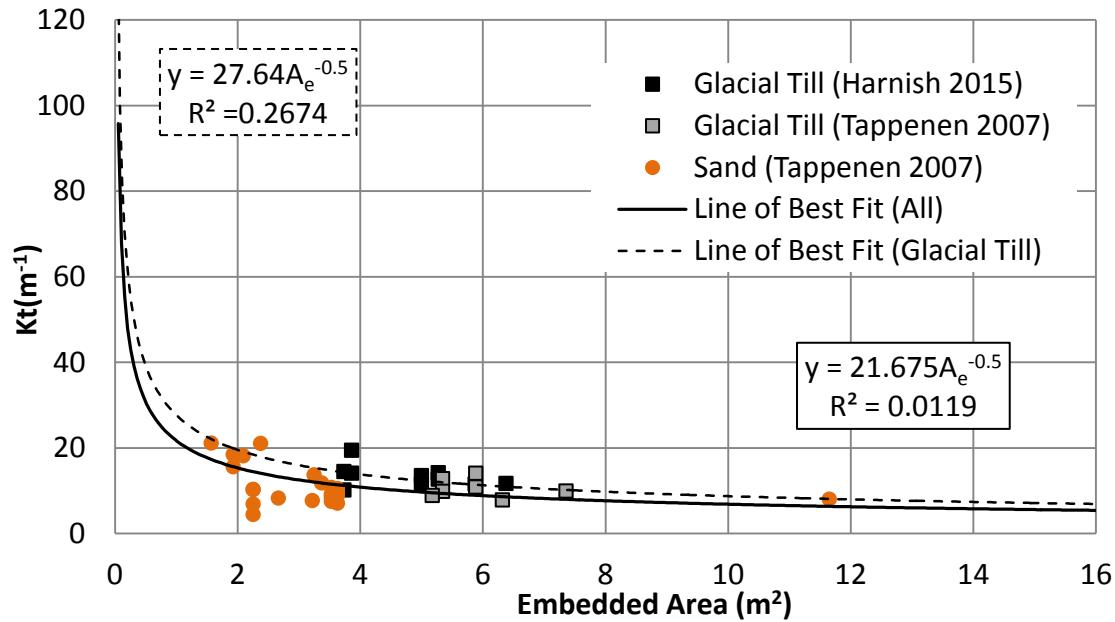


Figure 5-17: Torque to Capacity vs Embedded Area

5.7 Load Transfer Results

When load is applied to the head of a helical pile, it is transmitted to the soil through skin friction/adhesion along the pile shaft, and bearing on the helical plates and the pile toe. The distribution of this load depends on the pile geometry and soil stratification.

Seven test piles were instrumented with strain gauges to monitor the load transfer mechanism when subjected to vertical loads. The strain gauges were attached to the exterior pile wall at stations along the shaft and just above and just below the helices in order to monitor the shaft and helical loads. Each station had a pair of strain gauges. The locations of the strain gauge stations are indicated in Figure 5-18.

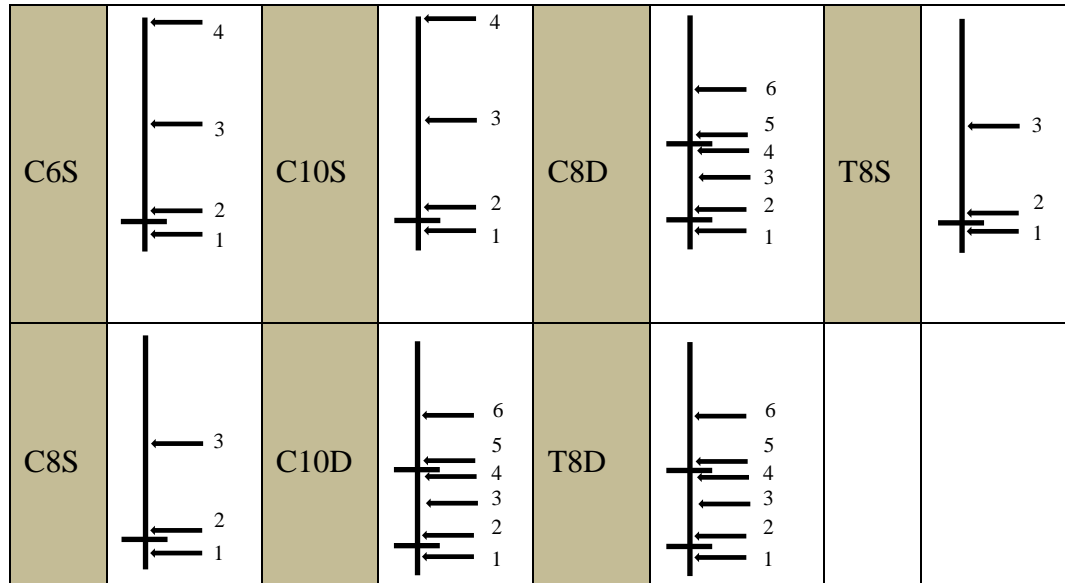


Figure 5-18: Locations of strain guage stations

The strain gauge measurements taken at each location are used to calculate the force at the pile cross-section of the strain gauge location, i.e.:

$$P_z = \epsilon A_p E_p \quad (5-2)$$

where; P_z is the pile calculated force, ϵ is the measured strain, A_p is the pile cross-sectional area, and E_p is the elastic modulus of the pile material. The results of strain gauge monitoring are analyzed to establish the load transfer mechanism for the test piles.

5.7.1 Load Transfer Curves for Piles Under Compression Loading

The pile force obtained from the strain gauge measurements by employing Equation 5-2, are used to establish the load transfer distribution along the pile shaft and through the helices.

Figure 5-19 shows the load transfer distribution for Pile C6S. As can be noted from Figure 5-19, the load at LV4 near the pile head is almost identical to the applied load, confirming the accuracy of the results. It is also noted from the figure that initially, the shaft transfers most of the load (the difference between loads LV4 and LV2). However, as the applied load increases, most of the load is transferred through the helix (the difference between loads LV1 and LV2) and the remaining load is transferred through the pile toe. Near failure, shaft resistance contributed approximately 15% of the load capacity, the helix provided 50% and the toe provided 35%. The large contribution of the toe resistance indicates it was well seated within the underlying hard soil between 7.0 and 8.0m depth (with $S_u > 500\text{kPa}$) as indicated in Figure 3-9.

Figure 5-20 shows the load transfer distribution for Pile C8S. Similar to Pile C6S, the load was initially taken by the shaft resistance (difference between LV2 and LV3). At the ultimate load, approximately 50% of the load resistance was provided by toe bearing while the helical plate provided only 20 %. Because the pile diameter is larger in this case, the shaft resistance provided a higher percentage contribution to the load carrying capacity, which amounted to 30% of the pile capacity. Again, the high percentage of load taken by the toe indicates it was situated in the hard material.

Figure 5-21 presents the load transfer for Pile C8D. The load was initially taken by the shaft, and at higher loads the shaft percentage contribution diminished. Near failure, the end/toe bearing provided only 15% of the total resistance while the lead helix provided approximately 21%. The resistance provided by the inter-helix zone (between the lead and top helices) accounted for 64% of the total resistance (difference between LV2 and LV4) as shown in Figure 5-21. It appears that very little capacity was provided by the shaft adhesion above the top helix.

As shown in Figure 5-22, Pile C10S derived its compressive resistance predominantly through end/toe bearing and helical bearing. The toe/end bearing provided approximately 26% of the total resistance while the lead helix provided near 40%. It can be noted from Figure 5-22 that the toe bearing was mobilized at the onset of loading while the lead helix was quickly mobilized once the load approached 300 kN. As the applied load approached failure, the toe resistance began to plateau and further capacity may have been attained via shaft friction.

Figure 5-23 shows that Pile C10D attained compressive capacity through lead helix bearing and shaft adhesion. Near failure, the lead helix provided approximately 62% of the total capacity, while the rear helix bearing and upper shaft friction accounted for a combined 35% of the total resistance. It can be noted from Figure 5-23 that toe/end bearing was mobilized at the onset of loading. As settlement and loading continued, the lead helix attracted significant portions of the applied load while the contribution of the toe capacity decreased. This decrease in toe resistance may be attributed to the breakthrough of a hard layer.

The general compressive load transfer mechanism revealed from these results indicate that the capacity of helical piles installed in over-consolidated glacial till is primarily provided via toe/end and lead helical bearing. This is attributed to the high stiffness and strength of soil within the helix/toe depth.

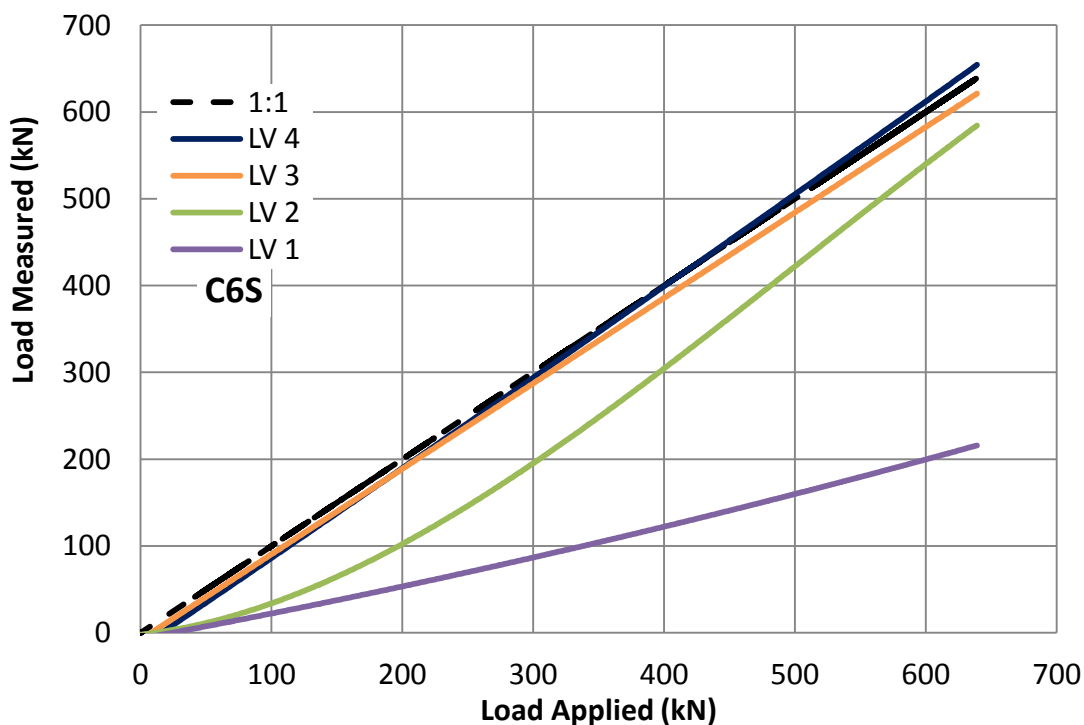


Figure 5-19: C6S Load Transfer Observations

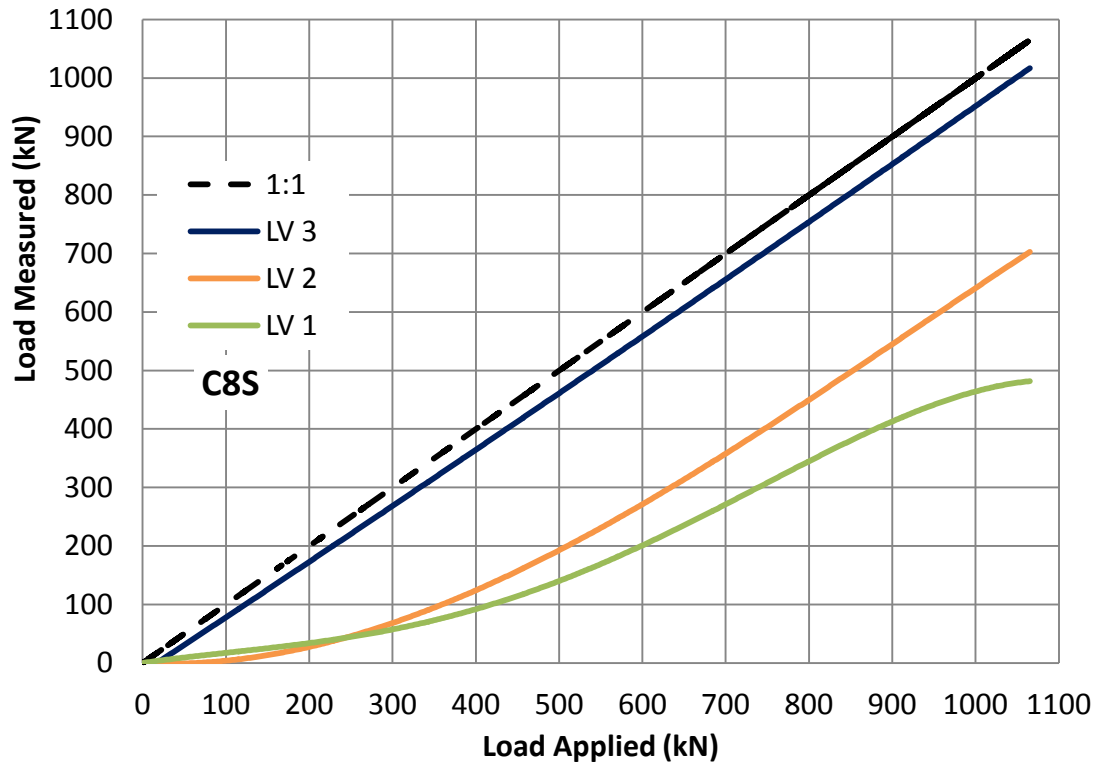


Figure 5-20: C8S Load Transfer Observations

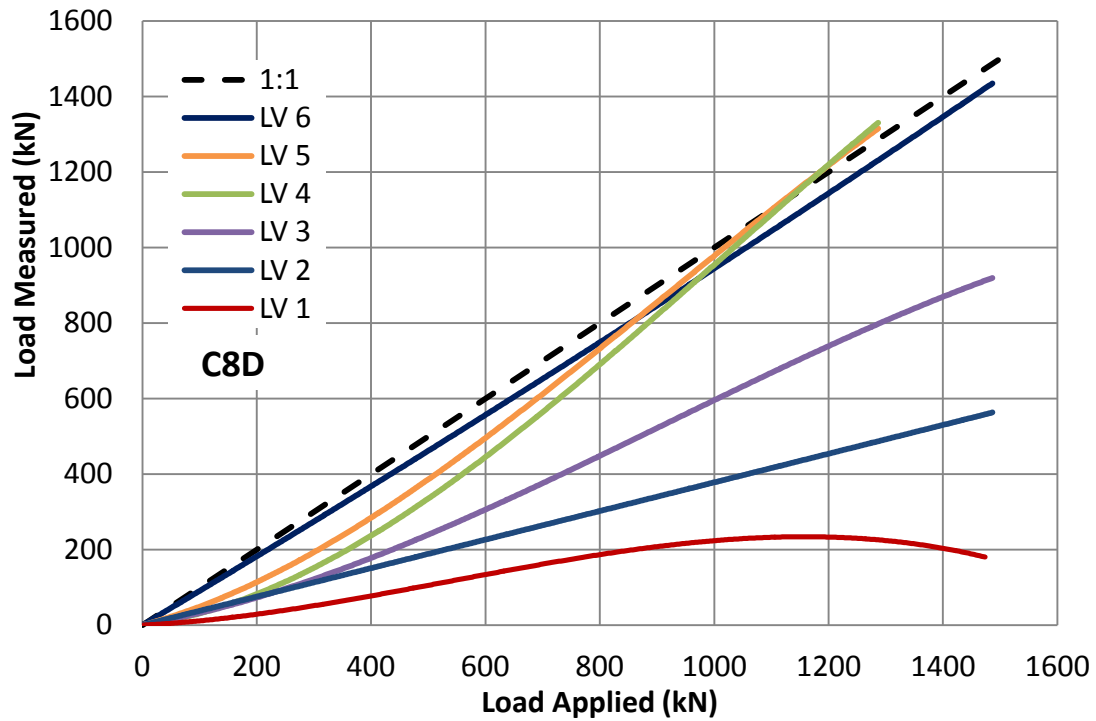


Figure 5-21: C8D Load Transfer Observations

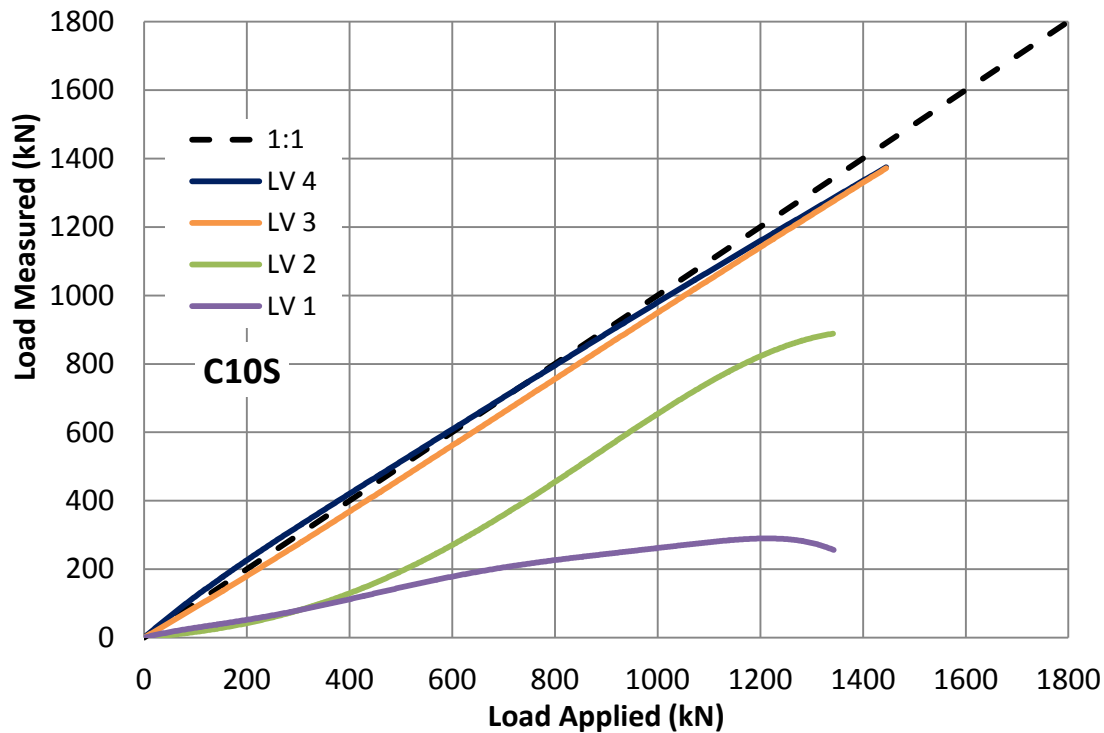


Figure 5-22: C10S Load Transfer Observations

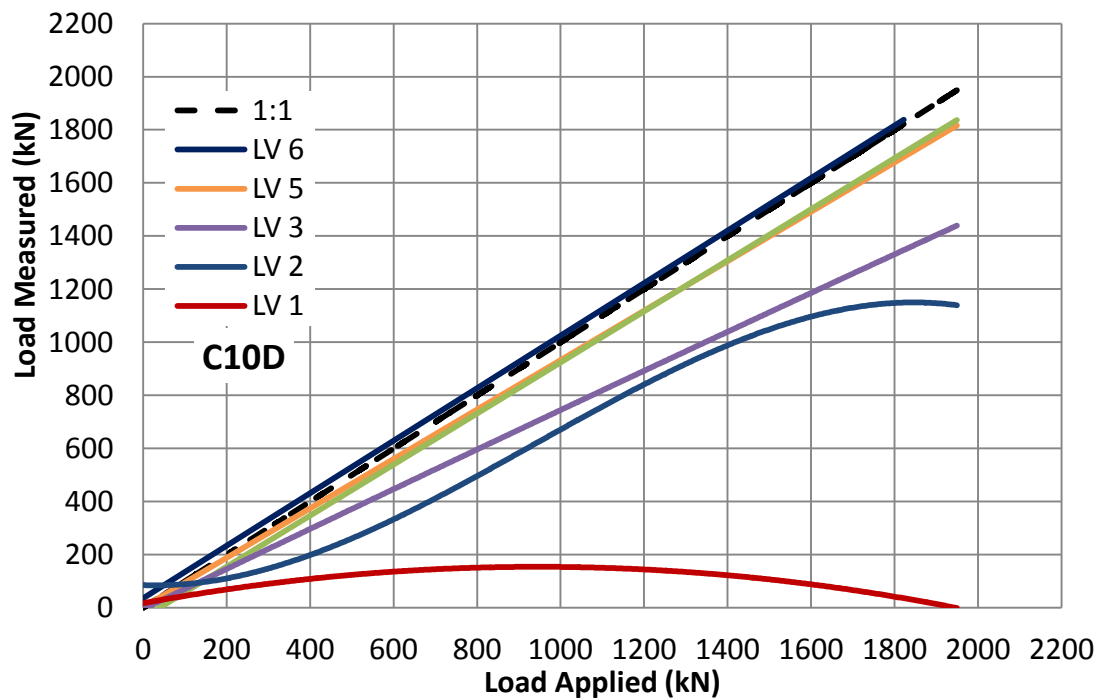


Figure 5-23: C10D Load Transfer Observations

5.7.2 Load Transfer Distribution for Piles Under Uplift Loading

Figure 5-24 presents the load transfer distribution for Pile T8S. Initially, the shaft provided most of the resistance. However, as the applied load increased, the shaft resistance and the anchoring (bearing) of the lead helix provided almost equal contributions to the total resistance. As indicated by Figure 5-24, the resistance provided by the helix increased dramatically as failure ensued. Figure 5-24 also shows the mobilization of the helix bearing did not initiate until the applied load reached approximately 400 kN. This is attributed to considerable soil disturbance just above the helix, which required some movement to re-establish firm contact between the helix and the soil. Near failure, the lead helix was fully engaged and provided 40% of the resistance while 60% was attributable to shaft resistance.

Figure 5-25 presents the load transfer curves for Pile T8D. The results demonstrate that the load was initially taken by the shaft resistance (up to an applied load of 600 kN). However, as the applied load increased the contributions from the top helix and the inter-helix zone increased. Near failure, the lead helix and inter-helix zone provided approximately 40 % and 15%, the rear helix about 20%, and the top shaft friction provided 25 %.

The tension load transfer mechanism indicated that the shaft contributed most of the load resistance initially. As the pile movement increased, the helix established firm contact with the soil above it, and its contribution to resistance eventually approached that attained from the shaft.

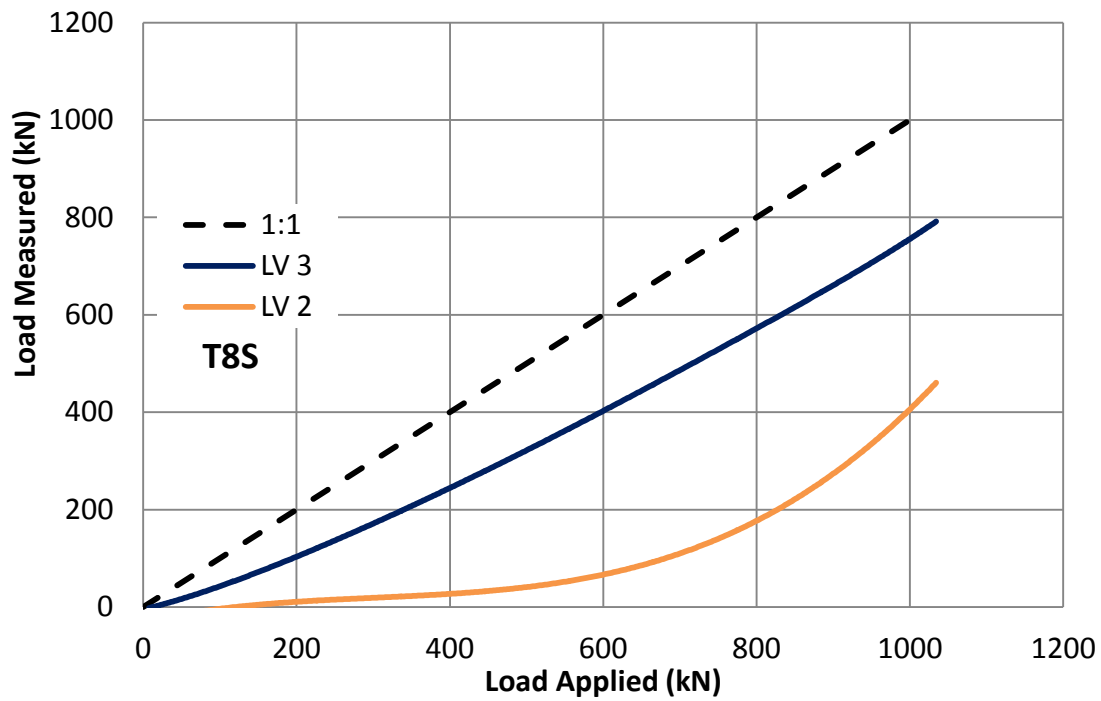


Figure 5-24: T8S Load Transfer Observations

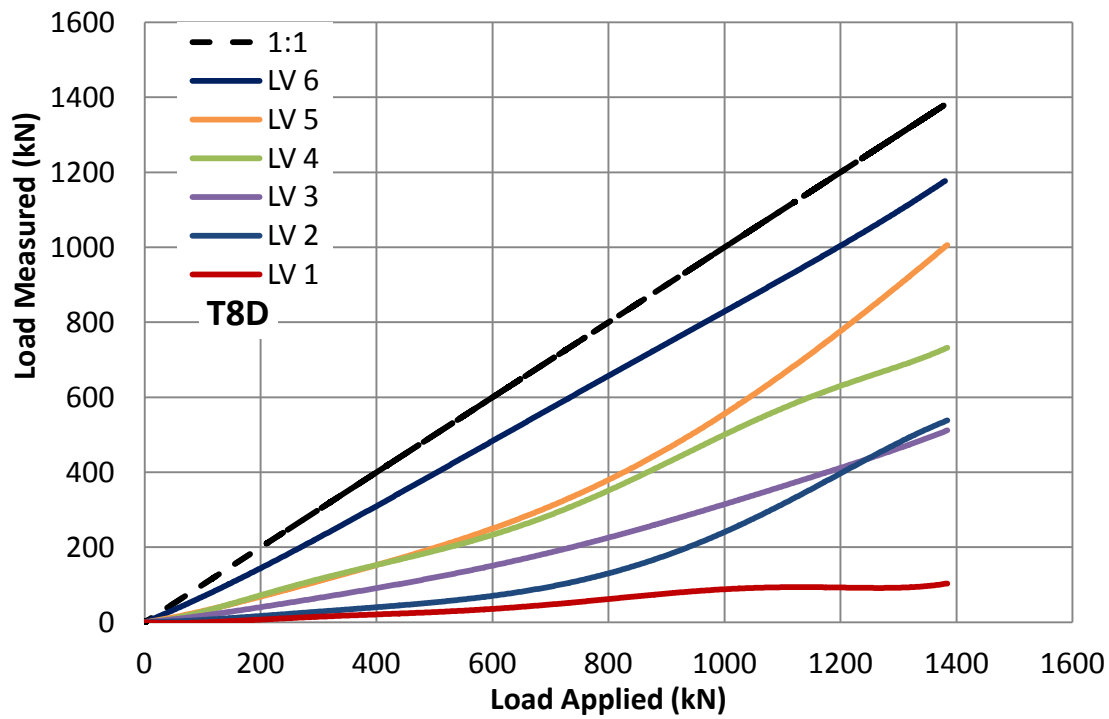


Figure 5-25: T8D Load Transfer Observations

5.7.3 Load Transfer Behavior

The changes in load distribution and load transfer mechanism were investigated by comparing the load transfer present corresponding to approximately 50 % and 100 % of the final interpreted failure load as summarized in Table 5-3-3.

For piles tested under compressive loading equal to 50% of its capacity, the shaft carried 33-60% of the applied load, and the lead helical plate and toe carried the balance roughly equally. At the ultimate load for single helix pile, the helical plate contribution increased by 8-33% while the shaft percentage of load decreased to only 15-30%. For the double helix pile, when the load approached the pile capacity, cylindrical shear was mobilized and contributed 33-64% of the resistance. It was observed that the rear helix in the double helical configuration piles did not contribute to load transfer.

For piles subjected to tension loading equal to 50% of its capacity, the shaft carried most of the load (59-99%). As the applied load approached the pile capacity, the lead helix and the inter-helical zone (cylindrical shear) proportion increased to 50-60%.

Given the presented data, it can be generally stated that at relatively small loads, the shaft carries most of the load, whereas at elevated loads a large percentage of the load is resisted by helical bearing. In addition, the percentage of load resisted by shaft friction in tension loading is higher than that for compressive loading, and represented significant contribution even at failure load. It is also noted that helical bearing is mobilized as the applied load increased (i.e. displacement/settlement increased). It is suggested that this settlement enabled the helical plate to compress any possibly disturbed soil within its zone of influence and hence transfer higher percentage of the applied load. Finally, when the lead helix and pile toe are embedded in very stiff/hard stratum, they provide most of the capacity which reduces load transfer through the rear helical plate.

Table 5-3: Load Transfer Summary

Pile ID	% of Max load	<u>Shaft Friction</u>			% Change	<u>Helical Plate Bearing</u>			% Change	Toe Bearing	% Change
		Above Rear Helix	Inter Helix			Lead	Rear				
C6S	50	33	-			33	-			33	
	100	15	-	-18	-	50	-	17	-	35	2
C8S	50	60	-			10	-			30	
	100	30	-	-30	-	20	-	10	-	50	20
C8D	50	9	52			13	0			26	
	100	0	64	-9	12	21	0	8	0	15	-11
C10S	50	35	-			30	-			26	
	100	28	-	-7	-	45	-	15	-	14	-12
C10D	50	6	29			44	0			21	
	100	5	33	-1	4	62	0	18	0	0	-21
T8S	50	99	-			11	-			-	
	100	61	-	-38	-	39	-	28	-	-	-
T8D	50	59	29			12	0			-	
	100	35	13	-24	-16	36	16	24	16	-	-

5.8 Accuracy of Capacity Prediction Approaches

It was found that the capacity of piles tested in this study could be predicted using three different approaches: theoretical calculation, empirical correlation to CPT measurements, and capacity to torque correlation. The accuracy of each method is discussed and compared.

The theoretical capacity was determined employing the individual plate bearing method (as inter-helical spacing was 3D), utilizing the average peak and remolded undrained shear strength presented in Table 3-2. The LCPC method (Bustamante and Ganeselli, 1982), which correlates the pile capacity to cone tip resistance as described in Section 2.2, was also used to predict the capacity of tested piles. Finally, pile capacity was predicted using the CTC relationships proposed by Perko (2009), Hoyt and Clemence (1989) and Tappenen (2007), as well as with the CTC factors developed in this thesis. All predicted capacities are summarized in Table 5-4.

Table 5-4: Predicted Capacity Summary

Pile Shaft Diameter (in)	Ultimate Calculated Capacity (kN)					
	6 5/8		8 5/8		10 3/4	
Helix Configuration (#, in)	Single 18"	Double 18"	Single 24"	Double 24"	Single 30"	Double 30"
IPB	865	1,057	1,330	1,661	1,776	2,223
LCPC	804	1,149	1,348	1,972	2,192	2,855
LCPC (mod)	570	790	941	1,256	1,576	1,959
K_t (9.22 m⁻¹) Tappenden	431	502	711	902	972	1,123
K_t (9.8 m⁻¹) Hoyt & Clarence	458	534	756	958	1,033	1,194
K_t (10.3)	481	561	795	1,007	1,086	1,255
K_t (27.64*A_e^{-0.5})	668	767	954	1,177	1,202	1,333
K_t (1433*D^{-0.92}) Perko 2009	599	699	776	984	867	1,001
K_t (221.05*D^{-0.536})	662	772	948	1,202	1,152	1,332

5.8.1 Individual Plate Bearing Predictions

In order to compare the accuracy of predictions, the ratio of predicted capacity (Q_p) to measured capacity (Q_u) is calculated.

Figure 5-26 shows the capacity calculated using the individual plate bearing method (IPB) as a ratio of the experimental pile capacity. It is noted from Figure 5-26 that using IPB method, Q_p/Q_u ranged from 1.00 to 1.82. The average over-prediction for all piles was 37% with coefficient of variation of 5%. This over-prediction is attributed to the use of unconservative soil shear strength (i.e. remolded strength even for the soil below helices) and/or reduced contributions of the two

helices due some overlapping. Perko (2009) and Hoyt and Clemence (1989) reported that the IPB is likely to over-predict pile capacity.

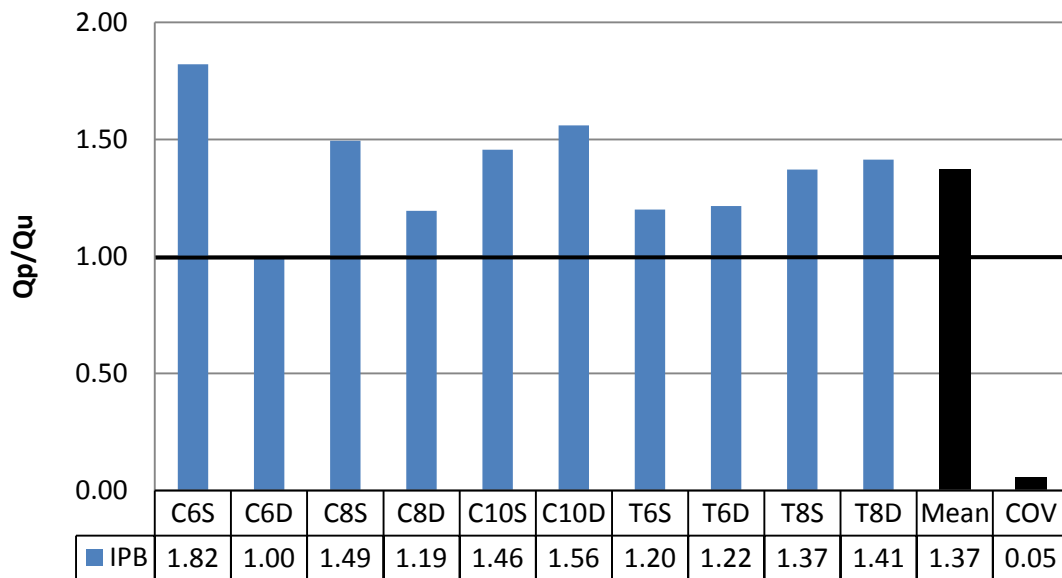


Figure 5-26: Individual Plate Bearing Prediction Ratio Q_p/Q_u

5.8.2 LCPC Method Predictions

The LCPC method correlates the pile capacity to the CPT tip resistance. All predictions were computed using the average CPT profile of CPT soundings 1, 2 and 3. As shown in Figure 5-27, the method over predicted the capacity by 8 to 200% of the measured capacity, with average prediction of 150% of the measured capacity and coefficient of variation of 9%. This over-prediction may be attributed to remolding the stiff clays/glacial tills, which was not accounted for in the LCPC method. Tappenen (2007) made similar observation and suggested that the LCPC method was not suitable for glacial tills.

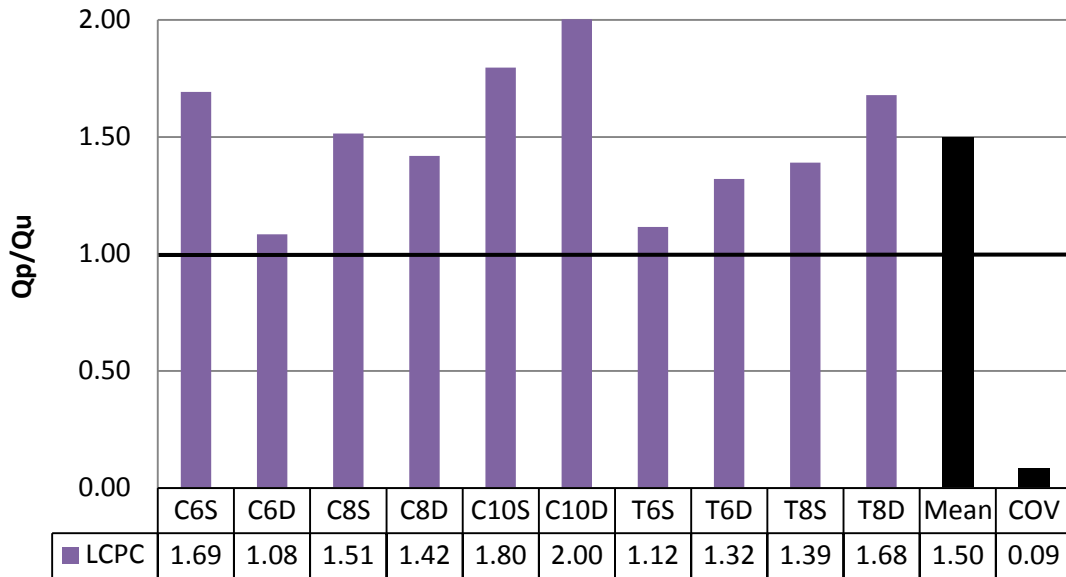


Figure 5-27: LCPC Method Prediction Ratio Q_p/Q_u

5.8.3 Modified LCPC Predictions

Tappenen (2007) recommended that the LCPC should be calibrated for glacial till soils. Thus, Tappenen (2007) suggested modifying the bearing coefficient term, k_c . Accordingly, $k_c = 0.30$ was used herein instead of the original value ($k_c = 0.45$). The predicted capacities using $k_c = 0.30$, shown in Figure 5-28, range from 75% to 137% of the measured capacities. The average prediction was 103% of the measured capacity with a coefficient of variation of 4%. This suggests that the LCPC method could be useful in predicting the helical pile capacity with “calibrated” k_c factors for different soil types, including glacial till.

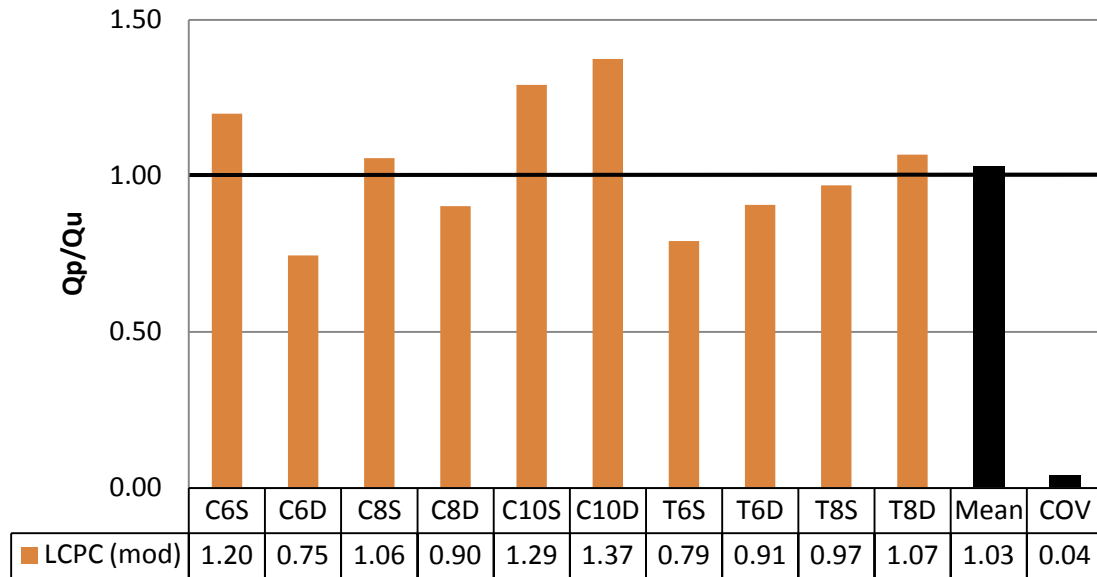


Figure 5-28: Modified LCPC Method Prediction Ratio Q_p/Q_u

5.8.4 Capacity to Torque Correlation Predictions

The CTC method was used employing six different correlations that use CTC factors (k_t) proposed by: Tapennan (2007), i.e. $K_t = 9.22 \text{ m}^{-1}$; Hoyt and Clemence (1989), i.e. $K_t = 9.8 \text{ m}^{-1}$; Perko (2009), i.e. $K_t = 1433 \times D^{0.92} \text{ m}^{-1}$; and present study, i.e. $K_t = 10.3 \text{ m}^{-1}$, $27.64 \times A_e^{-0.5} \text{ m}^{-1}$, and $513.36 \times D^{-0.727} \text{ m}^{-1}$. As shown in Fig. 5-29, most CTC predictions were below the measured capacity (i.e. conservative). The average Q_p is 0.71-0.98 Q_u , and the coefficient of variation ranged from 0.01 to 0.03. The results demonstrate the suitability of CTC method for design confirmation of large diameter helical piles as it gives consistently conservative and reasonably accurate prediction in comparison with theoretical calculations and CPT correlations.

A closer look at the results reveals that the average Q_p using CTC factors that do not account for pile geometry is 0.71-0.79 Q_u , while the CTC factors that account for the pile embedded area or pile shaft diameter resulted in more accurate average $Q_p = 0.82$ -0.98 Q_u . For example, Perko (2009) predicted $Q_p = 0.70$ -1.26 Q_u , as shown in Figure 5-29, with average $Q_p = 0.82 \text{ } Q_u$ and a coefficient of variation of 0.03. Furthermore, as expected, the site specific CTC factors provided enhanced accuracy, e.g. the relation based on the pile embedded area proposed in the current study.

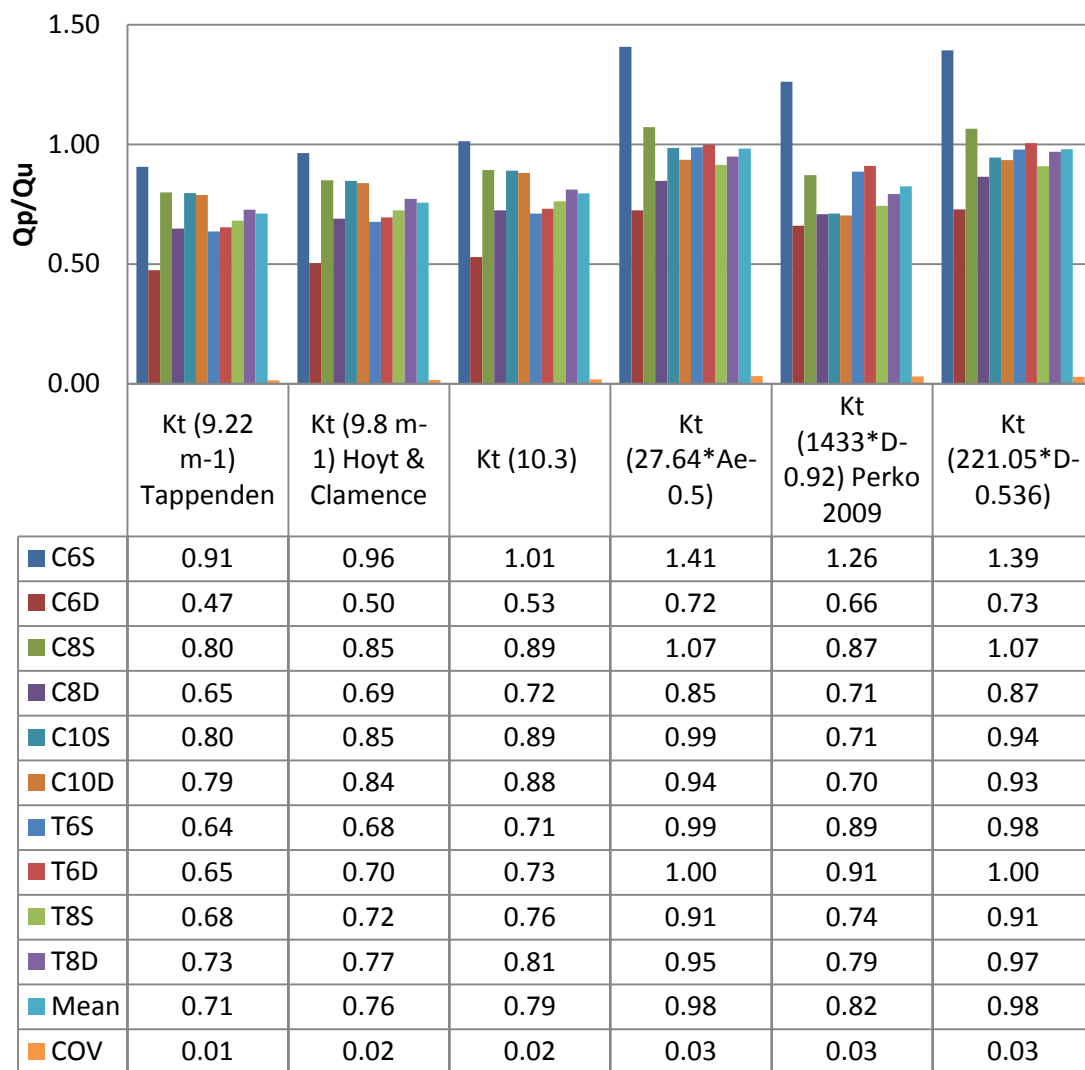


Figure 5-29: Torque-to-Capacity Prediction Ratio Q_p/Q_u

Desk design methods, whether theoretical or empirical, are based on often limited soil investigation data, which may not accurately reflect effects of pile installation on soil strength, or empirical correlations (e.g. correlations to SPT or CPT testing). As demonstrated in Figure 5-30, the individual plate bearing theory may dangerously over predict the pile capacity if proper remolded shear strength is not accounted for. It is suggested to utilize properly evaluated remolded shear strength in the IPB method. Similarly, the LCPC method seriously over-

predicted the pile capacity, again, because it does not account for soil strength reduction associated with pile installation. This can be practically accounted for by “calibrating” the bearing factor, k_c , to reflect site specific conditions. For example, it is suggested to use k_c value of 0.3 (LCPC mod) for helical piles installed in glacial tills.

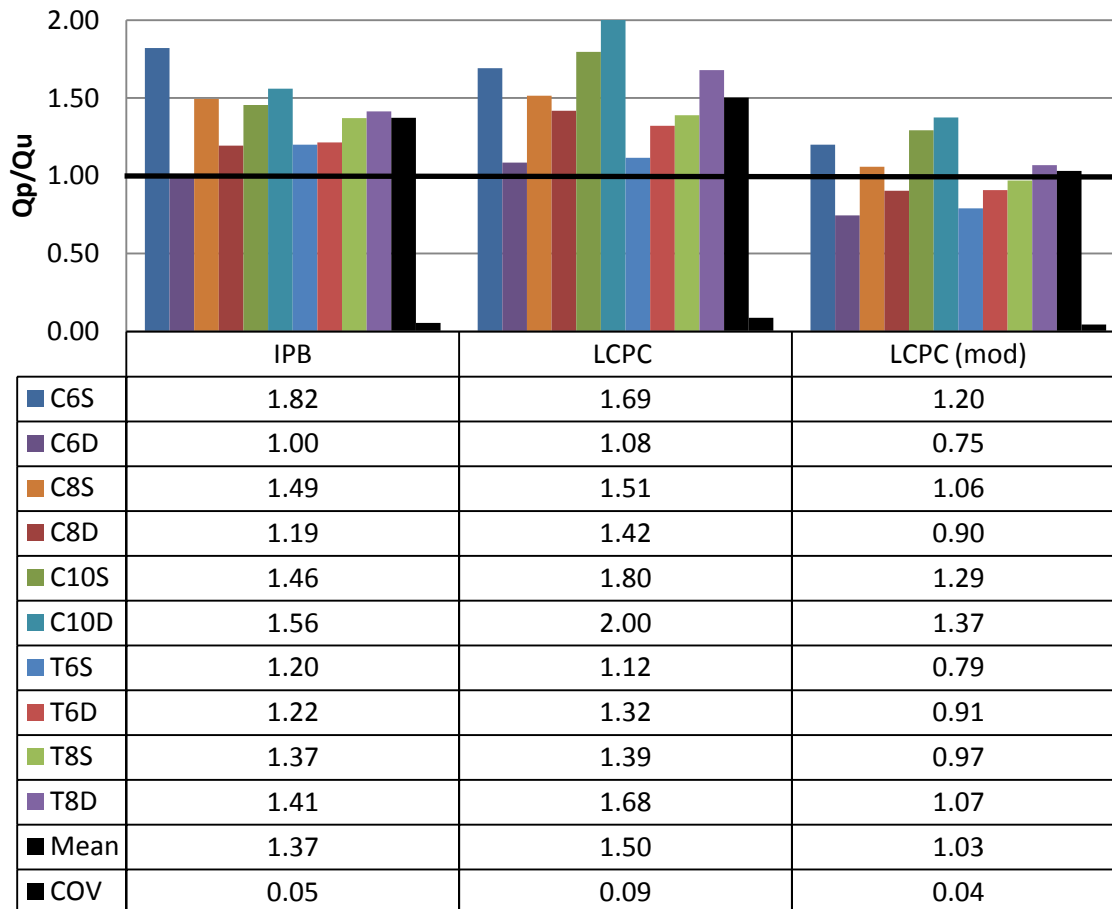


Figure 5-30: Comparison of Desk Design Prediction Ratio Q_p/Q_u

Chapter 6

6 Summary

In this study, a total of 17 helical piles with varying configurations were installed at a site consisting primarily of over-consolidated glacial till. All pile installations were monitored and the variations of installation torque, vertical crowd, and installation rate with depth were recorded. Six static compression load tests and four static tension load tests were conducted to establish the piles ultimate capacity. Seven test piles were fully instrumented to evaluate the load transfer behavior. The following conclusions may be drawn.

6.1 Conclusions

Installation Force Observations:

1. The installation torque measurements obtained by using the fabricated torque pin were demonstrated to be accurate and repeatable.
2. The installation rate (rotational speed) can have significant effect on the value of torque measured when employing hydraulic pressure gauge readings. It is recommended that a maximum speed of 5 RPM be maintained when taking the hydraulic pressure readings for torque measurement. However, this may differ depending on the machinery/pressure gauge combination.
3. The installation torque required to advance a helical pile is directly related to the pile embedded area and the soil shear strength. The torque can be estimated by integrating the soil resistance over the pile shaft and the helices (i.e. Eq. 4-7). The lead and rear helix torque contributions should be calculated using the peak undrained shear strength of the soil, while the pile shaft torque contribution should be calculated employing the remolded undrained shear strength of the soil.

Torque to Capacity Correlations:

4. Based on the measured pile capacities and installation torque obtained in the current study, three different CTC factors can be suggested for large diameter helical piles installed in sand and/or glacial till. They are as follows:

Sand & glacial till:

$$K_t = 10.3$$

direct correlation

$$K_t = 1433D^{-0.92} \quad \text{function of largest helix diameter (Perko, 2009)}$$

Glacial till

$$K_t = 27.64A_e^{-0.5} \quad \text{function of pile embedded area}$$

Static Axial Pile Testing:

1. The ultimate capacity of large diameter helical piles can be determined from the pile load test data employing the interpreted ultimate failure loads using the Elkasabgy and El Naggar (2015) and Fuller & Hoy (1970). Both criteria provided reasonable predictions for both compressive and tensile static pile capacity.
2. Significant settlement may be required to mobilize the bearing resistance provided by the lead helix for both compressive and tensile loading conditions. Furthermore, the rear helix provides significant additional capacity under compression loading and little additional capacity under tensile loading.

6.2 Recommendations for Future Work

1. The effects of vertical pressure (Crowd) on the generation of installation torque and thereby the validation of CTCs, are not entirely clear. Installation force monitoring investigated within this study indicates a clear trend in whereby crowd and torque increased almost proportionally to each other. It would be interesting to conduct installations while intentionally changing the crowd at the same depth and record the corresponding torque to better evaluate the effect of the crowd on the generated torque. Additionally, further experimental installation should be attempted whereby the applied crowd is held constant and/or minimized.
2. The residual axial loads locked in a helical pile post installation are assumed to be insignificant. However, the magnitude of applied crowd and some disparity observed

within the load transfer results indicate that there could be some axial residual load which should be accounted for when evaluating load transfer. This should be further investigated.

3. Experimental investigations similar to the current study should be attempted in different soil types and varying soil strength profiles. The results from such studies can be used to confirm the findings from this study (e.g. the method to calculate installation torque), and to calibrate the proposed CTC factor as a function of embedded pile area.
4. The results demonstrated that the individual plate bearing theory and the LCPC method can significantly over predict helical pile capacity in structured soils such as glacial till. The values of the shaft adhesion factor and the bearing capacity factors used in both methods should be evaluated for different types of soils, especially soils that are susceptible to significant remolding associated with helical pile installation.

References

- Abdelghany, Y. (2008). *Monotonic and Cyclic Behaviour of Helical Screw Piles Under Axial and Lateral Loading*. London, O.N.: The University of Western Ontario.
- Bradka, D. T. (1997). *Vertical Capacity of Helical Screw Anchor Piles*. Edmonton: University of Alberta.
- Bradka, T., & Kasprick, B. (2013, May 24). Personal communication.
- Bustamante, M., & Gianselli, L. (1982). Pile Bearing Capacity by Means of Static Penetrometer CPT. *Proceeding of the 2nd European Symposium on Penetration Testing*. 2, pp. 493-500. Amsterdam: Balkema Publisher.
- Butler, H., & Hoy, H. (1977). *Users Manual for the Texas Quick-Load Method for Foundation Load Testing*. Washington, D.C.: US Department of Transportation, Federal highway Administration.
- Canadian Geotechnical Society. (2006). *Canadian Foundation Engineering Manual 4ed*. Richmond, B.C: BiTech Publishers Ltd.
- Davisson, M. T. (1973). High Capacity Piles. *Proceeding of the Lecture Series, Innovations in Foundations Construction* (p. 52p). Illinois: ASCE.
- Elkasabgy, M. (2011). *Dynamic and Static Performance of Large-Capacity Helical Pile in Cohesive Soils*. London, O.N.: The University of Western Ontario.
- Elkasabgy, M. and El Naggar, M.H. 2015. Axial Compressive Response of Large-Capacity Helical and Driven Steel Piles in Cohesive Soil. *Canadian Geotechnical Journal*, Vol. 52, No. 2, pp. 224-243.
- Elsherbiny, Z. (2011). *Axial and Lateral performance of Helical Pile Groups*. London, O.N.: The University of Western Ontario.
- Fuller, F., & Hoy, H. (1970). *Pile Load Tests Including Quick-load Test Method Conventional Methods and Interpretations*.

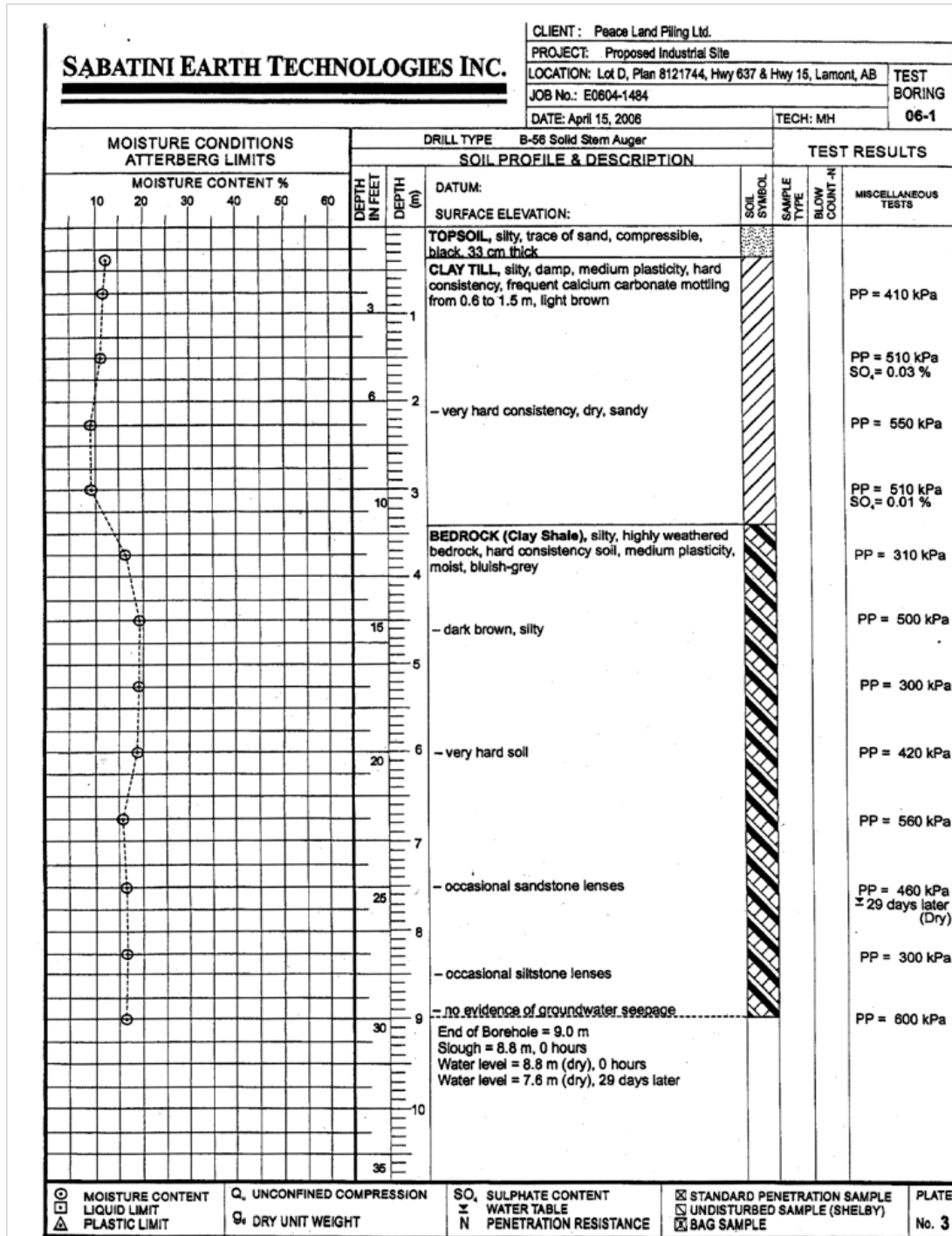
- Ghaly, A., & Clemence, S. (1998). Pullout Performace of Inclined Helical Screw Anchors in Sand. *Journal of geotechnical and Geoenvironmental Engineering*, 617-627.
- Ghaly, A., & Hanna, A. (1991). Experimetnal and theoretical studies on installation torque of screw anchors. *Canadian Geotechnical Journal*, 353-364.
- Hoyt, R. M., & Clemence, S. P. (1989). Uplift Capacity of Helical Anchors in Soil. *12th Internation Conference on Soil Mechanics and Foundation Engineering*, (pp. 1-12). Rio de Janiero, Brazil.
- Kulhawy, F. H. (2004). On the axial behaviour of drilled foundations. *American Society for Civil Engineering: Geo Support*.
- Kulhawy, F. H., & Hirany, A. (2009). Interpreted Failure Load for Drilled Shafts via Davisson and L1- L2. *2009 International Foundation Congress and Equipment Expo: Contemporary Topis in Deep Foundations*, (pp. 127-135).
- Kyfor, Z., Schnore, A., Carlo, T., & Baily, P. (1992). *Static Testing of Deep Foundations*. Washington: U.S. Department of Transportation: Federal Highway Administration.
- Livneh, B., & El Naggar, M. H. (2008). Axial testing and numerical modeling of square shaft helical piles under compressive and tensile loading. *Canadian Geotechnical Journal*, 1142-1156.
- Lunne, T., Robertson, P. K., & Powell, J. (1997). *Cone Penetration Testing : In Geotechnical Practice*. London UK: Blackie Academic and Professional.
- Meigh, A. C. (1987). *Cone Penetration Testing: methods and Interpretation*. Letchworth U.K: Adlard & Sons Ltd.
- Meyerhof, G. (1951). The Ultimate Bearing Capacity of Foundations . *Geotechnique*.
- Meyerhof, G. G. (1976). Bearing Capacity and Settlnent of Foundations. *Journal of Geotechnical and Geoenvironmental Engineering*, 195-228.

- Mitsch, M., & Clemence, S. (1985). The Uplift Capacity of Helix Anchors in Sand. . *Uplift Behaviour of Anchor Foundations in Soil*, (pp. pg 26-47). Michigan.
- Mooney, J. S., Clemence, S. P., & Adamczak . (1985). Uplift Capacity of helix Anchors in Clay and Silt. *American Scociety of Civil Engineering*, 48-72.
- Narasimha Rao, S., & Prasad, Y. (1993). Estimnation of uplift capacity of helical anchors in clays. *Journal of Geotechnical Engineering*, 352-357.
- O'Neill, M., & Reese, L. (1999). *Drilled Shaft: Construction, procedures and design methods*. FHWA-IF-99-025.
- Perko, H. A. (2001). Energy method for Predicting Installation Torque of Helical Foundation and Anchors. *GeoDenver: Geotechnical Special Publications*. Reston: ASCE Press.
- Perko, H. A. (2009). *Helical Piles: A Practical Guide to Design anf Installation*. New Jersey: John Wiley & Sons.
- Prakash, S., & Sharma, H. (1990). *Pile Foundation In Engineering Practice*. Toronto: John Wiley & Sons.
- Radhakrishna, H. (1976). *Helix Anchor Tests in Sand*. Ontario Hydro Research Division.
- Ramsey Industries. (2014). *Eskridge - Gear Drive, Brakes, Diggers and Anchor Drives*. Retrieved January 25, 2014, from Diggers: Product Specifications: <http://www.eskridgeinc.com/diggers/diggerprodspecs.html>
- Roberston, P., Campanella, R., Gillespie, D., & Greig, J. (1986). Use of piezometer cone data. *Proceedings of the ASTM Specialty Conference In Situ '86: Use of in situ tests in geotechnical engineering* (pp. 1263-1280). ASCE.
- Robertson , P. K. (1990). Soil classification using the cone penetration test. *Canadian Geotechnical Journal*, 151-158.
- Robertson, P. K. (2009). Interpretation of cone penetration tests - a unified approach. *Canadian Geotechnical Journal*, 1337-1355.

- Rogers, W. (2012). *Theoretical Installation Torque for Helical Pipe Piles - Part 1: Single Helix - Homogeneous Soils*. Quality Anchor Products Inc.
- Sakr, M. (2013). Relationship between Installation Torque and Axial Capacities of Helical Piles in Cohesive Soils. *The Journal of the Deep Foundation Institute*.
- Shetsen, I. (1990). Quaternary geology of Central Alberta. *Alberta Geological Survey*. Alberta Research Council.
- Skempton, A. W. (1951). The bearing Capacity of Clays. *Proceedings of the Bulding Research Congress*, (pp. 180-189).
- Tappenden, K. M. (2007). *Predicting the Axial Capacity of Screw Piles Installaed in Western Canadian Soils*. Edmonton: The University of Alberta.
- Terzaghi, K. (1943). *Theoretical Soil Mechanics*. New York: John Wiley & Sons.
- Transportaion Research Board. (2007). *National Cooperative Highway Research Program: Cone Penetration Testing*. Washington.
- Zhang, D. (1999). *Predicting Capacity of Helical Screw Piles in Alberta Soils, M.S. Thesis. Dept of Civil and Environmental Engineering*. University of Alberta.

Appendices

Appendix A: Borehole Logs



SABATINI EARTH TECHNOLOGIES INC.

CLIENT: Peace Land Piling Ltd.

PROJECT: Proposed Industrial Site

LOCATION: Lot D, Plan 8121744, Hwy 637 & Hwy 16, Lamont, AB

JOB No.: E0604-1484

DATE: April 15, 2006

TECH: MH

TEST BORING

06-1

MOISTURE CONDITIONS ATTERBERG LIMITS		DRILL TYPE B-56 Solid Stem Auger		SOIL PROFILE & DESCRIPTION		TEST RESULTS	
MOISTURE CONTENT %		DEPTH IN FEET	DEPTH (m)	DATUM: SURFACE ELEVATION:	SOIL SYMBOL	SAMPLE TYPE	BLOW COUNT -N
10 20 30 40 50 60				TOPSOIL, silty, trace of sand, compressible, black, 33 cm thick			
		3	1	CLAY TILL, silty, damp, medium plasticity, hard consistency, frequent calcium carbonate mottling from 0.6 to 1.5 m, light brown			
		6	2	- very hard consistency, dry, sandy			PP = 410 kPa
							PP = 510 kPa SO ₄ = 0.03 %
		10	3				PP = 550 kPa
							PP = 510 kPa SO ₄ = 0.01 %
		15	4	BEDROCK (Clay Shale), silty, highly weathered bedrock, hard consistency soil, medium plasticity, moist, bluish-grey			PP = 310 kPa
				- dark brown, silty			PP = 500 kPa
		20	6	- very hard soil			PP = 300 kPa
							PP = 420 kPa
		25	7	- occasional sandstone lenses			PP = 560 kPa
							PP = 460 kPa ± 29 days later (Dry)
		30	9	- occasional siltstone lenses			PP = 300 kPa
				- no evidence of groundwater seepage			PP = 600 kPa
		35	10	End of Borehole = 9.0 m Slough = 8.8 m, 0 hours Water level = 8.8 m (dry), 0 hours Water level = 7.6 m (dry), 29 days later			

⊙ MOISTURE CONTENT

□ LIQUID LIMIT

△ PLASTIC LIMIT

Q_u UNCONFINED COMPRESSION

γ_d DRY UNIT WEIGHT

SO₄ SULPHATE CONTENT

± WATER TABLE

N PENETRATION RESISTANCE

⊠ STANDARD PENETRATION SAMPLE

⊡ UNDISTURBED SAMPLE (SHELBY)

⊞ BAG SAMPLE

PLATE No. 3

Curriculum Vitae

Name:	Jared Harnish
Post-secondary Education and Degrees:	<p>Royal Military College of Canada Kingston, Ontario, Canada 2002-2006 B.A.</p> <p>The University of Western Ontario London, Ontario, Canada 2009-2013 B.Eng.</p> <p>The University of Western Ontario London, Ontario, Canada 2013-2014 MEng.</p>
Honours and Awards:	<p>Natural Sciences and Engineering Research Council (NSERC) Undergraduate Student Research Award 2012</p> <p>Undergraduate Thesis Competition 1st Place (Civil Engineering) The University of Western Ontario 2013</p> <p>Natural Sciences and Engineering Research Council (NSERC) Industrial Postgraduate Scholarship 2013-2015</p>
Related Work Experience	<p>Teaching Assistant The University of Western Ontario 2013-2014</p> <p>Special Projects Lead Helical Pier Systems 2013-2014</p>